NOTE TO USERS

This reproduction is the best copy available.

Numerical Study of a Tornado-Like Vortex in a Supercell Storm

by

Jorge Ruben Santos

Department of Atmospheric and Oceanic Sciences

McGill University

Montreal, Canada

June 2008

A thesis submitted to the

Faculty of Graduate Studies and Research

in partial fulfillment of the requirements for the degree of

Doctor of Philosophy

Your file Votre référence
ISBN: 978-0-494-66653-1
Our file Notre référence
ISBN: 978-0-494-66653-1

Abstract

Recent observations and numerical simulations have significantly improved our understanding of tornadic storms. However, our knowledge of tornadogenesis remains rudimentary. Necessary atmospheric conditions favoring the formation of tornadoes in supercell storms are known, but sufficient conditions remain elusive. The underlying reason is that the processes involved in environment-storm and storm-tornado interactions are not fully understood, as numerical models in the past lacked sufficient resolution to resolve these interactions satisfactorily. In this thesis, an attempt is made to fill this gap by performing a multi-grid high resolution simulation of a supercell storm spawning a tornado-like vortex. Four grids, with grid sizes of 600 m, 200 m, 70 m, and 30 m, are used to allow explicit simulation of storm-tornado interactions. Diagnostic analysis of the modeling results allows an investigation of the origin of rotation at both the storm scale and the tornado scale.

The simulation results showed that the origin of vertical rotation at storm scale during the early stage of storm development is due to tilting of the horizontal vorticity in the environment. This so called mesocyclone then further strengthens by the mechanism of stretching and Dynamic Pipe Effect and descends downwards. During the time of mesocyclone intensification, incipient surface vertical vortices form along the outflow boundary created by the rear flank downdraft due to the process of horizontal shear instability.

One of the surface vortices experiences an initial exponential growth in its vorticity by interacting with the descending mesocyclone and merging with multiple smaller satellite vortices. The tornado-like vortex (TLV) which forms has a maximum horizontal wind of 103 m s^{-1} and a minimum central pressure of 927 hPa. Vorticity budgets of the mesocyclone and the TLV are computed to assess quantitatively the importance of various processes for rotation.

Sensitivity experiments were also performed to determine the effect of varying the environmental conditions on the mesocyclone and surface vorticity. It was found that as the low-level vertical shear of the environmental wind increases, the mesocyclone intensifies and favors the intensification of near surface vorticity. The presence of drier layers in the upper and middle troposphere eventually produces a weaker mesocyclone and weaker outflow boundaries. On the other hand, inclusion of the ice phase processes produces a stronger mesocyclone and more intense outflow boundaries to enhance the intensification of near surface vorticity.

Résumé

Les résultats des observations et simulations numériques récentes ont significativement amélioré notre compréhension des orages à tornades. Cependant, cette compréhension de la genèse des tornades reste rudimentaire. Les conditions atmosphériques nécessaires à la formation des tornades au sein des orages supercellulaires sont connues. Néanmoins, les conditions atmosphériques suffisantes ne le sont pas. Cette méconnaissance est due à notre compréhension limitée des interactions entre environnement et orages et celles entre orages et tornades. Les modèles numériques précédents n'avaient pas une résolution suffisante pour capturer adéquatement de ces interactions. Dans cette thèse, nous tentons de changer cet état de fait en effectuant des simulations multigrilles à haute résolution afin de simuler des orages supercellulaires générant des vortex similaires à des tornades. Afin de permettre une simulation explicite des orages à tornades, quatre grilles sont utilisées: 600 m, 200 m, 70 m et 30 m. Les diagnostiques du modèle permettent d'étudier l'origine de la rotation aux échelles des orages et des tornades.

Les simulations ont montré que la genèse de la rotation verticale à l'échelle de l'orage, en début de développement, est due au basculement de la vorticité horizontale de l'environnement. Le mésocyclone résultant continue à s'intensifier dû à un mécanisme d'étirement, à un effet de tube dynamique, ainsi que dû au courant descendant. L'instabilité de cisaillement horizontal

génère ce courant descendant. Le flanc arrière du courant descendant crée un courant sortant de frontière. Pendant l'intensification du mésocyclone, des vortex verticaux se forment le long de ce courant sortant de frontière. Due à son interaction avec le mésocyclone descendant, la vorticité d'un des tourbillons de surface croît initialement de manière exponentielle et se joint à de multiples autres petits tourbillons satellites. Le vortex similaire à une tornade (VST) qui se forme a un vent horizontal maximum de 103 m s^{-1} et une pression centrale minimum de 927 hPa. Nous calculons le bilan de vorticité du mésocyclone et du VST afin de pouvoir évaluer les effets de divers procédés sur la rotation.

Nous avons également effectué des tests de sensibilité afin de déterminer l'impact du changement de conditions environnementales sur le mésocyclone et la mesure de tourbillon de surface. Il a été trouvé que lorsque le cisaillement environnemental vertical de basse altitude augmente, le mésocyclone s'intensifie. Ceci favorise à son tour l'intensification de la mesure de tourbillon au voisinage du sol. La présence des couches sèches de la haute et intermédiaire troposphère produit de faibles mésocyclone et courant sortant de frontière. Dû au processus de changement de phase de la glace, les mésocyclones et le courant sortant de frontière deviennent plus intenses, et intensifient à leur tour la tourbillon de surface.

Co-Authored Manuscripts

Chapters 2 and 3 of this thesis are in the form of articles submitted for publication in the *Journal of Atmospheric Sciences*. The results presented in these manuscripts originated from the research I conducted within the context of my Ph.D. studies. The first co-author of these papers, Dr. M. K. Yau provided normal supervision of the research project as well as some text editing. The second co-author, Dr. Badrinath Nagarajan, contributed to the setting up of the Linux Beowulf Cluster and installed the numerical model which was used to perform the research presented in this thesis and also some text editing of the first part of Chapter 2.

Statement of Originality

The main original contributions from this thesis are:

- An idealized high-resolution three-dimensional F4 tornado-like vortex (TLV) spawned by a supercell storm is simulated by using a mesoscale model. The analysis of TLV dynamics shows an imbalance between the radial pressure gradient and the centrifugal force during most of the whole life cycle of the TLV. However, when the surface winds of the TLV reached their maximum intensity, a quasi-cyclostrophic balance near the surface is achieved.

- A high-resolution multiscale analysis of the origin of rotation of the TLV and its parent system is achieved for the first time covering the whole life cycle of the storm and the whole life cycle of the TLV (including the genesis, intensification and weakening stages). The results showed that stretching is the most important mechanism in intensifying the vertical vorticity of the TLV and mesocyclone of the storm prior to the tornadic event.

- It is shown that the intensity of the outflow boundaries created by the storm's rear flank downdraft and the low level ambient vertical shear of the horizontal wind modulate tornadogenesis.

- Evidence is provided for the interaction between the storm's mesocyclone and the TLV. The presence of small scale vertical vortices near the surface, as observed in recent field experiments using mobile Doppler radars, is shown to play an important role during the TLV's intensification.

Acknowledgements

First and foremost, I would like to thank my thesis supervisor Professor M. K. Yau for his mentorship, guidance and the academic freedom provided to explore my ideas in this area of study. Dr. Yau's continuous support and invaluable help made possible the successful completion of this thesis.

I wish to thank Dr. Badrinath Nagarajan for his contribution to this thesis with his insight, thoughtful suggestions and assistance. I would also like to acknowledge Dr. Irena Paunova for all her help during the early stage of this thesis research.

Special thanks to the open source community, which through forums, online documentations and the provision of source codes made possible the solution to numerous technical problems during the setting up of the 128-nodes Linux Beowulf cluster used to perform the simulations presented in this thesis.

I would like to thank McGill's Atmospheric and Oceanic Sciences Department, and its Administrative and Academic Officers, Ornella Cavaliere, Karin Braidwood and Vaughn Thomassin, for all their assistance.

Thanks to Lydia Bourouiba for her generous contribution in completing the French translation of the abstract portion of this thesis.

I gratefully acknowledge the financial support of the Canadian Foundation

for Climate and Atmospheric Sciences (CFCAS).

I wish to thank Dr. Terrence Krauss for the support and encouragement to pursue my Ph.D. studies.

Many thanks to my dear friends Yosvany Martinez, Lily Ioannidou and Lucy-Ann Joseph for their moral support and unconditional help in overcoming difficult moments and providing encouraging words to continue moving ahead.

I wish to thank my parents, Cristina and Francisco Santos, who have always had confidence in me and given me the strength to achieve my objectives. Most of all, I want to express my heartfelt thanks to my dear wife, Silvia, for her love and patience throughout my pursuit of this degree.

Contents

List of Figures

List of Tables

Chapter 1

Introduction

1.1 Motivation

Tornadoes, with low-level wind speeds greater than 50 m s^{-1} (Bluestein and Unruh, 1989; Davies-Jones et al., 2001), are one of the most violent of atmospheric phenomena. A tornado is defined as a strongly rotating, narrow column of air, averaging about 100 m in diameter, which appears as the condensation funnel descending from the cloud base and/or as a swirling cloud of dust and debris rising from the ground. The condensation funnel associated with a tornadic vortex is called a funnel cloud. Although in many cases this funnel does not reach the surface, significant damages can still occur at the ground. Fujita (1981) proposed a scale for tornadoes based on the degree of damage inflicted (Fig. 1.1). There are six categories, ranging from F0 to F5; F0 being the weakest and F5 the strongest.

Tornadoes can also be classified in two types based on the characteristics of the convective system that spawns them. A Type I tornado forms within supercell storms characterized by a mesocirculation aloft. These su-

F-scale	Winds	Type of Damage
F0	18-32 ms^{-1}	Light Damage; some damage to chimneys; break branches off trees; push over shallow-rooted trees;damage signboards
F1	33-49 ms^{-1}	Moderate Damage; the lower limit (33 ms^{-1}) is the beginning of hurricane wind speed; peel surface off roofs; mobile homes pushed off foundations or overturned; moving autos pushed off the road
F2	50-69 ms^{-1}	Considerable Damage; roofs torn off frame houses; mobile homes demolished; boxcars pushed over; large trees snapped or uprooted; light-object missiles generated
F3	70-92 ms^{-1}	Severe Damage; roofs and some walls torn off well-constructed houses; trains overturned; most trees in forest uprooted, heavy cars lifted off ground and thrown
F4	93-116 ms^{-1}	Devastating Damage; well-constructed houses leveled; structures with weak foundations blown off some distance; cars thrown and large missiles generated
F5	117-142 ms^{-1}	Incredible Damage; strong frame houses lifted off foundations and carried considerable distance to disintagrate; automobile-sized missiles fly through the air in excess of 100 meters; trees debarked; incredible phenomena will occur

Figure 1.1: Fujita Scale (Fujita, 1981)

percell storms can be isolated or embedded entities in a line of thunderstorms (Browning, 1986). On the other hand, a Type II tornado is not associated with a mesocirculation. It is generally a small and weak vortex that forms along a stationary or slowly moving windshift line due to the rolling-up of the associated vortex sheet into individual vortices.

Significant tornadoes (stronger than F1) are almost always associated with supercell thunderstorms with a persistent region of rotation in a deep layer known as the mesocyclone. To a first approximation, the tangential winds in a mesocyclone may be modeled as a Rankine combined vortex (Davies-Jones et al., 2001), consisting of a core in solid-body rotation surrounded by a potential vortex where the tangential wind varies inversely with distance from the center. Core diameters vary from 3 to 9 km, with an average value of about 5 km. As a result of this mid-level rotation, part of the storm precipitation near the surface adopts a hook shape feature. This precipitation structure is clearly depicted by radar based reflectivity and is known as the hook echo region (HER). Tornadoes are usually formed at the tip of the HER.

Hook echoes are also known to be associated with commonly observed region of subsiding air in supercells, called the rear-flank downdraft (RFD). The role of the RFD has long been hypothesized to be critical in the genesis of significant tornadoes within supercell thunderstorms. At the tip of the HER, where the occlusion of the outflow boundaries created by the RFD and the forward flank downdraft (FFD) occurs, a tornado usually forms. The FFD is associated with an intense storm precipitation zone located ahead of the supercell storm.

Approximately 90 of the mesocyclones observed during the Joint Doppler Operational Project (JDOP) were associated with severe weather and 50 % of them produced tornadoes (Burgess and Lemon, 1990). As a result, Doppler radar identification of a mesocylone is considered a useful tool for issuing se-

vere weather warnings. However, the crucial question remains to be answered is why not all radar-observed mesocyclones produce tornadoes.

Blanchard and Straka (2002) documented a mobile radar signature of a spiraling hook echo in a nontornadic supercell similar in appearance to tornadic supercells. Trapp (1999) and Wakimoto and Cai (2000) also documented circulations in nontornadic supercells at levels close to the ground. Trapp (1999) studied tornadic and non-tornadic supercells to understand the likely factors leading to the failure of tornado formation. He found that the low-level mesocyclones associated with tornadic supercells had smaller core radii compared to non-tornadic supercells and they were associated with relatively intense vortex stretching. Recent observational data of tornadoes with resolution higher than 100 m reported by Wurman and Gill (2000) suggest the presence of subvortices in tornadic storms.

The association among hook echoes, RFD, and tornadoes is well established (Markowski et al., 2002a) although the dynamical relationship remains poorly understood. There are no obvious systematic differences in radar reflectivity structure (Markowski et al., 2002b) between hook echoes in tornadic and nontornadic supercells. Dual-Doppler radar observations from the Verification of the Origin of Rotation in Tornadoes Experiment (VORTEX) have shown that in most cases, the difference between tornadic and nontornadic supercell storms cannot be distinguished from the three-dimensional wind velocity measurements (Blanchard and Straka, 2002; Trapp, 1999; Wakimoto and Cai, 2000; Wakimoto and Liu, 1998). Further advances in the understanding of tornadogenesis are therefore needed to improve tornadoes forecast and warnings by reducing the false alarm rate based on mesocyclonic signatures.

The goal of this thesis is to advance our understanding of tornadogenesis in a supercell storm by numerical modeling. Specifically, the Canadian Mesoscale Compressible Community model (MC2) (Girard et al., 2005) will

be used to simulate a tornado-like vortex in a supercell. By employing high vertical and horizontal resolutions to resolve the flow near the ground, we will investigate the dynamics and the origin of rotation of the swirling flow in the hook echo region during the formation of a tornado-like vortex. Sensitivity experiments on varying the initial conditions will be performed and the effect on tornadogenesis studied. The sensitivity study will focus on the role of the vertical shear of the ambient horizontal wind at low levels, the influence of the upper and middle tropospheric moisture stratification, and the role of including ice phase microphysics.

1.2 Overview of Tornadogenesis in Supercell Storms. Observations and Numerical Modeling.

The most remarkable observational finding during the last 10 years is that the differences between tornadic and nontornadic supercells may be subtle. Even in dual-Doppler radar analyses of the wind fields just prior to tornadogenesis, no differences have been found in these two types of supercells.

Recent radar observations, which include data obtained from both airborne and ground based mobile Doppler radars, have resolved structures within hook echoes that were unresolvable or barely resolvable in earlier radar studies of supercell storms. Examples include the high resolution (less than 100 m spatially) data of tornadoes presented by Wurman and Gill (2000) and Bluestein and Pazmany (2000). The images presented by Bluestein and Pazmany (2000) are commencing to resolve small scale structures, possibly related to the existence of subvortices, within the hook echo region. The

multiple-Doppler radar observations in the last decade have also detected vorticity couplets in the hook echoes of tornadic storms (Bluestein et al., 1997; Rasmussen and Straka, 1996; Wurman and Gill, 2000). The understanding of the kinematics and dynamics of these small scale structures may start to shed some light on the mechanisms leading to success or failure in tornadogenesis.

Markowski et al. (2002b) used mobile mesonet data of the surface thermodynamics characteristics of hook echoes and RFDs associated with tornadic and nontornadic supercells to determine whether certain types of hook echoes and RFDs are favorable or unfavorable for tornadogenesis. They concluded from their analysis that:

- Tornado likelihood, intensity and longevity increase as the surface buoyancy, and the equivalent potential temperature in the RFD increase, and as the convective inhibition (CIN) associated with RFD parcels at the surface decreases.
- The presence of a circulation at the surface is not a sufficient condition for tornadogenesis.
- Baroclinicity at the surface within the hook is not a necessary condition for tornadogenesis.

Lemon and Doswell (1979) developed a conceptual model of a supercell (Fig. 1.2) based on extensive compilation of surface visual and radar observations. This model includes the FFD and the RFD, a surface gust front resembling a mid latitude cyclone, a hook shaped reflectivity region surrounding a cyclonic rotating updraft and a tornado, if present, that resides within the vertical velocity gradient between the updraft and RFD.

This model has undergone little modification since its appearance over 20 years ago. Lemon and Doswell inferred that the RFD typically originated

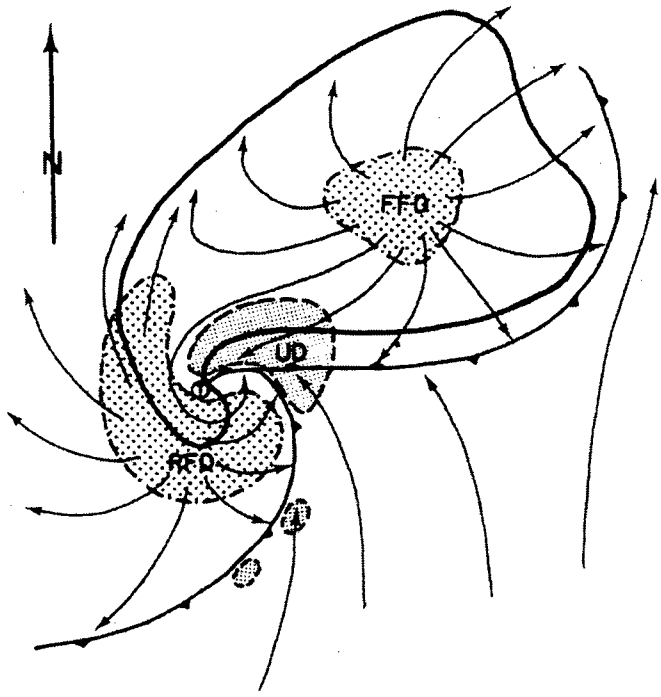

Figure 1.2: Lemon and Doswell conceptual model (Apadted from Markowski et al. (2002a)).

between 7 to 10 km on the relative upwind side of the updraft. Rotunno and Klemp (1982) showed that the RFD is initiated by a pressure fluctuation that depends on the vertical shear. Numerical simulation results confirmed this theoretical prediction, as did some later dual-Doppler radar findings.

Klemp and Rotunno (1983) used a numerical model with a horizontal resolution of 250 m and obtained a large hook echo with a strong low level updraft. The simulated low-level vorticity field is elongated along the rear flank gust front. After 60 min of integration the solution revealed many details of the low level mesocyclonic flow.

Rotunno and Klemp (1985) showed that baroclinic generation of horizontal vorticity along the storm's low level cold pool was important to the development of the low level rotation. They demonstrated that low level rotation is initially horizontal (horizontal vorticity generated by the cold pool's solenoid) and subsequently reoriented to produce vertical circulation.

Grasso and Cotton (1995) simulated an intense tornado like vortex. This vortex was resolved using 100 m horizontal and 25 m vertical grid spacings. Surface friction was also included. Their simulation generated a tornado like vortex with 50 m s^{-1} tangential winds and updraft speeds of over 50 m s^{-1}. Analysis showed that the low pressure at the base of the updraft generates vertical motion near the surface. A vortex formed in region of strong gradient of the vertical velocity near the low pressure and then tilting and stretching of additional vorticity lowered the subcloud pressure field further. The vortex continues to build toward the surface via this process.

Wicker and Wilhelmson (1995) presented another tornado scale simulation. The life cycles of two tornadoes-like vortices were simulated on a 125 m grid during a 40 min period. Maximum ground relative wind speed exceeded 55 m s^{-1} for over 5 min. Vertical vorticity near the surface also exceeded

0.25 s^{-1}. The vortices appeared to have been generated from strong vertical motion that periodically intensified at the base on the storm. Updraft in the storm at the height of 3 km accelerated over 10 m s^{-1} within a few minutes, immediately preceding the tornado like vortices in the boundary layers. An analysis showed that updraft acceleration was driven by rapid changes in the vertical pressure gradient aloft due to increase midlevel rotation in the storm's mesocyclone. Tornado demise occurs when the updraft over the tornado weakens significantly. At this time, the occlusion downdraft which wrap around the tornado produces an associated low-level divergence. Being cut off from its source of positive vorticity, the vortex then dissipates.

Markowski et al. (2003) conducted idealized numerical simulations of an axisymmetric, moist, buoyant rotating updraft which is designed to emulate that of a supercell storm. The horizontal and vertical grid resolutions are $\Delta r = 40$ m and $\Delta z = 40$ m respectively. After analyzing the results of the four experiments it was concluded that the angular momentum brought to the surface increases with increasing temperature deficits, while low-level convergence is stronger when the downdraft has small temperature deficit compared to the cold downdraft case. In this numerical simulation there is an association between relatively warm rear flank downdraft and the likelihood of tornado, intensity and longevity (small dew point depression and relatively warm rear flank downdraft). The simulation results of Markowski et al. (2003) were consistent with those found in observed temperature deficit within RFD (Markowski et al., 2002b).

1.3 Thesis outline and objectives

Recent observations (Bluestein et al., 2003a,b; Markowski et al., 2002b) are starting to shed some light in tornado structure and evolution together with

the low level flow of the storms. However, the relatively low temporal and spatial resolutions of the measuring instruments preclude a detailed picture of tornadogenesis and the interaction of tornadoes with their parent systems. Numerical models have given some insight in terms of the possible mechanism for tornado formation in supercells, but the model-grid spacing used are still too coarse to resolve the tornado itself.

The main goal of this thesis is to better understand tornadogenesis in supercell storms and the impact of the environmental parameters on the modulation of tornado formation. Specific objectives of this research are:

- to simulate numerically an idealized tornado-like vortex that occurs in a supercell storm using a nesting grid with resolutions of 600 m, 200 m, 70 m, and 30 m and to investigate the interaction between the different storm components (i.e. RFD and storm mesocyclone) with the tornado-like vortex (TLV);
- to identify the mechanism leading to the origin of rotation on the TLV and storm scales;
- to study the sensitivity of tornadogenesis to the variation of low level vertical shear of the environmental wind and the upper and middle tropospheric moisture stratification.

The outline of the thesis is as follows. In Chapter 2, an idealized high resolution TLV in a supercell storm is simulated by using a non-hydrostatic high-resolution model. The interaction between the TLV and its parent system is analyzed and the results are compared with current conceptual models.

In Chapter 3, the origin of rotation in the simulated supercell and the spawned TLV is investigated. The tornado wind structure and the main forces

acting during the evolution of the tornado vortex are analyzed. Also a series of sensitivity experiments are performed to determine the impact of the ambient low level vertical wind shear and the upper and middle tropospheric moisture stratification in modulating the evolution of the storm and tornadogenesis.

Conclusions are provided in Chapters 2, and 3 and are also summarized in Chapter 4.

Chapter 2 and 3 are presented in the form of two manuscripts with some unavoidable overlaps.

Chapter 2

Tornadic Supercell Simulation

The conditions leading to the formation of a tornadic supercell have long been surmised. They are supported by numerous observations and numerical modeling results. Nevertheless in many cases, only necessary conditions for the formation of tornadoes exist and sufficient conditions remain elusive. The main reason is the poor understanding of the mechanism in storm-tornado interactions. In this chapter, a high-resolution supercell storm simulation is performed to obtain a tornado-like vortex. The mechanism leading to the formation of this vortex is investigated to shed light on tornadogenesis.

Simulation of a Tornado-Like Vortex in a Supercell Storm, Part I: Results on storm scale and tornado scale.

Jorge Ruben Santos

M. K. Yau

Badrinath Nagarajan

Department of Atmospheric & Oceanic Sciences, McGill University,

Montreal, Canada

ABSTRACT

An idealized numerical simulation of a supercell storm was performed using the Canadian Mesoscale Compressible Community model to study the formation, development, and dissipation of a F4 tornado-like vortex (TLV).

The model was initialized using a horizontally homogeneous sounding characterized by a convective available potential energy of 2100 J kg^{-1} and a bulk Richardson number of 24.4. The storm scale features and the event of tornadogenesis are investigated using four nesting domains with horizontal resolutions of 600 m, 200 m, 70 m, and 30 m respectively.

The simulated storm exhibited an intense TLV situated at the tip of a hook shaped precipitation region at the surface. The intensification of the TLV was associated with an upper-level mesocyclonic circulation, a low-level jet, and mergers of several surface vortices. The vortex reached a maximum surface wind of 103 m s^{-1} and a central pressure of 927 hPa, characteristic of an F4 tornado.

The weakening stage of the vortex was dominated by the presence of an intense downdraft through the center of the vortex, creating a divergence flow at the surface to dissipate the TLV. The investigation of a weaker F1 vortex revealed an absence of the interaction with an upper level mesocyclonic circulation and the merging with other surface vortices, resulting in a significantly weaker vortex. Our results therefore suggest an important role played by the mesocyclone and vortex mergers in the formation and development of an intense tornado.

2.1 Introduction

Tornadoes are severe weather events and they present a hazard over the globe (Feuerstein et al., 2005). In the past 30 years, there has been progress in understanding tornadic storms. However, knowledge of the mechanism for tornadogenesis remains rudimentary. Similar environments that produce strong rotating supercell storms often fail to generate a tornado and only between 30 % and 50 % of mesocyclones are conducive to tornadogenesis (Burgess et al., 1993). It is clear that the mechanisms for storm-environment and storm-tornado interactions are not fully understood. Better understanding of the interactions is required to improve the forecast of these severe weather events.

Based on the results of observations and numerical models, Lemon and Doswell (1979) proposed a conceptual model of a tornadic supercell storm. The essential components include the hook echo region (HER), the rear flank downdraft (RFD), and the forward flank downdraft (FFD). Intense tornadoes with high values of low level vorticity tend to form near the tip of the HER which is marked by strong horizontal gradients in vertical motion and temperature.

Unfortunately, the presence of these components seems only to be necessary but not sufficient for a supercell storm to become tornadic. In general, it is difficult to distinguish between a tornadic and a non-tornadic supercell storm based on radar reflectivity signatures of hook echoes (Markowski et al., 2002b). Furthermore, dual-Doppler radar wind observation from the Verification of the Origin of Rotation in Tornadoes Experiment (VORTEX) indicate no systematic difference between tornadic and non-tornadic supercells (Blanchard and Straka, 2002; Wakimoto and Cai, 2000; Wakimoto and Liu, 1998). Recently, Markowski et al. (2002a) found some differences in surface thermodynamic fields between significant tornadic, and weakly tor-

nadic or non-tornadic supercell storms. They showed that tornado intensity and longevity increase with an increase in surface buoyancy and equivalent potential temperature in the RFD but also concluded that the presence of a circulation center at the surface and baroclinity within the HER are not necessary conditions for tornadogenesis. Dupilka and Reuter (2006a,b) studied the environmental parameters from an observational dataset containing tornadic and non-tornadic storms over Alberta, Canada. They found that significant tornadoes were associated with environments characterized by stronger shear than those in weak or non-tornadic events. High values of storm relative helicity were also correlated with the occurrence of significant tornadoes.

Recent high resolution (about 100 m) observations obtained from ground-base mobile radars or Doppler On Wheels (DOW) in tornadic supercell storms have depicted the presence of small scale vortices (or satellite vortices) in the region of the outflow boundaries of RFD (Bluestein et al., 1997; Bluestein and Pazmany, 2000; Bluestein et al., 2003b; Wurman and Gill, 2000). An understanding of the kinematics and dynamics of these small scale features may shed some light on tornadogenesis.

Additional insight into the physical processes contributing to tornadogenesis has been gained from numerical modeling. Consistent with observations, three-dimensional idealized numerical simulations of tornadic storms have generated tornado-like vortices (TLVs). Some early work by Klemp and Rotunno (1983), using a grid size of 250 m, captured a large hook echo region associated with a strong low level updraft and a low level mesocyclonic flow. Rotunno and Klemp (1985) showed that baroclinic generation of horizontal vorticity along the outflow cold pool was important to the development of the low level rotation through vorticity tilting. Numerical simulations performed by Finley et al. (1998); Grasso and Cotton (1995); Wicker and Wilhelmson (1995) using grid sizes from 100 m to 125 m also reproduced hook and bounded precipitation regions with rotation at both the mid- and low-levels.

Markowski et al. (2003) carried out a series of sensitivity experiments on an axisymmetric, moist buoyant rotating updraft with a resolution of 40 m. They suggested that the intensity of the near ground circulation depends on the thermodynamic characteristic of the rotating air mass. These results were consistent with those found in Markowski et al. (2002a).

Although the three-dimensional numerical studies mentioned above capture the main features of a tornadic storm, the horizontal grid resolution remains too coarse to properly resolve the air flow in the low and upper levels. To investigate storm-tornado interaction processes a higher resolution numerical simulation is needed and it is the purpose of this paper to fill the gap.

The main goal of this work is to better understand tornadogenesis by simulating numerically an idealized tornado-like vortex in a supercell storm using four nesting grids with resolutions of 600 m, 200 m, 70 m, and 30 m respectively. We will analyze not only the low-level storm boundaries and the contribution of small scale vortices, but also the role played by the mesocyclone and its interaction with the tornado-like vortex. The organization of the paper is as follows. Section 2 provides a brief description of the model, the initial conditions, and the nesting strategy. Section 3 presents the results for both the coarse resolution (600 m) run encompassing the supercell storm and the high resolution (30 m) run depicting the life cycle of the TLV. Particular attention will be focused on the interaction of the mesocyclone and the small scale vortices, as well as the process of vortex mergers. Section 4 contains a summary and conclusions.

2.2 Model strategy

The simulations were performed using the Canadian Mesoscale Compressible Community Model (MC2) which is a fully-compressible, nonhydrostatic, limited-area model capable of one-way self-nesting. Interested readers are referred to Benoit et al. (1997) for a complete description of the MC2 dynamics and Mailhot et al. (1998) for a complete description of the MC2 physics. The MC2 model has been applied to simulate the Pine Lake tornadic storm over the province of Alberta in Canada (Milbrandt and Yau, 2006a,b). For the idealized simulations performed here, we neglect the effect of topography, Coriolis force (Weisman and Klemp, 1982), boundary layer and surface processes, as well as short- and long-wave radiation. Cumulus convective parameterization is not used but explicit warm rain microphysics following Kong and Yau (1997) is allowed.

2.2.1 Initial and boundary conditions

Fig. 2.1 depicts the domains D1, D2, D3, D4 with a grid size of 600, 200, 70 and 30 m respectively. Each domain employs a one-way nesting procedure of the lateral boundary conditions. For the 600 m run, the lateral boundary conditions are kept constant. For the 200 m, 70 m and 30 m simulations, the initial and lateral boundary conditions are provided respectively by the 600 m, 200 m and 70 m runs. The number of grid points, the initiation time, and the frequency of updating the lateral boundary conditions are given in Table 2.1.

The 600 m, 200 m, and 70 m domains employed a vertical grid spacing of 50 m from the surface to 3.4 km, followed by a gradually increasing grid size with height, reaching 1 km at the model top (16 km). For these three

domains, the first momentum level is at a height of 25 m. For the 30 m domain, the first momentum level is set at 15 m. The run is initialized with a horizontally homogeneous thermodynamic profile (Fig. 2.2), whose analytic representation is given by the following expressions:

$$\bar{\theta}(z) = \begin{cases} \theta_o + (\theta_{trp} - \theta_o)\left(\frac{z}{z_{trp}}\right)^{1.5}, & z \leq z_{trp} \\ \theta_{trp} exp\left[\frac{g}{c_p T_{trp}}(z - z_{trp})\right], & z > z_{trp} \end{cases} \tag{2.1}$$

$$H(z) = \begin{cases} 1 - \frac{3}{4}\left(\frac{z}{z_{trp}}\right)^{1.5}, & z \leq z_{trp} \\ 0.25, & z > z_{trp} \end{cases} \tag{2.2}$$

where $\bar{\theta}(z)$ and $H(z)$ are the environmental potential temperature and the relative humidity profile respectively. The tropopause height is given by z_{trp} = 12 km, surface potential temperature is θ_o = 302 K, and the tropopause temperature is set at T_{trp} = 217.18 K (or θ_{trp} = 349 K). Fig. 2.2 shows the sounding on a skew-T plot. There is a well-mixed boundary layer (1000-850 hPa) and a moist tropospheric layer. The sounding has a moderate value of convective available potential energy (CAPE) at 2100 J kg^{-1}. This thermodynamic profile is similar to the one used by Markowski et al. (2003) in their Experiment 1 and Experiment 2.

The vertical wind shear profile is the same as in Wicker and Wilhelmson (1995) (Fig. 2.3) and it represents a composite of hodographs in environments that produced tornadic storms over Oklahoma (Brown et al., 1973; Davies-Jones et al., 1990; Wicker et al., 1984). The hodograph is characterized by a clockwise rotation of the horizontal winds with height over the lowest 5 km. From 5 km to 7 km, the winds mainly indicate speed shear. Above 7.5 km, the winds are kept at a constant value.

The Storm Relative Helicity (SRH) for the hodograph is 310 m^2 s^{-2} for the 0-1 km layer and 480 m^2 s^{-2} for the 0-3 km layer. The definition of SRH

is:

$$H(z) = -\int_0^z \mathbf{k} \cdot \left(\vec{\mathbf{V}} - \vec{\mathbf{C}}\right) \times \frac{\partial \vec{\mathbf{V}}}{\partial \mathbf{z}} \mathbf{dz} \tag{2.3}$$

where $\vec{C}$ is the velocity of the storm motion, $\vec{V}$ is the horizontal wind vector and z is the vertical height.

Another important parameter used to characterize the environmental winds is the Bulk Richardson Number (BRN) given by:

$$BRN = \frac{CAPE}{0.5 * (\Delta \bar{U}^2 + \Delta \bar{V}^2)} \tag{2.4}$$

where $\Delta \bar{U}$ and $\Delta \bar{V}$ are the zonal and meridional components of the difference between the 0-6 km and 0-500 m density weighted layer mean winds. The computed BRN for the sounding is 24.4, within the range of values for quasi-steady supercell storms (Weisman and Klemp, 1982).

Convection in the model is initiated by specifying an ellipsoidal thermal bubble with a temperature perturbation of 4 K and a horizontal (vertical) radius of 10 km (1.5 km). The bubble is centered at 1.5 km above the surface and is situated at the center of domain D1 (Fig. 2.1). To keep the storm near the center of the domain during its evolution, the storm propagation velocity (11.8 m s^{-1} in the x direction) is subtracted from the initial wind velocity. Therefore all subsequent analysis is in storm-relative coordinates.

The 600 m run is integrated for 90 min, the 200 m run 30 min, the 70 m run 26 min, and the 30 m run 15 min. The time steps for the four runs are respectively 1 s, 1 s, 0.5 s, and 0.1 s.

2.3 Results

2.3.1 Storm scale

The results from the 600 m run are analyzed to understand the storm scale features. Following the initiation of convection, two storm systems developed. One system corresponds to a right moving supercell while the other is a left mover (Klemp and Rotunno, 1987). These systems are depicted as S1 and S2 in Fig. 2.1. S1 intensifies into a supercell and will be the focus of this study, whereas S2 fails to intensify and propagates toward the left of the mean wind (Fig. 2.1). The mechanisms leading to the formation of S1 and S2 are explained in Klemp and Rotunno (1987). Briefly, the development of vertical rotation in S1 and S2 occurs through the vertical tilting of the environmental horizontal vorticity, resulting in a pair of vortices. The presence of the downdraft splits the storm system into a cyclonic and an anticyclonic rotating pair. The interaction of the updrafts with the counter-clockwise rotating winds of the environment (see Fig. 2.3) favors the development of S1 and leads to the weakening of S2.

As will be shown later, the development of the TLV is related to the mesocyclone in S1. We therefore examine first the salient features surrounding the hook echo region in S1 over an 18 km x 18 km area delineated by x=(63 km,81 km), and y=(99 km,117 km). Fig. 2.4 depicts the time evolution of the maximum vertical velocity (Wmax) at three levels. Two major maxima appear at each height with the first maximum occurring at around 20 min after the model has gone through the spin-up phase. The second absolute maximum occurs at about 66 min at 3 km, 70 min at 1 km, and 75 min at 0.1 km. We will show below that the descent of the absolute maximum is related to the intensification of the mesocyclone cumulating in a tornadic event at the surface around 77 min.

Figure 2.5 shows the horizontal and vertical structures around the hook echo region at 75 min, close to the time of tornadogenesis. Despite the coarse resolution of 600m, a maximum in surface vertical vorticity (ζ) appears at the tip of the hook-shaped region of the supercell storm (Fig. 2.5 a). This vorticity maximum is related to the TLV, and its location within the parent system is in agreement with the conceptual model of Lemon and Doswell (Lemon and Doswell, 1979). The vertical cross-section along the line 1-2 in Fig. 2.5 a shows an intense mesocyclonic circulation between 2 and 4 km shown in Fig. 2.5 b. Note that the surface maximum in ζ is located underneath the mesocyclone and a strong vertical gradient of vertical motion extends from the surface to a height of 2 km, indicative of strong convergence below 2 km. Horizontally, strong gradients of vertical motion in the hook echo region is revealed at an altitude of 1 km (Fig. 2.5 c). The strong downdrafts are associated with the outflow boundaries at the surface marked by large horizontal temperature gradients (Fig. 2.5 d). Note that along the thermal boundaries where the cold downdraft air meets the warm inflow air from the environment, strong horizontal shear of the horizontal wind develops. This shear will be shown to contribute to the generation of the initial seed of vertical vorticity along the thermal boundaries to the east of the hook and plays an important role in the generation of the TLV. Another important feature captured is the low-level jet located in the cold channel (depicted by the red-dash circle in Fig. 2.5 d). The jet appears to originate from the RFD that is driven by evaporative cooling in the rain shaft.

The alignment of the vertical velocity and vertical vorticity fields depicted in Fig. 2.5 b is conducive to the intensification of the mesocyclone. To clarify this point, we plotted in Fig. 2.6 a time-height section of maximum vertical vorticity and Wmax over the same area as in Fig. 2.5 a after 60 min. A well-defined mesocyclonic circulation is evident at 68 min between 1.5 km and 4 km. With time, the mesocyclone intensifies and descends. This is

accompanied by a descending updraft pulse, the locus of which is given by the solid dashed line. Note the strong vertical gradient in Wmax below 2 km after 70 min, indicative of the development of low-level horizontal convergence. This process continues until a maximum in the vorticity near the surface is reached at 77 minutes when tornadogenesis occurs.

The intensification and descent of the mesocyclone can be explained as follows. Wicker and Wilhelmson (1995) has shown that a low pressure exists in the mesocyclone as a result of the dynamic forcing associated with the velocity field. At 68 min, the minimum low pressure of the mesocyclone is located around 2.5 km. This creates an upward pressure gradient force causing convergence and vortex stretching below so the mesocyclone descends. In turn the descent of the mesocyclone results in additional upward pressure gradient force lower down and the Dynamic Pipe Effect (DPE) (Leslie and Klemp, 1971; Smith and Leslie, 1979) is in operation. Through a bootstrap process, the storm mid-level circulation is brought down by the continuous intensification of the rotation below the mesocyclone as a consequence of increasing convergence at the lower levels.

It is worth noting that the intensification and descent of Wmax in Fig. 2.6 after 68 min prior to the tornadic event is a feature also found within the storm that spawned the Del City tornado (see Fig. 11 a in Wicker and Wilhelmson (1995)).

Thus far, we have shown that the 600 m run qualitatively reproduces the main features of the Lemon and Doswell conceptual model, particularly in the location of the TLV with respect to a hook shaped precipitation region, the updraft, and the RFD. Similar to Wicker and Wilhelmson (1995), the simulation reproduced the horizontal structure of the updraft,downdraft, and a surface vorticity maximum. Our results indicate that the appearance of the TLV is preceded by the downward shift of Wmax and ζ associated with a

mesocyclone. The strong horizontal shear along the boundary between hot-humid environmental air and cold air due to evaporation from the RFD is the site of incipient surface vortices. The alignment of the mesocyclone with the low level vortex and the existence of a low-level jet are highly suggestive of their link to the vortex intensification process. However, a 600 m run cannot resolve the TLV in its details. We resort therefore to the 30 m simulation to investigate the process of formation and intensification of the TLV and its interaction with the mesocyclone.

2.3.2 Tornado-like vortex

2.3.2.1 Overall evolution

The 30 m simulation is initialized at 66 minutes (Table 2.1). For convenience, the reference time in the figures for the 30 m run will be relative to the initial time. Fig. 2.7 shows the time series of the minimum central pressure (MCP), maximum horizontal wind speed (Vmax), and maximum vertical vorticity ζ at the surface following a 900 m x 900 m square with the MCP of the TLV at its center. Using Vmax as the criterion for intensity, the life cycle of the TLV can be classified into three stages: the genesis stage, the intensification stage, and the weakening stage. The genesis stage spans the period 250-400 s with Vmax between 22 and 32 m s^{-1} accompanied by a slow decrease in MCP. The intensification stage starts at around 400 s and extends to 530 s. There are a number of peaks in Vmax during this time with the strongest wind speed occurring at 510 s. The MCP and ζ also undergo oscillation but in general the vorticity increases and the MCP decreases and extreme values of ζ and MCP are preceded by peaks in Vmax. The largest value of Vmax reached is 103 m s^{-1} at 510 s. The weakening stage sets in after 530 s. The maximum

wind and vertical vorticity decrease rapidly while the MCP indicates a fast filling of the TLV.

A snap shot of the TLV (denoted by the letter T) and its surrounding close to the time of its maximum development at 530 s is depicted in Fig. 2.8. Unlike the horizontal sections in the 600 m run (Fig. 2.5), small scale features like vortices and vortex couplets begin to emerge. These features have also been found in recent observations (Bluestein et al., 1997; Bluestein and Pazmany, 2000; Rasmussen and Straka, 1996; Wurman and Gill, 2000). Although many surface vortices (Fig. 2.8 b) develop near the tip of the hook shaped precipitation region delineated by the 1 g kg^{-1} contour, only one of them reaches F4 intensity. This TLV is characterized by a low central pressure of 927 hPa (Fig. 2.8 a) and a large vertical vorticity (Fig. 2.8 b) associated with strong horizontal wind gradients. Note that the TLV is located in a zone with strong gradients of vertical motion (Fig. 2.8 c) and temperature (Fig. 2.8 d), and it has a cold core structure.

2.3.2.2 Tornado-like vortex life cycle

The detail of the life cycle of the TLV in its three stages is presented below.

- *Genesis Stage*

The initial seed of surface vertical vorticity is generated at the surface along a line depicted in Fig. 2.9 a at 271 s. This line of vorticity is the manifestation of a vortex sheet originating from strong horizontal wind shear produced at the boundary of two air masses of different virtual potential temperatures (Fig. 2.9 b). The air to the east of the vorticity line is associated with the inflow of warm air and the air to the west of the line is associated

with storm outflow with colder temperatures. We will zoom into the region marked by the dashed square in Fig. 2.9 a to follow the time evolution of the incipient TLV.

Fig. 2.10 depicts the development of the northern tail end of the vortex sheet from 250 s to 271 s. The 8 panels are plotted every 3 s. As time progresses, a center of maximum vorticity, originally located around x= 78.6 km and y= 117.5 km at 250 s, starts to amplify rapidly. At 259 s, the incipient TLV is located around x= 78.1 km and y= 117.5 km at the lobe of the cold outflow boundary (indicated by the -3 K contour of perturbation potential temperature) in a region with strong horizontal shear. The spatial distribution of vorticity in the vortex sheet (Fig. 2.10) and its initial evolution is characterized by:

- A change in sign in the spatial gradient of the vertical vorticity component (VVC) across the vortex sheet, which is a necessary condition for shearing instability as indicated by Rayleigh (1880).
- The fastest growing mode occurs at a wavelength of approximately 7 times the width of the transition zone in the vortex sheet, close to the 7.5 times found by Miles and Howard (1964) from linear theory.
- The fastest growing mode (Fig. 2.11), represented by the time evolution of the VVC perturbation (ζ') of the vorticity sheet in Fig. 2.10 between 256 s and 275 s, grows exponentially with time (Fig. 2.11). This perturbation is computed by taking the difference between the actual VVC and the average vertical vorticity computed over the domain presented in Fig. 2.10. The exponential growth of this perturbation resembles the one predicted by linear theory.

The above characteristics are common features also found in the development of two dimensional shear instabilities. Although some uncertainty

remains in the mechanisms that control the evolution of a three dimensional vortex sheet, our results are highly suggestive that horizontal shear instability (HSI) is a dominant mechanism during the genesis of surface vertical vorticity. We remark that the initial evolution of the simulated vortex sheet presented here is similar to the results reported in Lee and Wilhemlson (1997), where vortices are generated at the leading edge of a dry outflow air mass in the presence of horizontal wind shear.

The relation between the small scale surface vortices and the mesocyclone during this stage is illustrated by the plot of surface vorticity and the 1.6 km horizontal wind field and pressure deficit at 337 s in Fig. 2.12. The incipient TLV is marked by the letter T and other surface vortices can be seen developing along the vorticity line. It is clear that there are two well-defined scales during this tornadogenesis event: the incipient TLV with a horizontal scale of around 300 m and the mesocyclone with a diameter of about 4 km. The separation distance in the horizontal direction between the surface incipient TLV and the center of the mesocyclone, defined by the absolute minimum pressure deficit (relative to the pressure in the far environment at the same level) at an altitude of 1.6 km, is about 2.5 km.

- *Transition to the Intensification Stage*

The transition to the intensification stage is marked by the interaction between the mesocyclone and the incipient TLV depicted in Fig. 2.13, which is a vertical cross-section of Fig. 2.12 parallel to the x axis through the center of the TLV.

Note that in the figures for the 30 m runs that follow, the origin of the x and y axes are chosen to ensure that the TLV is located at the center of the figures.

In Fig. 2.13 panel a shows that at 340 s, a strong pressure deficit exists for x < 1.2 km. The strongest value lies between 1 and 1.5 km above ground level (AGL) and is associated with the mesocyclonic circulation. Near the ground, at a distance of x = 2.5 km, a surface vortex marked by the letter T has emerged. At 360 s (panel b), the near surface vortex has the strongest pressure deficit around 0.25 km AGL and is beginning to interact with the mesocyclone. At 390 s, the mesocyclonic circulation shows a downward and eastward intensification and stronger interaction with the vortex occurs. The pressure deficit in the vortex continues to increase and extends upward at 400 s (panel d) and 430 s (panel e). At 460 s (panel f), the pressure deficit minimum of the mesocyclone has merged with that of the vortex with values reaching -30 hPa, revealing a picture of the connection between the tornado vortex signature (TVS) aloft and surface vortices during tornadogenesis. Note that the patch of pressure deficit below the mesocyclone to the west of the TLV is related to a low-level jet. This association is illustrated more clearly in Fig. 2.14 which depicts the surface pressure deficit (panel a) at 460 s with the TLV at the center and the signature of the low level jet to the west. A similar pattern can be detected in the plot of the surface wind speed (panel b).

As the mesocyclone intensifies downward, the induced rotating winds near the surface favors the occlusion of the line of vorticity generated by horizontal wind shear. This allows other vortices to merge with the intensifying TLV. Three main merging events occur at 430 s , 490 s and 507 s respectively, and each merger is associated with a peak in maximum surface vertical vorticity shown in Fig. 2.7. The evolution of a representative merger event is illustrated in Fig. 2.15. At 500 s, a main vortex is centered at (x,y)=(0.4 km, 0.4 km) in panel a). Two smaller vortices are detected; a weak one centered at (0.4 km, 0.2 km) and a stronger one at (0.18 km, 0.75 km). The weak vortex starts to merge with the main vortex at 503 s (panel b). This merging is completed at

507 s while the second stronger vortex has rotated from the northwest to the west of the main vortex (panel c). Merging of the second vortex takes place at 513 s (panel d). The process continues at 522 s (panel e) and is completed at 533 s (panel f). The merged main vortex shows a spiral band structure around its center, reminiscent of the case of a hurricane.

In passing, we mention that there are many studies in the last 20 years on vortex-vortex interactions. A review of different types of vortex interactions in rotating fluids, including merger processes, is presented in Hopfinger and van Heijst (1993). Most of the laboratory experiments have concentrated on flow regimes characterized by small Rossby numbers, where the results can be interpreted using quasi-geostrophic theories. On the theoretical side, studies of vortex interactions are focussed on pure two dimensional flows. These laboratory and theoretical studies have revealed that the merger of two identical like-signed vortices occur usually in a time scale that is smaller than the individual vortex turnover time. In contrast, the time scale of merger in our simulation is around 20 s and the eddy turnover time of the TLV is 1 s. So our merger time scale is much longer than the orbital time scale of the simulated vortex. It is also worth mentioning that in our simulation, the flow is characterized by a Rossby number of the order 30 computed as follows. The Rossby number can be defined as the ratio between the vorticity of the TLV and the background vorticity. From the simulation, the vertical vorticity of the TLV is on the order of ζ =1 s^{-1}. The background vorticity can be estimated from the average radius and tangential velocity of the mesocyclone with R=2000 m and V=30 m s^{-1}. Assuming solid body rotation, the background vorticity is calculated as $f = 2\ V\ R^{-1} = 0.03\ s^{-1}$, thus the equivalent Rossby number $\zeta\ f^{-1} \approx 30$. This flow regime is completely different from the ones described in the experiments cited in Hopfinger and van Heijst (1993) with small Rossby numbers and their conceptual results therefore cannot be extrapolated to the present case.

- *Structure at the Intensification Stage*

A representative picture of the TLV structure during the intensification period is depicted in Fig. 2.16 at 480 s. At this stage of the evolution the TLV is characterized by high values of vorticity and a large gradient of pressure deficit at the surface (Fig. 2.16 a). The horizontal winds at the surface are depicted in Fig. 2.16 b with an strong updraft wrapping around the TLV in the south-west corner at 150 m AGL. Fig. 2.16 a also shows the west-east vertical cross section along the line 3-4 and the south-north section along the line 1-2, which are shown respectively in panel c and panel d. From these two panels, it can be observed that there is a lack of symmetry in the vertical structure of the TLV, which is characterized by a westward tilt in the vertical vorticity field (Fig. 2.16 c). The TLV is embedded in a zone dominated by strong updraft gradient along the TLV axis suggesting that stretching is an important mechanism in the maintenance and intensification of the vortex (Fig. 2.16 e). The TLV is also characterized by a cold structure as shown in (Fig. 2.16 f).

Finally at 500 s, the TLV starts to interact with the low-level jet, whose location was already depicted in Fig. 2.14. As this jet approaches the TLV from the west (Fig. 2.17 b), a vortex associated with this high speed feature (Fig. 2.17 a at (0.18 km, 0.75 km)) begins to merge with the TLV. As a result of the interaction of the jet with the TLV, maximum winds of 103 m s^{-1} develop at the surface. During this time the weakening stage starts to set in and downdrafts start to fill the vortex in Fig. 2.17 e. Nevertheless maximum vorticity of 2.1 s^{-1} and minimum central pressure of 927 hPa are reached at 530 s with maximum surface winds of 92 m s^{-1}.

- *Weakening Stage*

At 540 s, the vortex starts to lose its identity by becoming a wider structure as indicated by the surface vertical vorticity (Fig. 2.18 a). The TLV structure is mainly characterized by strong downdrafts filling the vortex completely (Fig. 2.18 e), thus creating divergent winds at the surface (Fig. 2.18 b). Despite the presence of this strong downdraft the horizontal swirling winds remains intense (Fig. 2.18 b). The vertical structure of the vertical vorticity field, depicted in Fig. 2.18 c, d and e, is characterized by a disorganized feature with a closed vertical circulation.

This TLV, according to the Eqn. 2.5 given by Feuerstein et al. (2005) relates the Fujita scale (F) to the maximum wind speed (v in m s^{-1}), which would be classified as an F4 tornado at 507 s.

$$v(F) = 6.30(F+2)^{3/2} \tag{2.5}$$

2.3.2.3 Other weak tornadoes

During the weakening stage of the F4 vortex, some other vortices continued to be generated but none of them developed as strongly. We will describe one of these vortices: a cyclonic vortex of a cyclonic-anticyclonic pair located at (x,y)=(81 km, 110.7 km) at 530 s in Fig. 2.8 b.

This vortex pair (Fig. 2.19 a) is located about 2 km east of the F4 TLV at 550 s and developed along the vorticity line mentioned previously. The vertical section of the minimum pressure deficit associated with the cyclonic vortex (Fig. 2.19 b) indicates no interaction with any mesocyclonic circulation aloft. A time series of the maximum surface winds, vertical vorticity and minimum central pressure at the surface (Fig. 2.20) for only the cyclonic vortex indicated that the surface winds peaked at 42 m s^{-1} at 550 s, making

it an F1 tornado. The major differences during intensification between the F1 and the F4 vortices are the absence of interaction with a mesocyclonic circulation aloft and vortex merging in the former case. For the anticyclonic vortex of the F1 pair, a similar analysis (not shown) indicated smaller absolute values in terms of pressure deficit and vertical vorticity compared to the cyclonic one.

2.4 Summary and conclusions

An idealized F4 tornado-like vortex in a supercell storm is simulated using a three-dimensional nested grid model (MC2). The simulated supercell storm spawned one intense TLV with maximum surface winds of 103 m s^{-1} and minimum central pressure of 927 hPa.

Tornadogenesis was initiated at the surface along an outflow boundary characterized by a significant horizontal shear across and strong temperature gradient separating two different air masses. One air mass originated from cooling of the rain shaft of the RFD while the other is the warm environmental air being ingested into the storm.

Vertical vorticity maxima start to develop along this line with an initial exponential growth. Horizontal shear instability seems to be the main mechanism leading to the formation of these vortices. Only one vortex among many is found to become an intense tornado (F4). Its intensification stage is marked by an interaction with the mesocyclone of the storm. As the intensifying mesocyclonic circulation starts to descend due to a Dynamic Pipe Effect and intense stretching, near surface induced cyclonic wind circulation starts to strengthen creating a spiraling inward motion. Thus the newly developed vortices begin to orbit around the TLV and merge with it. At the end of

the intensifying stage, the maximum value of the horizontal wind reaches 103 m s^{-1}. The onset of the weakening stage is characterized by the presence of strong downdrafts through the TLV center. At the beginning of this phase, the maximum (minimum) in surface vorticity (surface central pressure) is reached and the maximum surface wind is 93 m s^{-1}. As the downdraft over the tornado reaches the ground, a divergence flow is created and the TLV decays.

Other weaker vortices developed in areas of high horizontal wind shear near the hook region. In one of them the swirling winds at the surface reached a maximum of 42 m s^{-1} and the minimum central pressure was 987 hPa. However in this case, the weaker vortices did not interact with the mesocyclone nor merged with other surface vortices during their lifetime.

Although the present idealized simulation produced a realistic tornadic supercell with all the features consistent with the Lemon and Doswell conceptual model, other physical processes including ice microphysics (ice, snow, graupel, and hail) and a more realistic representation of the boundary layer with a proper parameterization of subgrid processes should be investigated. In particular, we acknowledge that the neglect of atmospheric boundary layer (ABL) processes in the current simulation may underestimate the interaction of the TLV with the surface. On the other hand, an accurate representation of the ABL in high-resolution simulations remains challenging. There is likely to be a double counting of parameterized ABL processes with the explicitly resolved eddy transports in small grid sizes. For this reason we neglected the ABL processes in all current simulations. A sensitivity run including the ABL processes was performed. However, the simulated storm failed to develop a TLV in that experiment (not shown).

Nevertheless the use of a three dimensional model with a warm rain microphysics has served well as a first step in identifying the interactions among

the different components of the supercell storm system during tornadogenesis. In the second part of this series (Santos et al., 2008b), a vorticity budget analysis during tornadogenesis and sensitivity experiments on varying the initial conditions and adding ice microphysics will be presented. The sensitivity analysis will focus on the impact of varying the low level shear and midlevel humidity.

Acknowledgements

This research reported here is sponsored by the Canadian Foundation for Climate and Atmospheric Sciences (CFCAS). We would like to thank all the operational staff of the Network and Communications Services (NCS) of McGill University for help in the setup and operation of the Beowulf Linux cluster used for our simulations.

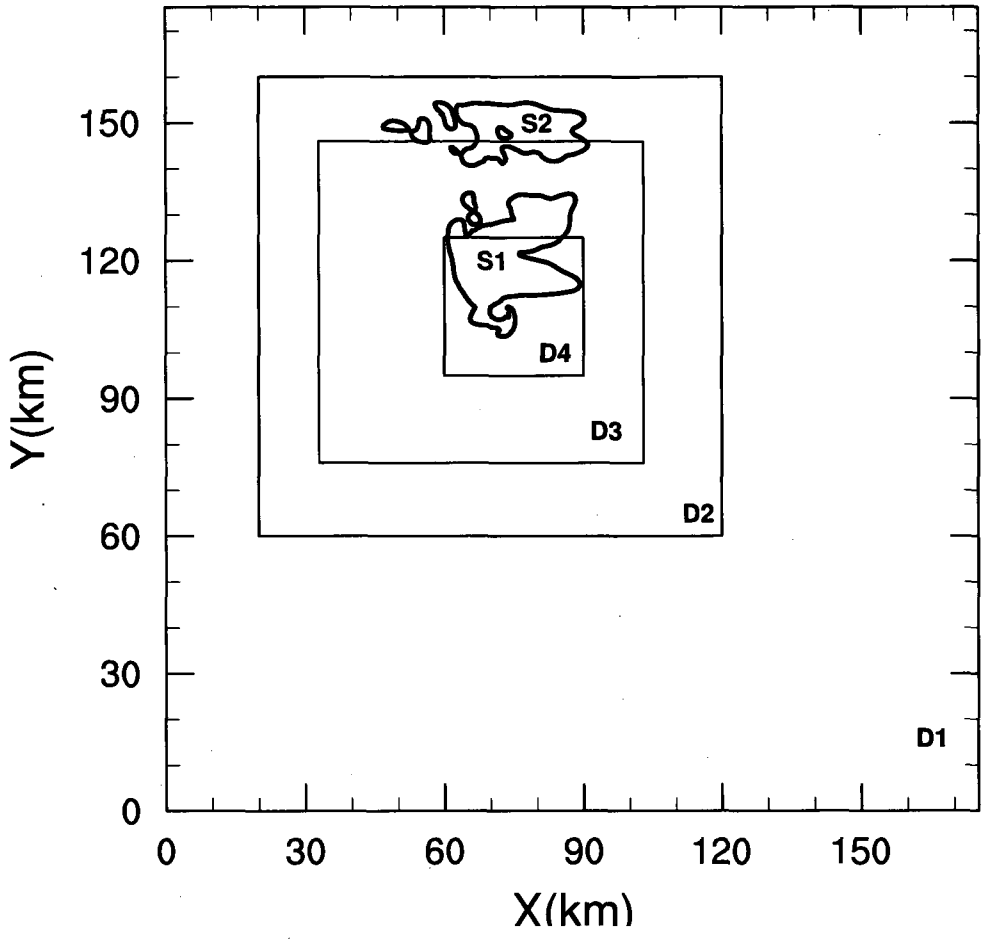

Figure 2.1: The domains of the simulation. D1, D2, D3 and D4 correspond respectively to domains with grid size of 600 m, 200 m, 70 m and 30 m respectively. S1 (S2) is the right (left) moving storm.

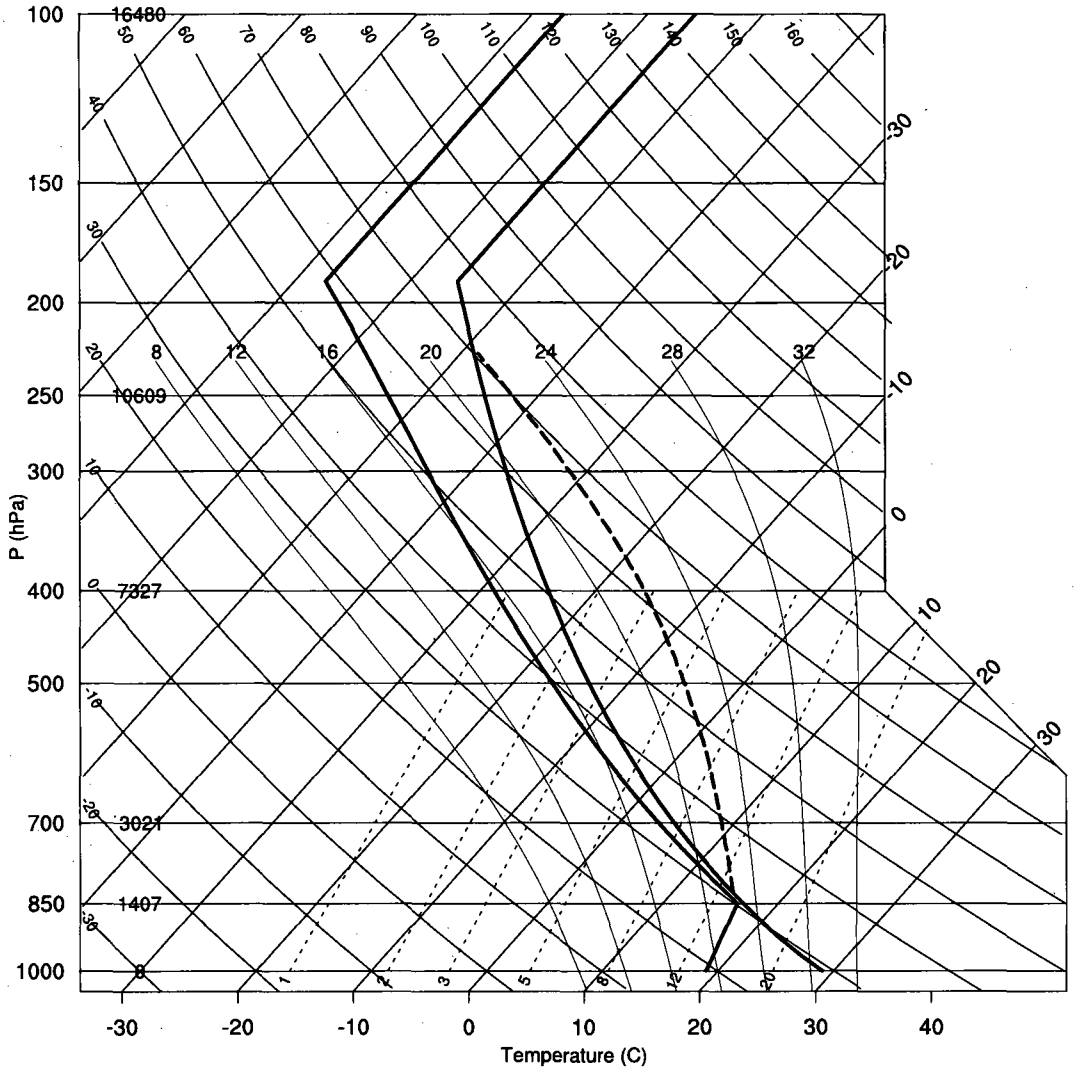

Figure 2.2: Skew-T plot of sounding used to initialize domain D1 in Fig. 2.1.

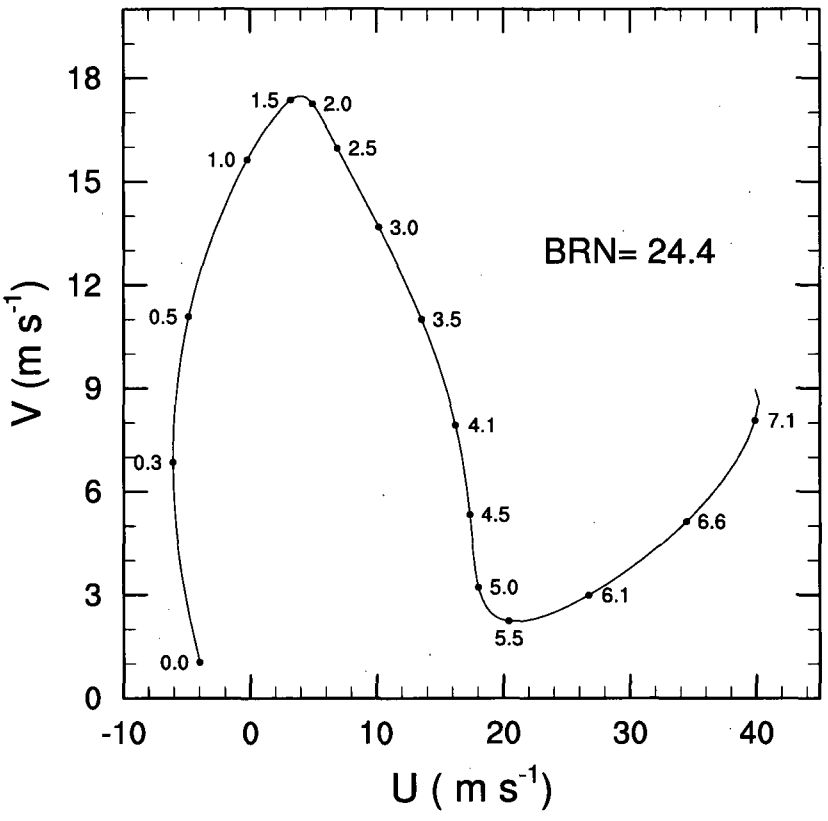

Figure 2.3: Wind hodograph used to initialize domain D1 in Fig. 2.1. The numbers on the hodograph refer to the heights in km. BRN stands for Bulk Richardson Number.

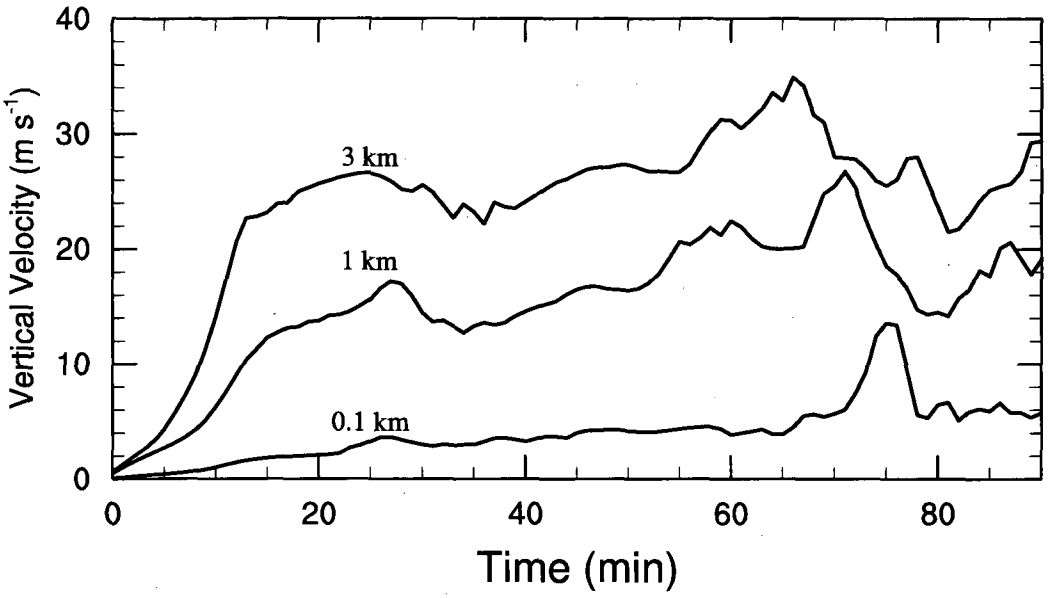

Figure 2.4: Time series of maximum vertical velocities at three heights: 3 km, 1 km and 0.1 km. The maximum value is over an area of 18 km x 18 km delineated by x = (63 km, 81 km) and y=(99 km, 117 km).

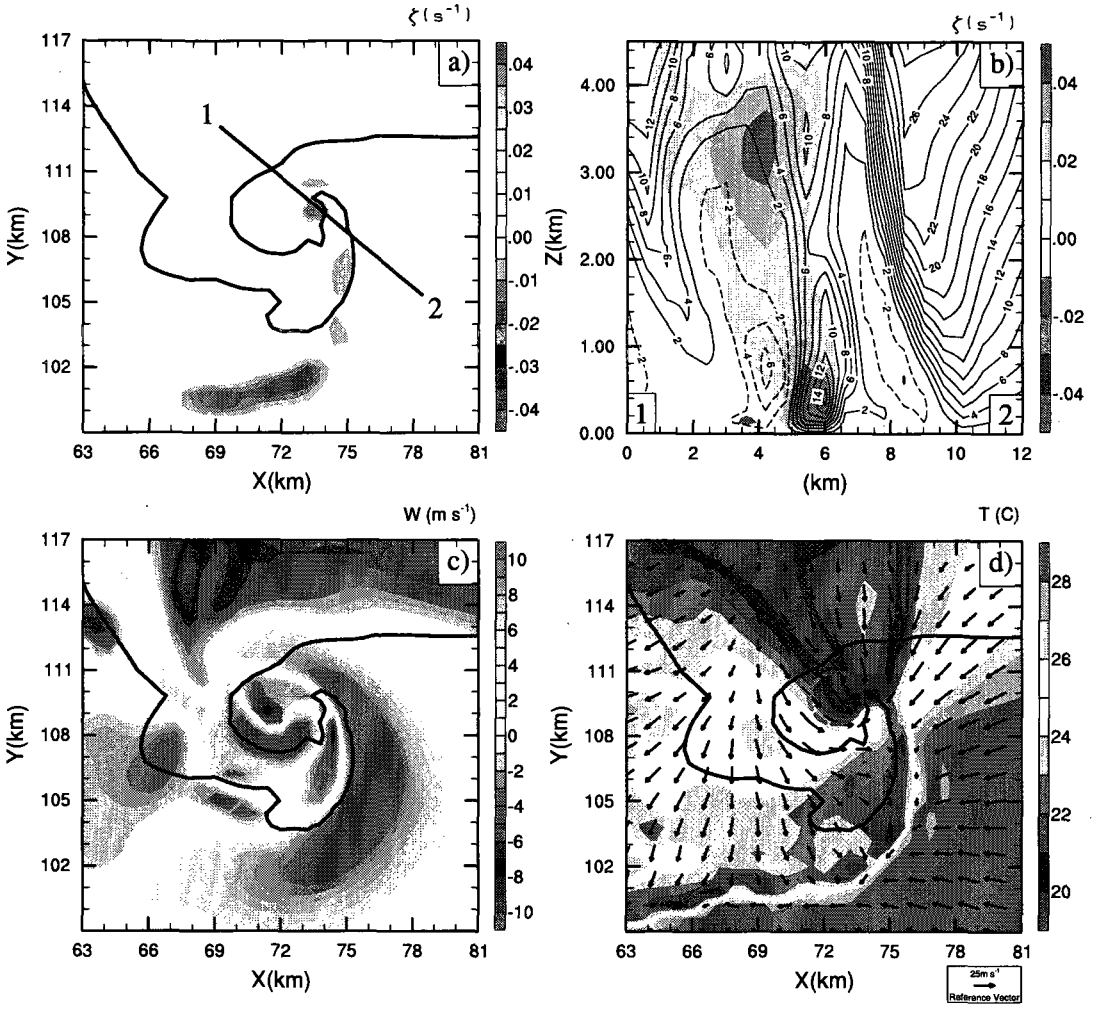

Figure 2.5: Plot of a) surface vertical vorticity, b) vertical cross section of vertical vorticity (color shaded), updraft (solid contour) and downdraft (dashed contour) with contour interval of 2 m s^{-1}, c) vertical velocity at 1 km AGL and d) surface air temperature and horizontal wind vectors. All panels are at 75 min of model integration. The surface rain water mixing ratio of 1 g kg^{-1} is denoted by the thick solid line in panels a) , c) and d).

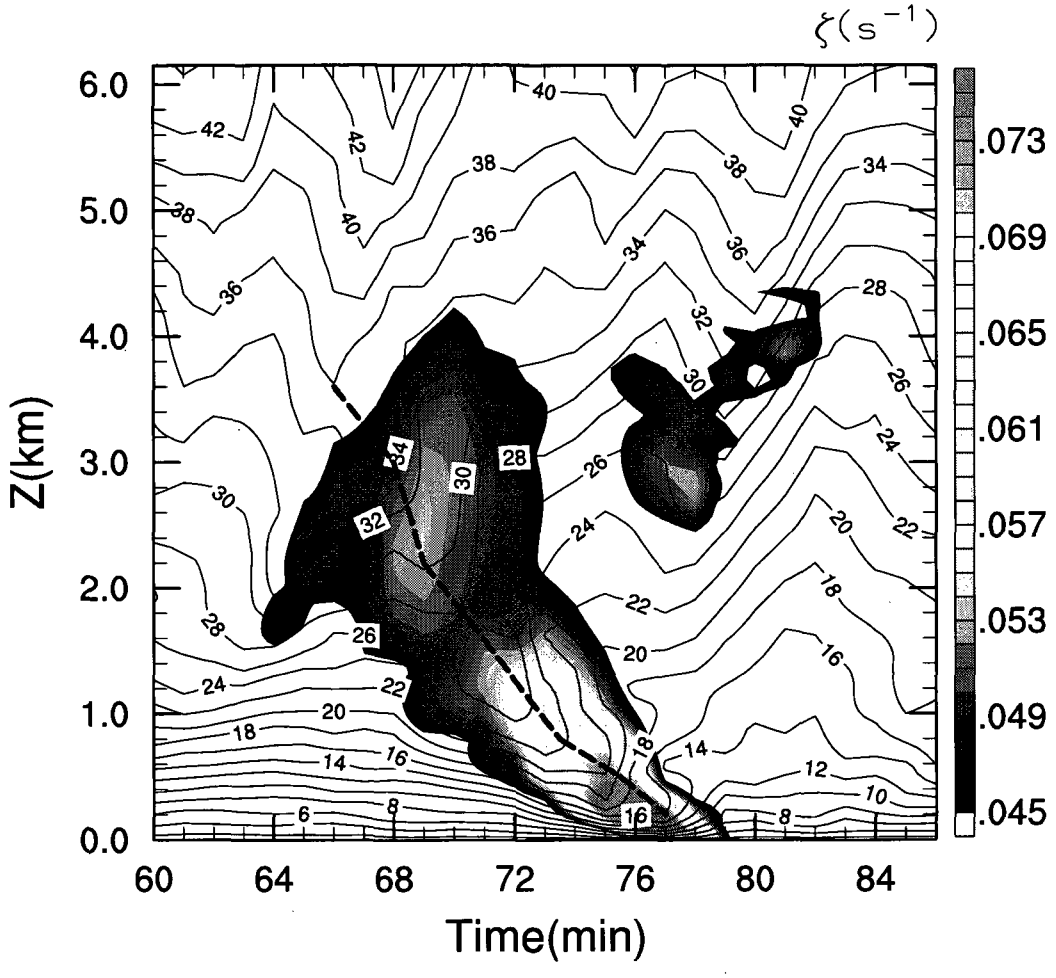

Figure 2.6: Time series of maximum vertical motion (solid lines in m s^{-1}) and maximum vertical vorticity (color shaded). The dashed line denotes the locus of the downward movement of the intensifying updraft as a function of time. The maxima are taken over the same area as in 2.5 a).

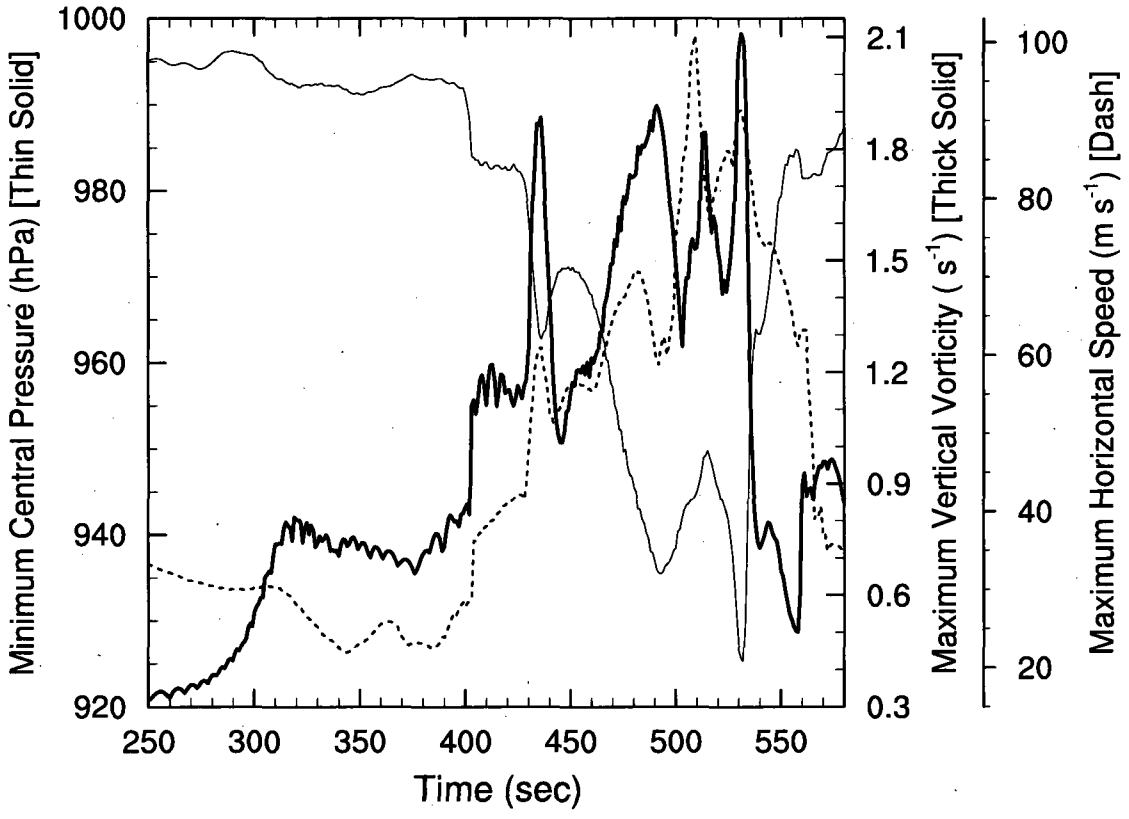

Figure 2.7: Time series of minimum central pressure (thin solid), maximum vertical vorticity (thick solid), and maximum wind speed (dashed) for the tornado-like vortex at the surface. The minimum/maximum is over a 900 m x 900 m area centered on the minimum central pressure of the vortex.

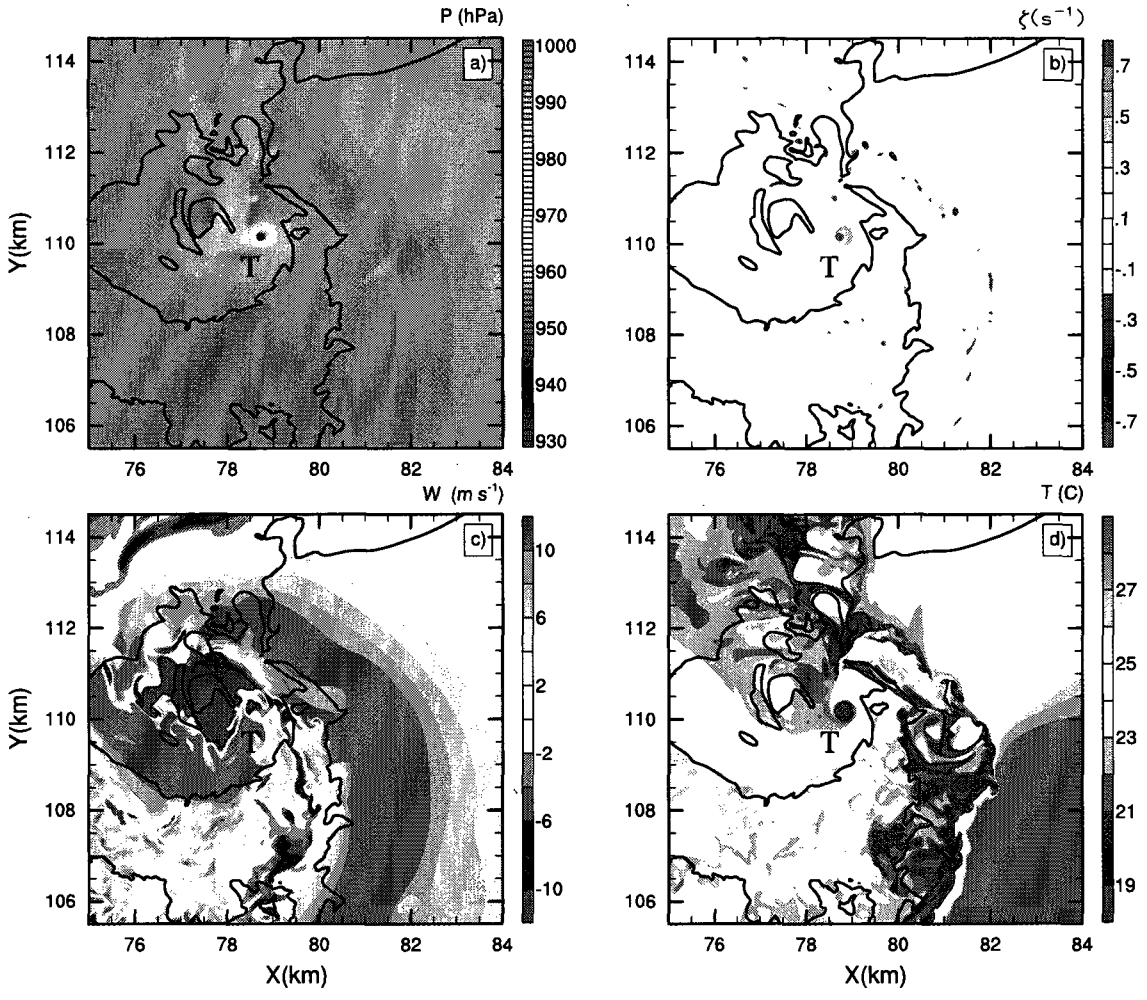

Figure 2.8: Plot of a) surface pressure, b) surface vertical vorticity, c) vertical motion at 1250 m AGL and d) surface air temperature. All panels at 530 s. The surface rain water mixing ratio of 1 g kg^{-1} is denoted by the solid line.

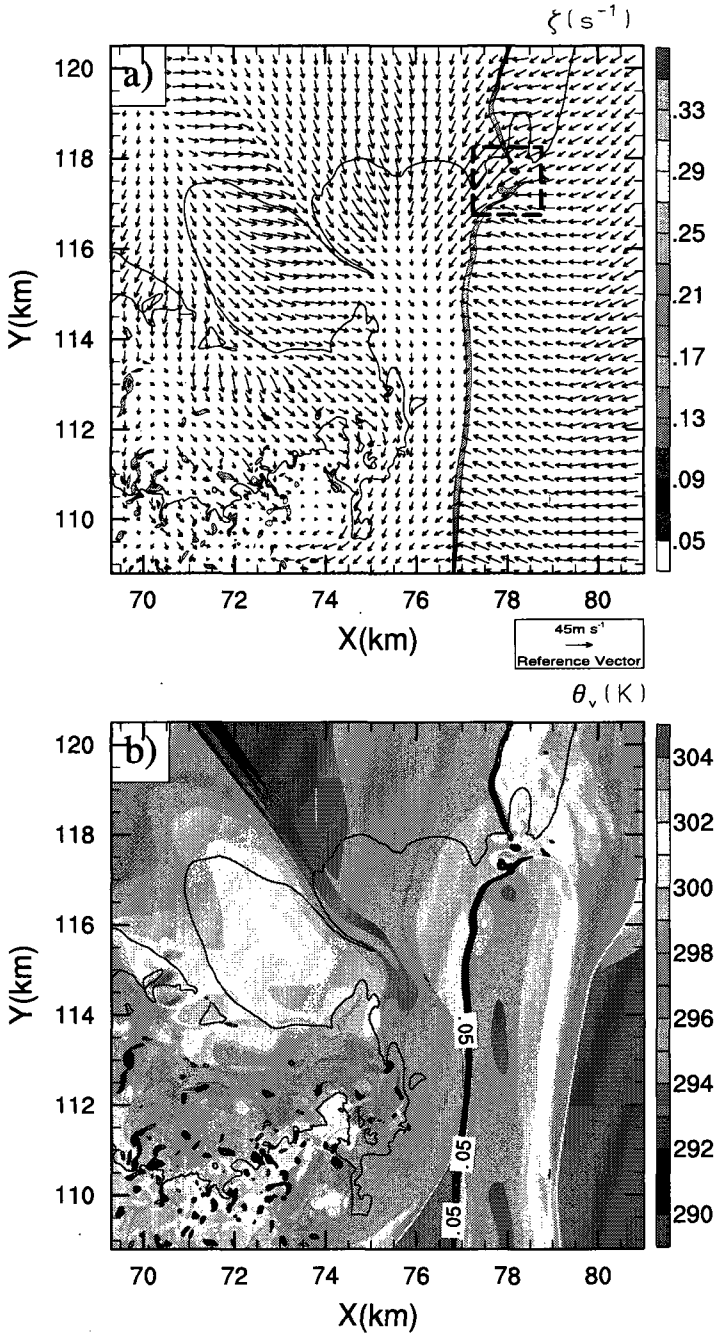

Figure 2.9: Plot of a) vertical vorticity and horizontal wind vector at the surface, b) virtual potential temperature at the surface. Surface rain mixing ratio (1 g kg^{-1} contour) in thin solid line. The thick solid line in the bottom panel represents the vorticity line with marked values in units of s^{-1}. Time is at 271 s.

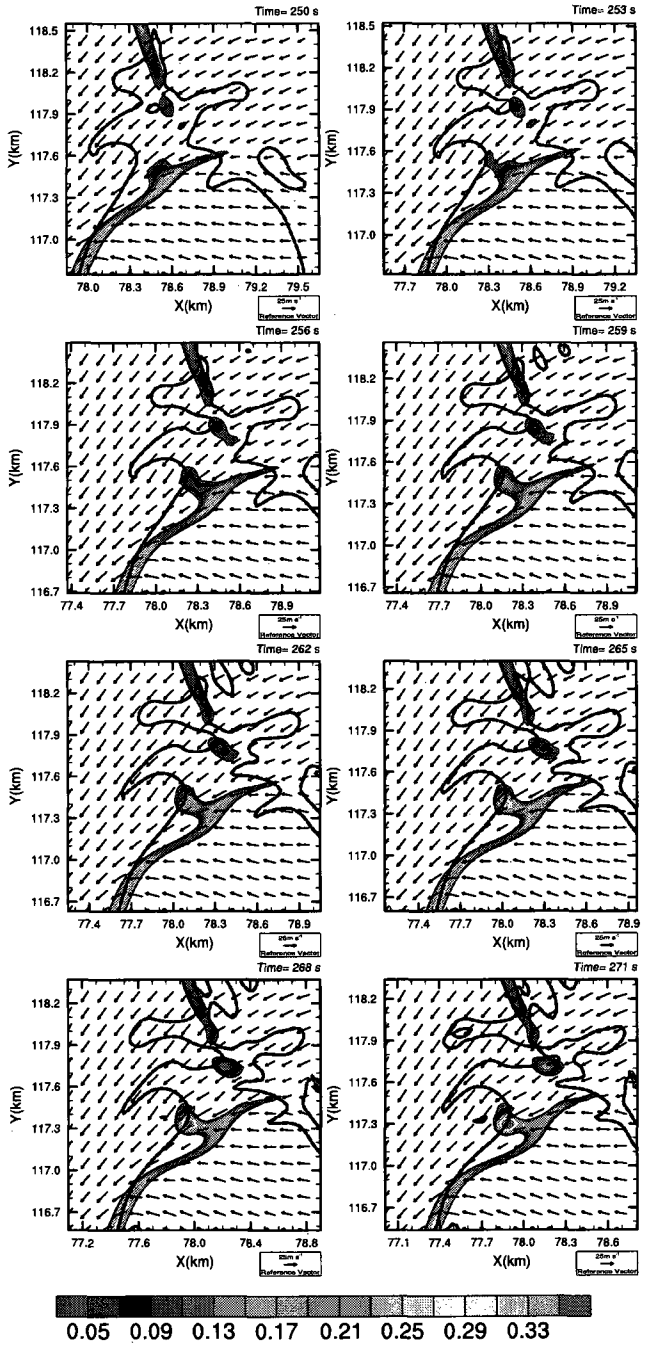

Figure 2.10: Plot of vertical vorticity at the surface (color shaded in units of s^{-1}) and horizontal wind vectors from 250 s to 271 s. The thick line denotes the contour of the -3 K perturbation potential temperature.

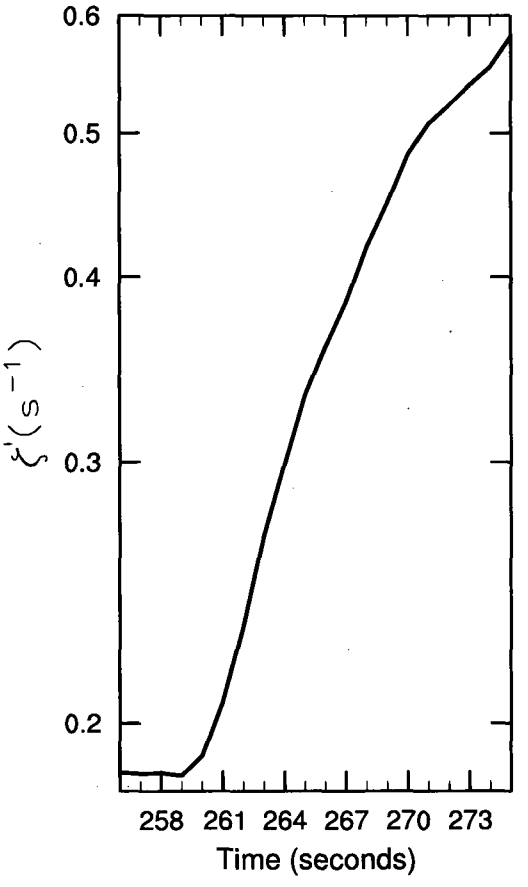

Figure 2.11: Initial growth rate of the vertical vorticity pertubation associated with the genesis of the TLV.

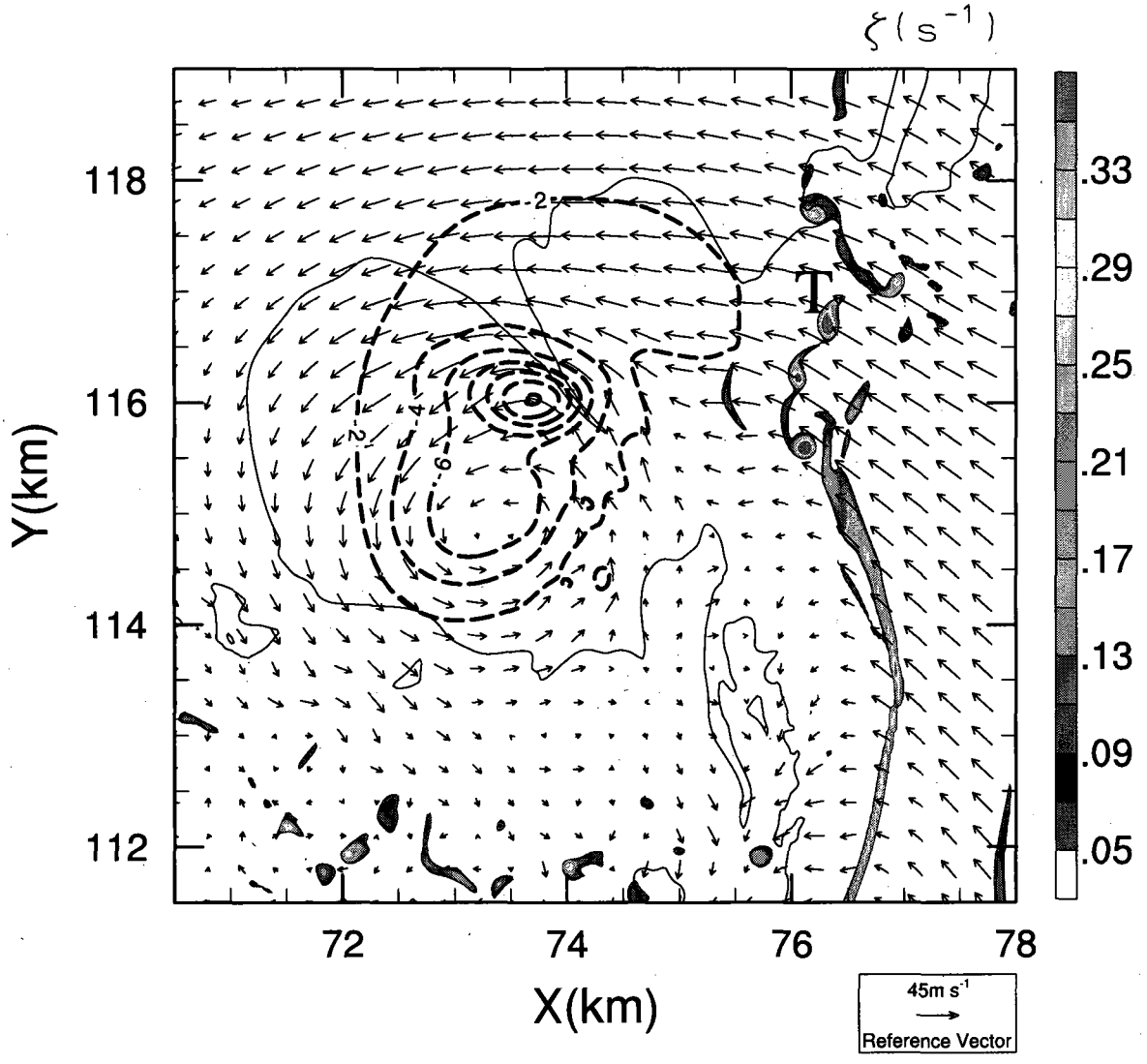

Figure 2.12: Surface vertical vorticity (color shaded), horizontal wind vectors at 1600 m AGL, and pressure perturbation (dashed) at 1600 m AGL with contour interval of -2 hPa at 337 s. The surface rain water mixing ratio of 1 g kg^{-1} is denoted by the thin solid line. Letter T shows the location of the TLV.

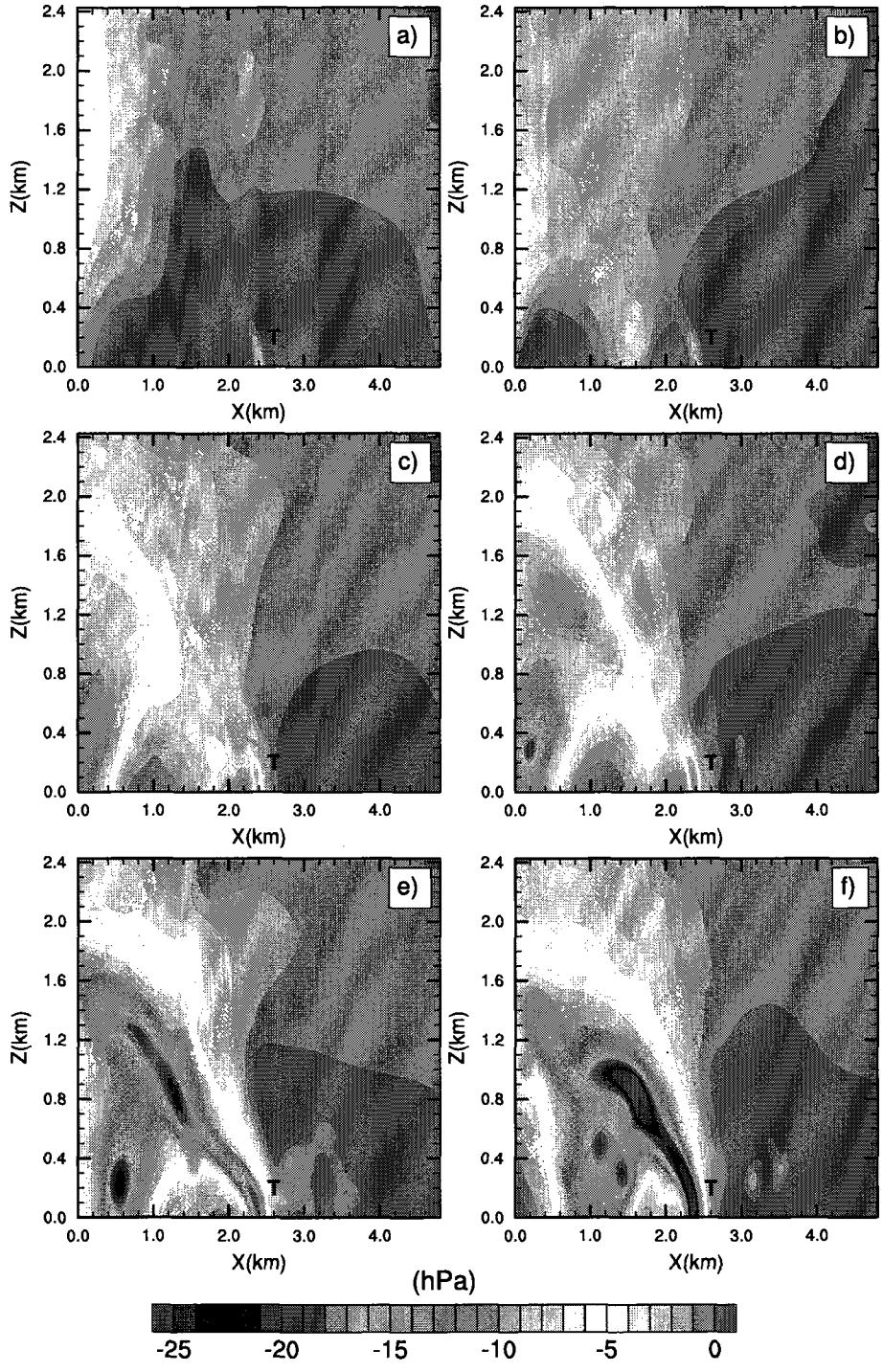

Figure 2.13: Vertical cross section of the pressure deficit at a) 340 s, b) 360 s, c) 390 s, d) 400 s, e) 430 s and f) 460 s.

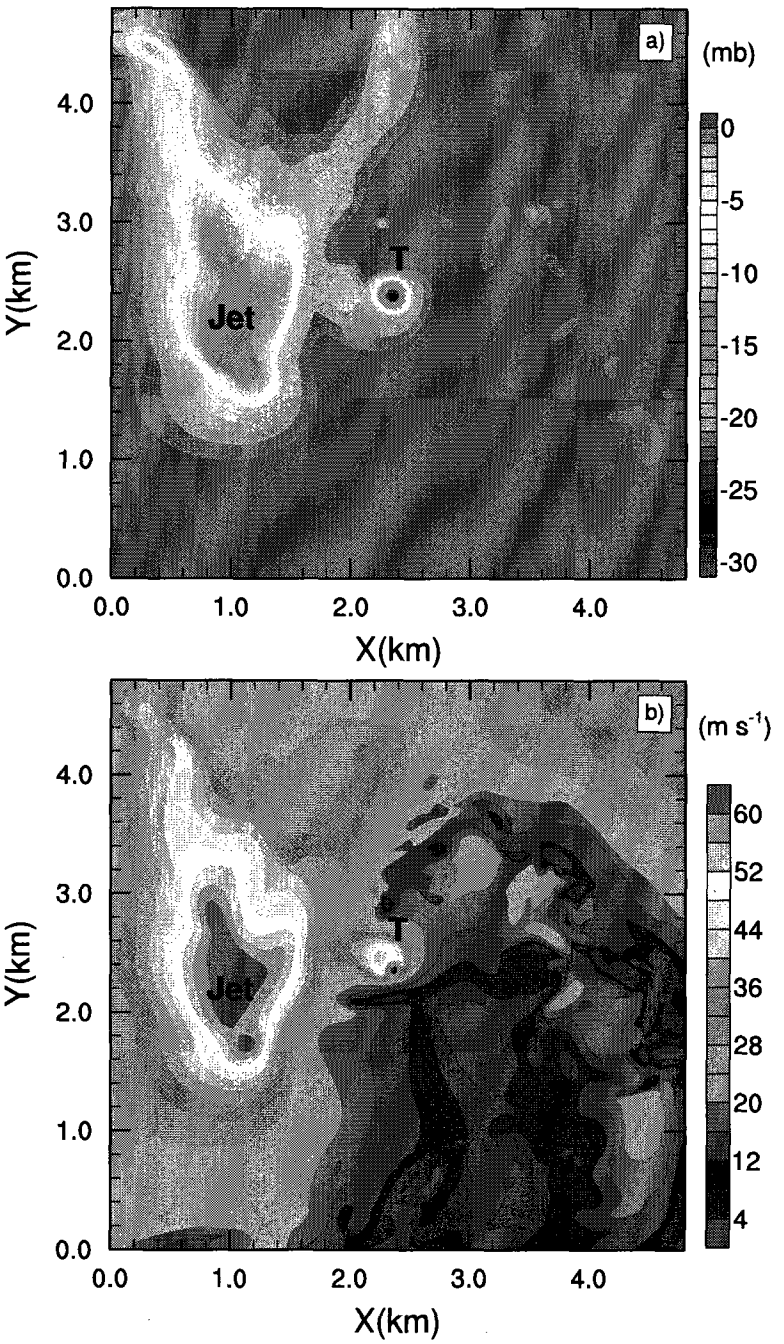

Figure 2.14: Plot of a)surface pressure deficit, and b) surface wind speed at 460 s.

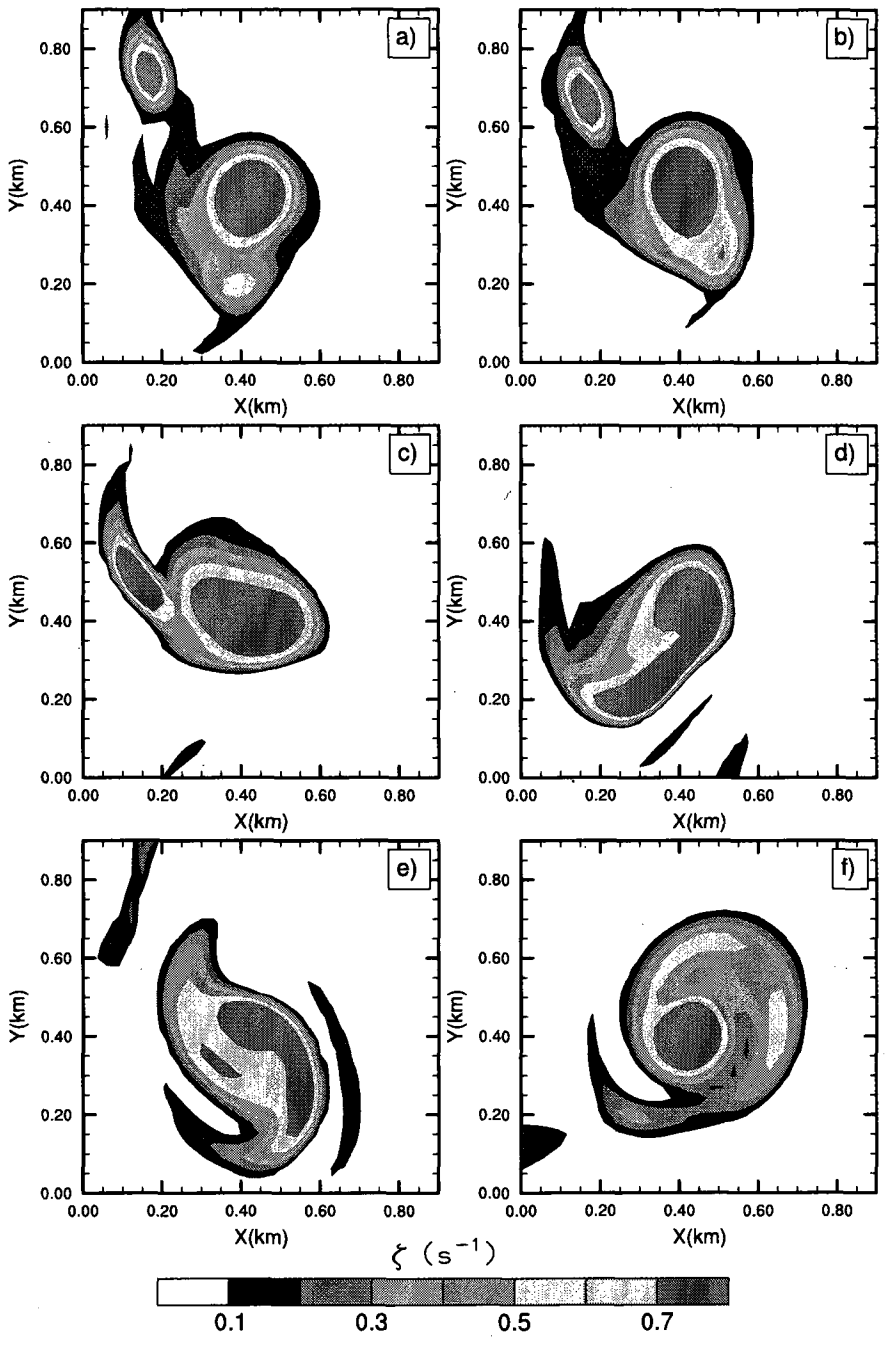

Figure 2.15: Vertical vorticity at the surface at a) 500 s, b) 503 s, c) 507 s, d) 513 s, e) 522 s, and f) 533 s.

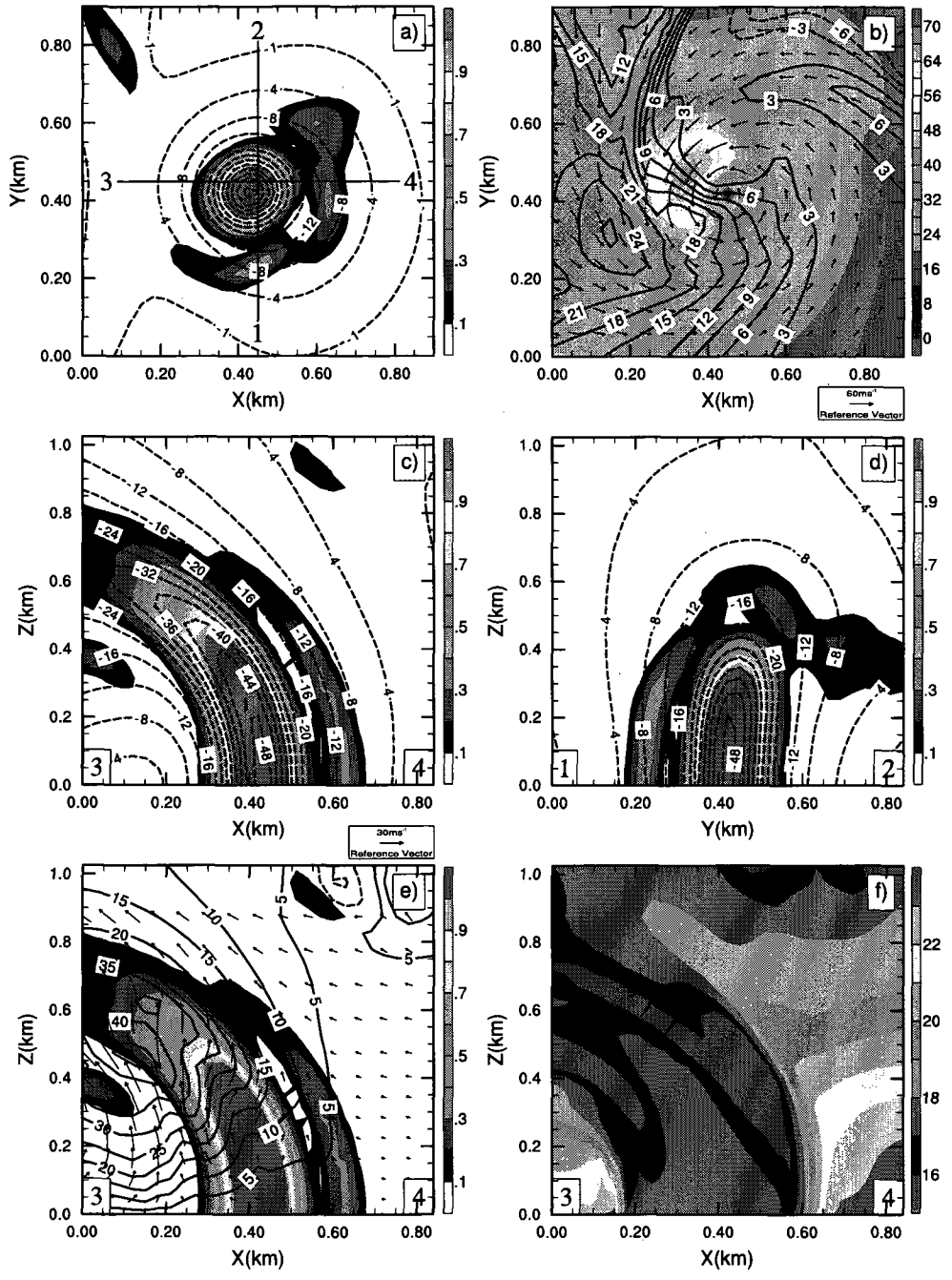

Figure 2.16: Plot of a) vertical vorticity [s^{-1}](shaded) and pressure deficit (dashed) every -4 hPa contour at the surface, b) updraft (downdraft)[m s^{-1}] in solid lines (dashed) at 150 m AGL and horizontal wind vectors at the surface. Surface speed (shaded), c) west-east cross section of vertical vorticity (shaded) and pressure deficit (dashed), and d) as in c) but for south-north cross section, e) west-east cross section of vertical vorticity (shaded), updraft (downdraft) in solid (dashed) and wind vectors, and f) west-east cross section of temperature [^oC]. All panels at 480 s.

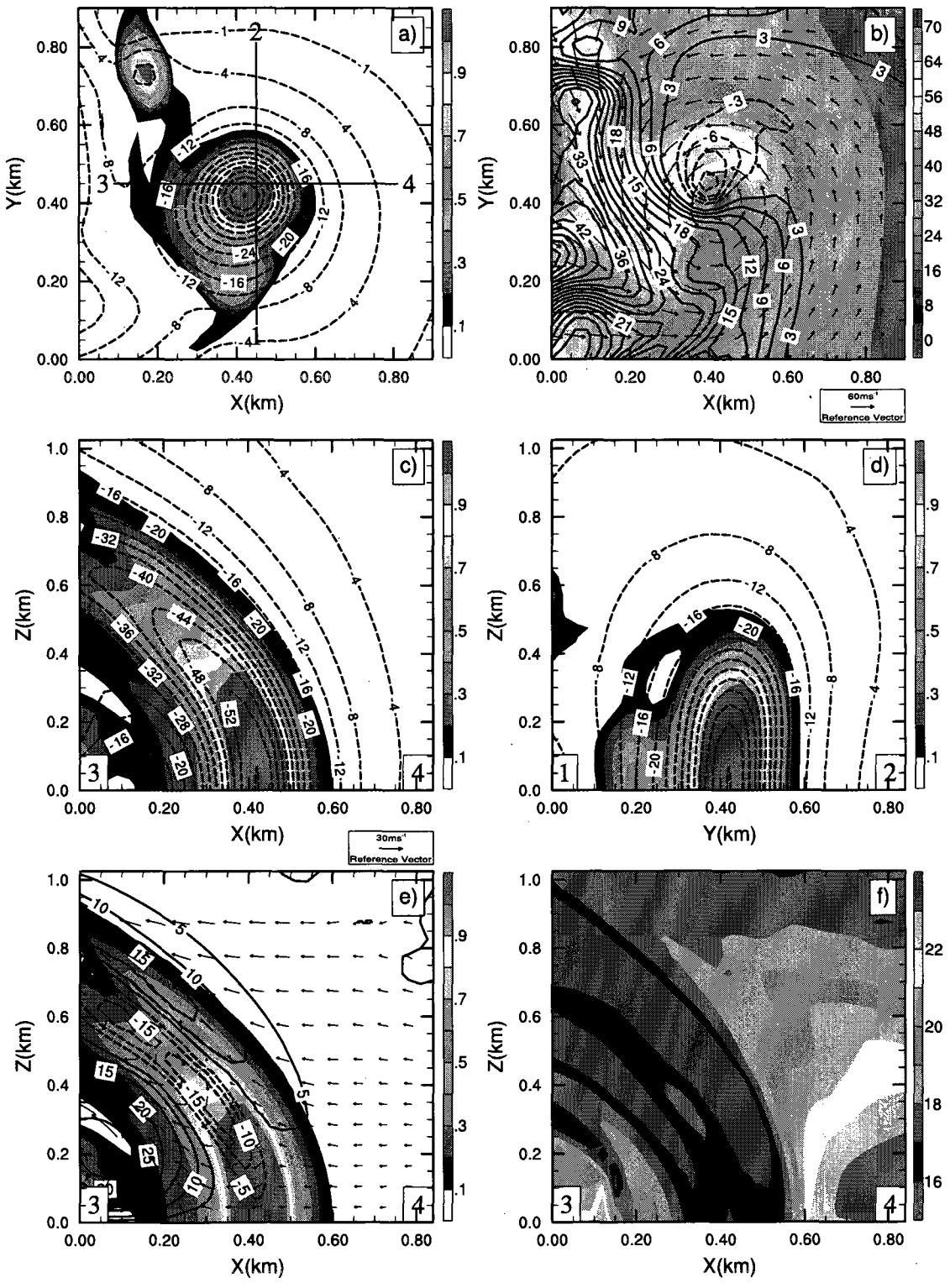

Figure 2.17: Same as 2.16 but at 500 s.

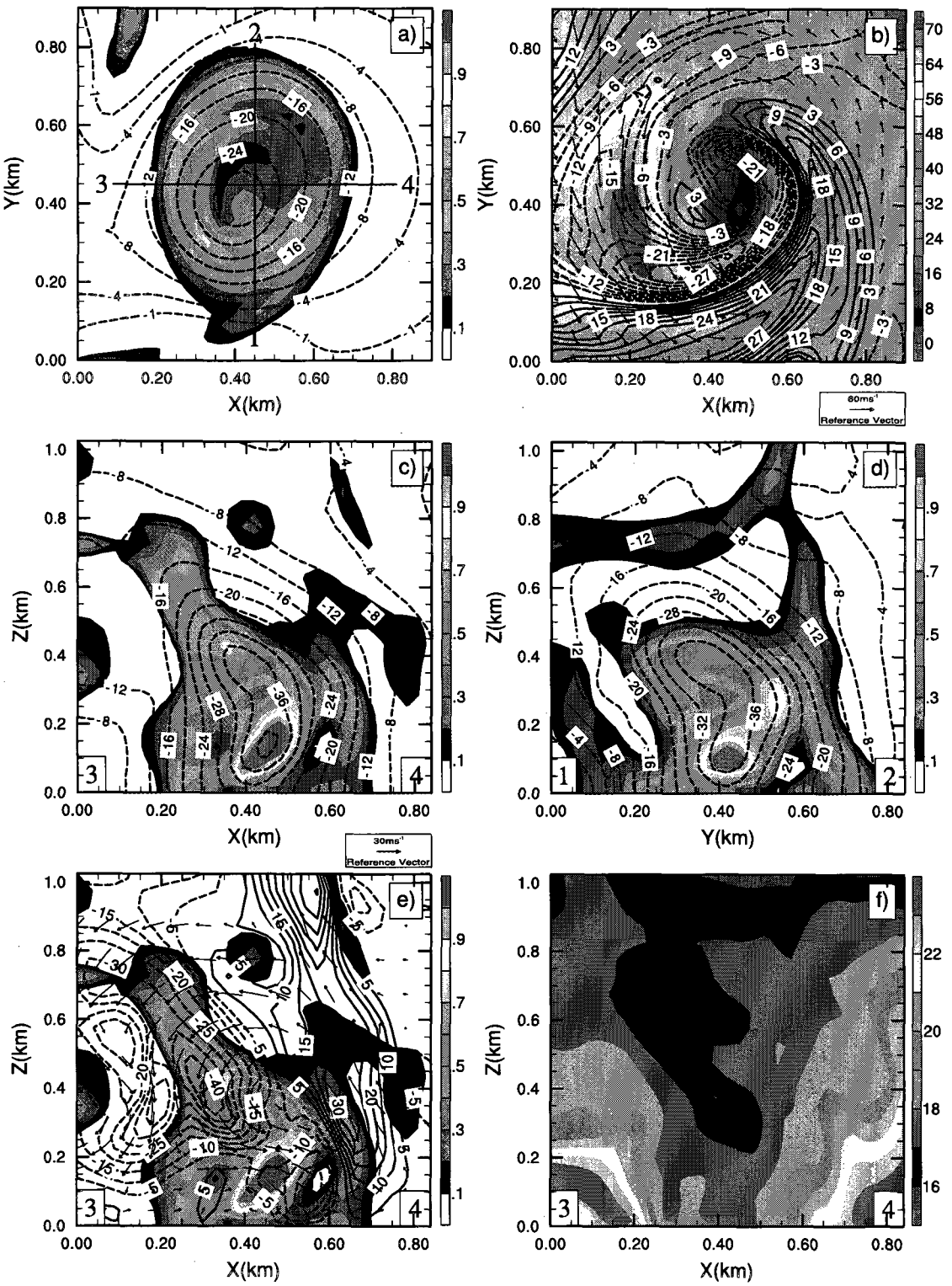

Figure 2.18: Same as 2.16 but at 540 s.

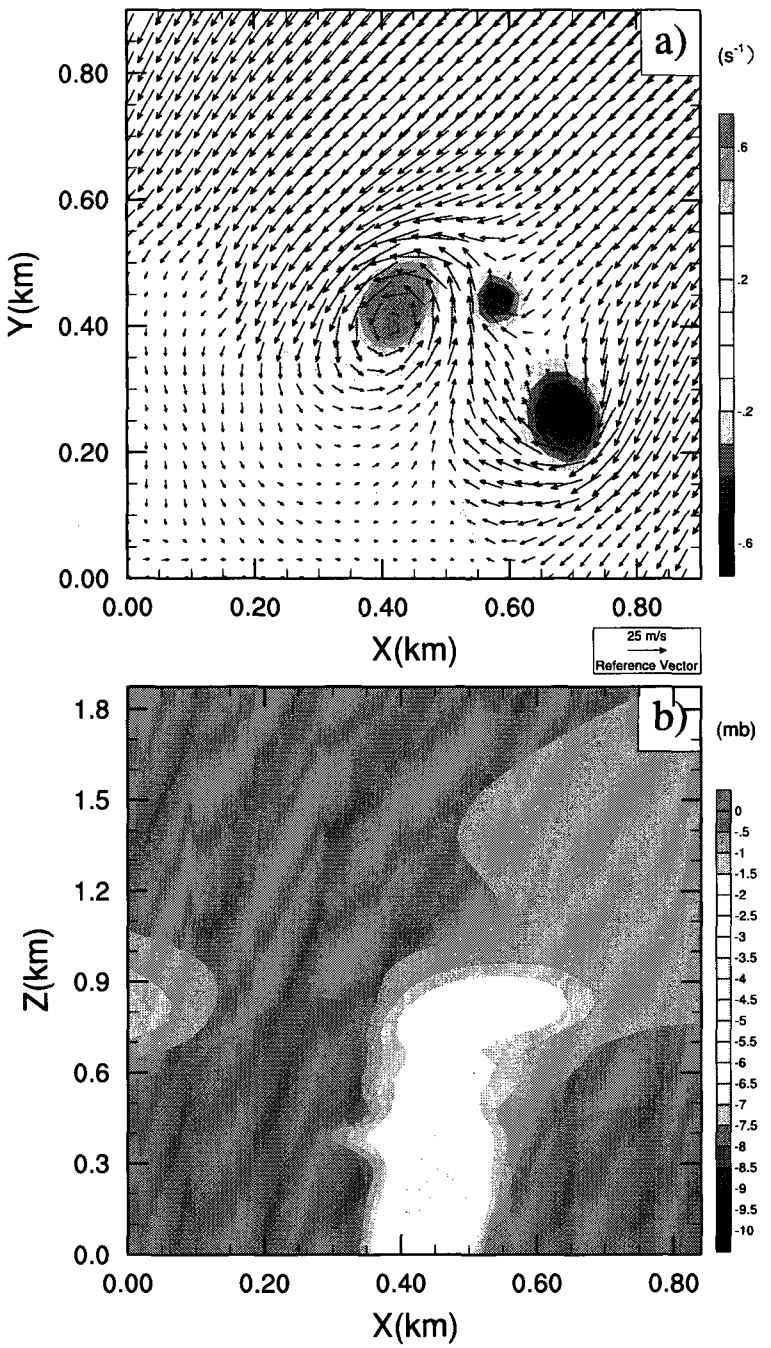

Figure 2.19: Plot of a) surface vertical vorticity (shaded) and horizontal wind vectors, and b) vertical section of the minimum pressure deficit at 550 s.

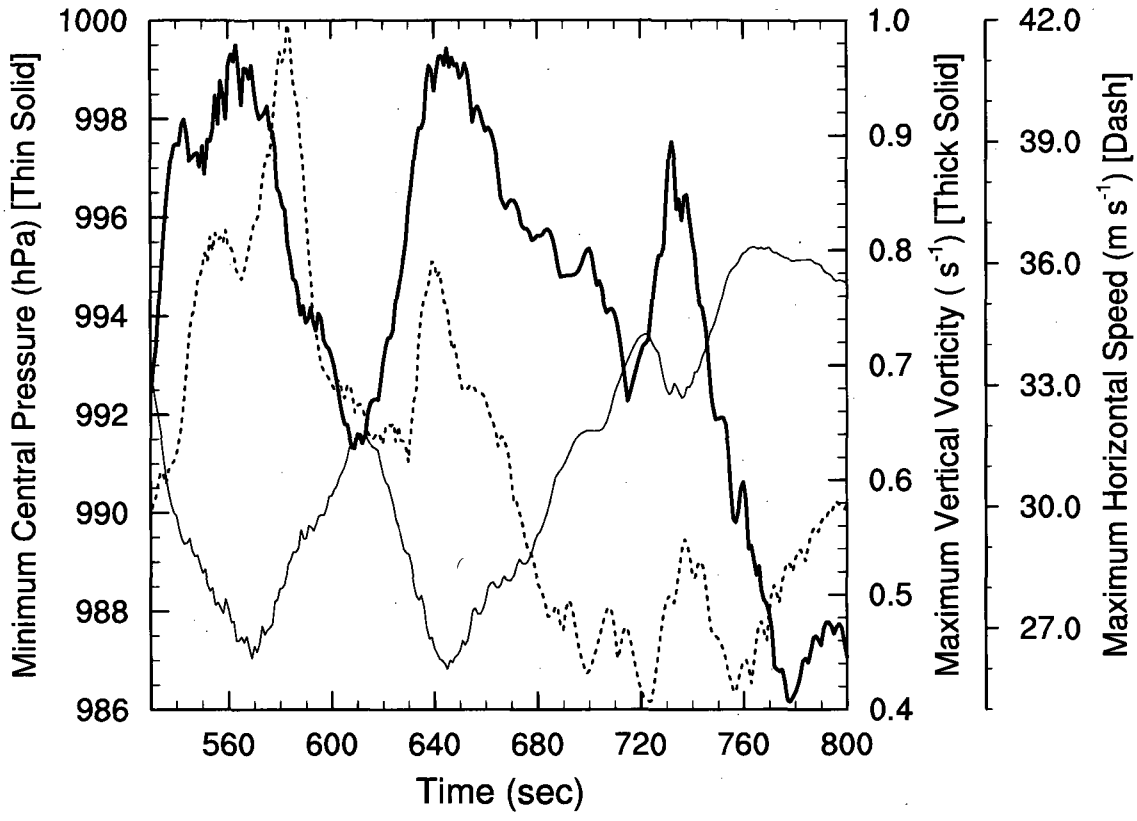

Figure 2.20: Time series of minimum central pressure (thin solid), maximum vertical vorticity (thick solid) and maximum wind speed (dashed) at the surface for the weak vortex.

Horiz. Resol. (meters)	Model Initiation Time (minutes)	Update frequency of Lateral Boundaries (seconds)	Number Grid Points X x Y x Z
600 m	0	Constant in Time	300 x 300 x 100
200 m	60	15	500 x 500 x 100
70 m	64	15	1000 x 1000 x 100
30 m	66	5	1000 x 1000 x 100

Table 2.1: Nesting Domains.

Chapter 3

Origin of Rotation and Sensitivity Analysis in a Tornadic Supercell

The lack of a thorough understanding on storm-environment and storm-tornado interactions precludes the definition of sufficient conditions for tornadogenesis. In this chapter, a multi-scale numerical simulation of a supercell storm spawning a tornado-like vortex is analyzed through computation of the storm scale and tornado scale vorticity budgets, force balance of the mean tangential wind and sensitivity experiments. The results shed light on the mechanism that favor tornadogenesis.

Simulation of a tornado-like vortex in a supercell storm, Part II: Vorticity budget and sensitivity experiments.

Jorge Ruben Santos

M. K. Yau

Badrinath Nagarajan

Department of Atmospheric & Oceanic Sciences, McGill University,

Montreal, Canada

ABSTRACT

Santos et al. (2008a) reported on a qualitative description of a multi-grid simulation of a supercell storm spawning a tornado-like vortex (TLV). In this second paper of the series, results of a quantitative analysis of the vorticity budgets during tornadogenesis, the evolution of the force balance for the mean flow of the TLV, as well as sensitivity experiments on varying the initial conditions and the parameterization of the microphysical processes are presented.

The vorticity budgets cover both the storm scale and the TLV scale. For the storm scale, the major mechanisms for producing midlevel rotation are tilting and stretching. The mesocyclone intensifies and descends and becomes vertically aligned with the maximum vorticity center near the surface. For the tornado scale, the major terms in the vorticity budget are stretching and advection. The flow is subcyclostrophic during the development of the TLV but a state of quasi-cyclostrophic balance appears when the TLV reaches its

maximum intensity. The results of the sensitivity experiments indicate that an environment with a larger storm relative helicity produces a stronger mesocyclone and a stronger downdraft. In turn, stronger horizontal convergence and horizontal shear appear near the surface to favor tornadogenesis. A drier environment above the cloud base eventually produced a weaker storm while the inclusion of ice phase processes generates more vigorous updrafts and downdrafts, stronger surface horizontal convergence and horizontal shear to favor tornadogenesis.

3.1 Introduction

Atmospheric conditions that affect the formation of supercell storms have been well studied (Browning, 1986; Klemp and Wilhelmson, 1978; Klemp et al., 1981; Weisman and Klemp, 1982, 1984). Moderate to strong thermodynamic instability (Convective Available Potential Energy CAPE $>$ 2000 J Kg^{-1}), together with a vertical distribution of the environmental wind such that the Bulk Richardson Number is less than 35, are necessary conditions for quasi-steady organized convection such as supercell storms (Weisman and Klemp, 1982). The supercells are generally associated with strong midlevel rotation (mesocyclones) and the strength of which is well predicted by Storm Relative Helicity (SRH) (Droegemeier et al., 1993). Although sometimes tornadoes are spawned by these convective systems, the presence of rotation alone is not a sufficient condition for a supercell storm to become tornadic. It is known that only between 30 to 50 percent of the mesocyclones are associated with tornadic events (Burgess et al., 1993). Dupilka and Reuter (2006a,b) studied the environmental parameters from an observational dataset containing tornadic and non-tornadic storms over Alberta, Canada. They found that significant tornadoes were associated with environments characterized by stronger shear than those in weak or non-tornadic events. High values of storm relative helicity were also correlated with the occurrence of significant tornadoes. Nevertheless, no sufficient conditions have been found for a rotating supercell to produce a tornado.

In a supercell storm, vortices of different scales can sometimes be found. Their diameters range from 3-10km for the midlevel mesocyclones to an average size 100-300 meters for tornadoes. The understanding of the interaction between the vortices of different scales seems to be a crucial first step to disentangle the complex conditions for tornadogenesis.

Although recent observational studies (Bluestein et al., 2003a, 2007, 2003b; Markowski et al., 2002b) using mobile Doppler radars are starting to shed some light on the structure of tornadoes, as well as the kinematics and thermodynamics characteristics of the storm environment, the temporal and spatial resolutions of the measurements are still too coarse to depict the complete life cycle of tornadoes and their interaction with the parent system. As a result, the use of high-resolution numerical models has become an extremely useful tool as an alternate avenue of attack.

Three-dimensional simulations of tornadic supercell storms containing tornado-like vortex (TLV) have been performed by Grasso and Cotton (1995); Wicker and Wilhelmson (1995), where TLVs with tangential velocities of 50 m s^{-1} and updrafts over 50 m s^{-1} were generated. However the resolutions in these simulations are still insufficient to address the problem of vortex interactions. To fill this gap, Santos et al. (2008a) simulated an idealized F4 tornado-like vortex in a supercell storm using a numerical model with warm rain microphysics and four nesting domains having horizontal resolutions of 600 m, 200 m, 70 m, and 30 m respectively. Their simulated supercell spawned an intense TLV with maximum surface winds of 103 m s^{-1} and minimum central pressure of 927 hPa. They found that tornadogenesis was initiated at the surface along an outflow boundary characterized by significant horizontal shear and strong temperature gradients separating two different air masses. Horizontal shear instability leads to the formation of small vortices near the surface along the vortex sheet. Only one vortex among many became tornadic and its intensification stage was marked by an interaction with the mesocyclone of the storm. As the intensifying mesocyclonic circulation start to descend due to a Dynamic Pipe Effect and intense vortex stretching, near surface induced cyclonic wind circulation starts to strengthen creating a spiraling inward motion. Thus the newly developed vortices begin to orbit around the TLV and merge with it. At the end of the intensifying stage,

the maximum value of the horizontal wind reaches 103 m s^{-1}. Other weaker vortices also developed in areas of high horizontal wind shear near the hook region. However in this case, the weaker vortices did not interact with the mesocyclone nor merged with other surface vortices during their lifetime.

The work of Santos et al. (2008a) represents a qualitative description of the results of the simulations. In this second paper, we will present a quantitative analysis of the vorticity budget during tornadogenesis and the evolution of the force balance for the mean flow of the TLV. Sensitivity experiments on varying the initial conditions and the parameterization of the microphysical processes will also be performed. Specifically, the objective of this paper is three-fold:

1. To compute the vorticity budgets on the storm scale and on the tornado scale to determine the mechanism for the origin and intensification of rotation.

2. To compute the evolution of the azimuthally averaged mean winds of the TLV and its balance of forces.

3. To perform sensitivity experiments on

    - Changes in the low level ambient vertical shear of the horizontal winds.
    - Modification of the upper- and middle-tropospheric humidity.
    - Inclusion of ice phase microphysics.

This paper is organized as follows. Section 2 summaries the modeling methodology. In section 3 the vorticity budgets are presented. Section 4 contains the results of the different sensitivity experiments. Section 5 is the summary and conclusions.

3.2 Modeling strategy

The model and experimental setup for the control simulation, with 4 nesting grids at resolutions of 600 m, 200 m, 70 m, and 30 m respectively, are described in Santos et al. (2008a). To summarize, the idealized numerical simulation is performed using a three-dimensional fully Compressible Community Model (MC2) (Benoit et al., 1997). Convection is initiated by specifying an ellipsoidal thermal bubble with a temperature perturbation of 4 K with a horizontal (vertical) radius of 10 km (1.5 km). The bubble is centered at 1.5 km above the surface and situated at the center of domain. The initial conditions are horizontally homogeneous as depicted in the thermodynamic and horizontal wind profiles in Fig. 3.1 a and Fig. 3.2 a.

The vorticity budgets will be computed for both the 600 m and 30 m model output. The mean winds and force balances for the TLV would be calculated from the 30 m simulation data. Five sensitivity experiments, as listed in Table 3.1, are performed with a resolution of 600 m. Experiment CH is the same as the 600 m run in the control simulation described in Santos et al. (2008a). Its initial conditions are given by the sounding and hodograph depicted respectively in Fig. 3.1 a and Fig. 3.2 a. Experiments LH and SH explore the effect of varying the vertical distribution of the environmental wind below 4 km and their hodographs are given respectively in Fig. 3.2 b and c. The storm relative helicity (SRH) for experiments CH, LH, and SH are compared in Fig. 3.2 d. Here SRH is defined in eqn. 3.1 as

$$H(z) = -\int_0^z \hat{\mathbf{k}} \cdot \left(\vec{\mathbf{V}} - \vec{\mathbf{C}}\right) \times \frac{\partial \vec{\mathbf{V}}}{\partial \mathbf{z}} \mathbf{dz}, \tag{3.1}$$

where $\vec{C}$ is the velocity of the storm motion, $\vec{V}$ is the horizontal wind vector, and z is the vertical height.

The designation CH, LH, and SH can therefore be interpreted as Control Helicity, Large Helicity (or large shear below 4 km), and Small Helicity (or small shear below 4 km) respectively. Note that the shape of the hodographs remains unchanged in the three experiments, and that their Bulk Richardson number varies from 24.4 to 27.5, still within the range for quasi-steady supercells. Experiment DRY is designed to test the effect of a drier environment above 850 hPa and its sounding is given in 3.1 b. Experiment ICE includes the microphysical processes of ice/snow and graupel/hail (Kong and Yau, 1997; Misra et al., 2000).

3.3 Vorticity Budget of Tornadic Supercell Storm

Tornadic supercell storms are long-lived and well-organized convective systems with strong rotating updrafts and heavy precipitation. Santos et al. (2008a) has shown that the structures of their simulated supercell agree with the conceptual model proposed by Lemon and Doswell (1979). The interaction of the mesocyclone with surface vortices was found important for tornadogenesis. We therefore first perform a vorticity budget of the supercell with focus on the evolution of the mesocyclone.

The equation governing the evolution of the vertical component of vorticity is given by

$$\frac{\partial \zeta}{\partial t} = -\vec{V} \cdot \nabla \zeta + \vec{\omega_h} \cdot \nabla_h w - \zeta \nabla_h \cdot \vec{V_h} - \hat{k} \cdot \rho^{-2} \nabla \rho \times \nabla p, \qquad (3.2)$$

where ζ, $\vec{\omega_h}$, $\vec{V}$, w, ρ and p denote the vertical component of the vorticity, the horizontal vorticity vector, the three-dimensional wind vector ($\vec{V} = u\hat{i} + v\hat{j} + w\hat{k}$), the vertical velocity, the air density, and the pressure respectively. The term on the left is the local time tendency. The first term on the right

represents the advection of vertical vorticity, the second term the tilting of horizontal vorticity into the vertical plane, the third term the stretching or divergence effect, and the fourth term the solenoidal or baroclinic effect.

Fig. 3.3 depicts the outline of the hook echo and the vertical vorticity in a subdomain of the 600 m run. The horizontal sections at three vertical levels (200 m, 1850 m, and 3000 m) and at two times are displayed. The time 62 min lies within the genesis stage of the tornado vortex and the time 75 min is within the intensifying stage (see Santos et al. (2008a) for an explanation of the different stages). The letter M denotes the location of the vertical vorticity maximum. At 62 min, the hook echo is not well defined and the maximum vertical vorticities at different levels are not vertically aligned. The hook can be recognized quite readily at 75 min and a spiral band of vorticity around the hook becomes evident at 1.85 km and 2 km. Relative to the picture at 62 min, the vorticity near the surface at 200 m has intensified and the maximum vorticity centers are more or less aligned in the vertical.

The development of vertical vorticity in the supercell storm is illustrated by the time height series in Fig. 3.4. The maximum at each level represents the maximum value in the subdomain shown in Fig. 3.3. We focus on the vorticity budget after 20 min to avoid the problem of spin-up of the model. At about 25 min, the vorticity tendency (panel a) indicates a positive increase at around 0.6 km. The positive tendency increases with height from 25 to 40 min. Inspection of panel c and panel b shows that the positive vorticity tendency originates from the tilting term and strengthened by the stretching term. Titling and stretching continue to contribute to a positive tendency from 40 min to 55 min, especially from 2.5 km to 4 km in altitude. The contribution of tilting to vertical vorticity at midtropospheric levels in a tornadic thunderstorm is well-known as reported in (Klemp and Rotunno, 1983, 1987). Specifically, the ambient horizontal vorticity associated with the vertical shear of the environmental wind is being tilted upward by the updraft

of the storm to generate vertical vorticity. This is the first seed of midlevel rotation, or the mesocyclone in the supercell storm.

At around 60 min, the stretching term intensifies the storm's mesocyclonic circulation between 2 km and 4 km AGL (panels a and b). As discussed in Santos et al. (2008a), the mesocyclone descends and intensifies as a result of the Dynamic Pipe Effect. The three-dimensional advection (panel d) increases its influence as a result of the downward descent of the mesocyclone. The stretching term reaches its maximum value near the surface during tornadogenesis around 75 min, so is the three dimensional advection. There is also a small contribution from the tilting term at this time near the surface.

We mention that throughout the model integration, the contribution of the solenoidal term is several orders of magnitude smaller than the other terms in the vorticity Eqn. 3.2. The effect of the solenoidal term is thus negligible (not shown).

3.3.1 Vorticity Budget of Tornado-Like Vortex

Santos et al. (2008a) suggested that the initial seed of vertical vorticity for the TLV near the surface arises from horizontal shear instability. This instability is located along an outflow boundary with strong temperature and horizontal wind gradients separating two air masses. One air mass originated from the rear flank downdraft (RFD) and the other from ingestion of warm and humid air in the environment.

After the appearance of the initial seed of vorticity, the budget was calculated in a box of dimension 800 m x 800m x 600 m following the minimum central pressure of the TLV. Figure 3.5 depicts the maximum vorticity and the budget terms at five times: 300 s (genesis stage), 430 s (beginning of

intensification stage), 510 s (time when TLV achieves maximum horizontal wind speed at the surface), 530 s (time for maximum vorticity and minimum pressure at the surface), and 540 s (weakening stage). Panel a shows that at 300 s and 430 s, the maximum vertical vorticity is located near the surface. The vorticity decreases almost linearly with height till about 280 m. Above this level, the vorticity remains approximately constant to 600 m. During these stages, the TLV intensifies mainly near the ground due to stretching and vertical vorticity advection (panel c and panel e). At 510 s, there is a large vorticity increase below 500 m (panels a, b). Vorticity advection (panel e) and stretching (panel c) are the main source terms above 300 m. Below this level, stretching and tilting (panel d) are the major contributors to the positive vorticity tendency but counteracted by the negative vorticity advection (panel e) below 200 m. Note that the solenoidal term (panel f) is four orders of magnitude smaller than the rest of the tendency terms in the vorticity equation.

At 530 s, the TLV attains the maximum vorticity value of 2.1 s^{-1} at the surface (panel a). However, the weakening process is beginning to set in. Negative vorticity tendency can be detected from 200 m to 400 m AGL (panel b). The major causes of the weakening are the negative advection of vorticity and negative stretching as downdrafts start to dominate. At 540 s, the decay of the tornado scale vortex is evident at all levels particularly below 160 m (panel a).

3.3.2 The Evolution of the Mean Structure of the TLV

The mean structure of the TLV and its evolution will be investigated by an analysis of the azimuthally averaged tangential wind, radial wind, and vertical vorticity fields. The azimuthal average is centered on the minimum central

pressure of the vortex. The reason is that relative to the wind structure, the pressure pattern is more symmetric and the track of the TLV is better described by the minimum pressure. Fig. 3.6 depicts the time series of the maximum mean (azimuthally averaged) tangential wind and the radius of maximum wind (RMW) at the surface. During the genesis stage, the surface tangential wind grows quasi-linearly until about 400 s and its RMW is around 70 m. Two periods of rapid intensification followed. The first period starts around 430 s when the tangential wind increases from 22 to 44 m s^{-1} in 15 s. Another steep increase occurs from 450 s to 510 s when the mean tangential wind reaches a peak of 56 m s^{-1}. In terms of the RMW, it is of interest to note that an abrupt change in the mean tangential wind is accompanied by a contraction of the RMW, consistent with the conservation of angular momentum in an inviscid fluid. During the last period of intensification and the weakening stage, the RMW increases quite dramatically and the TLV adopts a broader structure.

It should be pointed out that the simulated tangential wind around the TLV is asymmetric. Although the mean tangential wind peaks at 56 m s^{-1}, the actual maximum wind speed has a magnitude of 103 m s^{-1}, almost double the mean value. Our simulated results are consistent with observations. Bluestein et al. (2003a) reported an observed mean tangential wind speed of 25-30 m s^{-1} in tornadoes, whereas the actual maximum wind speed ranges between 60-70 m s^{-1}. They also observed contractions in the vortex core every time the tornadoes showed a steep increase in tangential velocity (see Fig. 3 in Bluestein et al. (2003a)). However, unlike the broadening of the core of the TLV near the end of the intensifying stage and the weakening stage in our simulation, observations in general indicate a shrinking of the core with intensification. A possible explanation for our TLV core broadening is its interaction with a low level jet (see Fig. 2.17 b in Santos et al. (2008a)), thus introducing a broad asymmetric structure in the simulated surface wind

distribution.

The time development of the mean tangential wind (v_t), radial wind (v_r), and vertical vorticity (ζ) at the surface as a function of radius are depicted in Fig. 3.7. The profiles are plotted for the times 300 s, 430 s, 510 s, 530 s, and 540 s. The tangential winds (panel a) increase from the center of the TLV to the RMW, and decrease with radius thereafter. The exception being at 530 s when two radii of maximum wind are found. At 510 s the surface winds reach their maximum intensity, and the tangential wind increases linearly with radial distance in the inner core. The vertical vorticity is almost constant within 80 m from the center (panel c). Although these features are characteristic of those found in solid body rotation, the TLV at its maximum intensity is not represented well by a Rankine vortex. Such a vortex exhibits a potential flow outside the RMW with zero vertical vorticity, quite unlike the situation at 510 s shown in panel c. Indeed if the mean tangential wind and the mean vertical vorticity were written as $v_t = ar^{-\alpha}$, where a, α are constants and r the radius, and ζ is given by Eqn. 3.3

$$\zeta = \frac{1}{r}\frac{\partial(rv_t)}{\partial r}, \tag{3.3}$$

then panel b shows that $\zeta > 0$ and $0 < \alpha < 1$ outside the RMW. A potential flow, on the other hand, would have $\alpha = 1$ and $\zeta = 0$ outside the RMW. We also note that at 530 s, there are two RMWs. The inner RMW disappears at 540 s and only the outer RMW remains.

The structure of the mean radial wind is depicted in Fig. 3.7 panel b. The dominant feature during the intensification period is the convergence flow near the surface. Upward motion is therefore produced and the TLV can be described by an upward moving spiraling flow. As the maximum intensity is reached at 510 s, weak divergent flow starts to develop near the center of

the TLV. Further development of the downdraft is evident at 530 s and 540 s when the divergent flow expands to 180 m and 160 m respectively (panel b). Note also that the radial gradient of vorticity changes sign at 530 s and 540 s (panel c).

To determine the extent of cyclostrophic balance in the mean structure of the TLV, we first define the balance as an equality between the centrifugal force and the radial pressure gradient force:

$$\frac{V_c^2}{r} = -\frac{1}{\rho}\frac{\partial p}{\partial r}, \tag{3.4}$$

where V_c, ρ, p and r are the azimuthal wind in cyclostrophic balance, the air density, the pressure, and radial distance respectively.

The degree of cyclostrophic imbalance is given by the difference between the actual centrifugal forces and the centrifugal force of a flow in cyclostrophic balance with the form

$$Ai = \frac{V^2}{r} - \frac{V_c^2}{r}, \tag{3.5}$$

where V is the actual mean azimuthal wind. A negative value of A_i means that the actual tangential wind is smaller than the cyclostrophic wind. The flow is subcyclostrophic with an acceleration toward the center. On the other hand, a positive value of A_i means that the actual tangential wind is larger than the cyclostrophic wind. The flow is supercyclostrophic with an acceleration away from the center.

Fig. 3.8 depicts the field of Ai at different heights (15 m, 105 m, 195 m, 285 m and 405 m) and times (300 s, 430 s, 510 s, 530 s and 540 s) covering the lifecycle of the TLV. At 300 s (genesis stage), the flow at the 5 levels is subcyclostrophic resulting in acceleration of the mean radial wind (panel

a) toward the center of the TLV. At 430 s (start of the intensifying stage), the flow is subcyclostrophic less than 90 m from the center but approaches cyclostrophic balance at larger distance except at an altitude of 405 m (panel b). At 510 s, when the surface wind of the TLV reaches its maximum intensity, the flow is approximately cyclostrophic below 200 m but supercyclostrophic aloft (panel c). When the TLV enters its weakening stage (panel d and panel e), the flow is no longer in cyclostrophic balance.

3.4 Sensitivity Experiments

As mentioned previously, five sensitivity experiments were performed as listed in Table 3.1. The vertical shear of the environment wind below 4 km increases from experiment SH, CH, to LH, as does the storm relative helicity. In Experiment DRY, a drier humidity profile similar to the one in Wicker and Wilhelmson (1995) is used. However, the vertical distributions of temperature and the horizontal winds remain the same as in the control experiment CH. In Experiment ICE, ice microphysics is included. Since the evolution of the storm in the different experiments behaves differently, the integration is extended to 135 min to allow for slower storm development in some experiments. For comparison purposes, experiments SH and LH will be compared to CH; so will experiments DRY and ICE.

3.4.1 Effect of Low level Wind Shear and Storm Relative Helicity

Two different approaches have been used to understanding rotation in supercell storms (Weisman and Rotunno, 2000). One approach focuses on the

production of rotation as a consequence of the interaction between environmental vertical wind shear and the storm updraft (Rotunno and Klemp, 1982, 1985). The second approach considers the effect of streamwise storm relative helicity or the advection of ambient streamwise vorticity (Davies-Jones, 1984). Our interpretation of the sensitivity experiments SH, CH, and LH follows the helicity school of thought.

Fig. 3.9 a presents a comparison of the evolution of the maximum vertical velocity in the storm. After about 50 min, the maximum updraft speed generally increases with a decrease in low level shear. For example, experiment SH which has the smallest low level shear exhibits the strongest updraft. This scenario is consistent with the interpretation by Weisman and Klemp (1982) that in strong shear environments, entrainment becomes large and mixing between the updraft and the ambient environment is enhanced to produce a weaker updraft.

With regard to storm rotation, Fig. 3.10 panels a, b and c indicate that before 40 min, the mesocyclone from 1 km to 3 km in LH is stronger than in CH, which in turn is stronger than in SH. This result can be explained by the fact that experiment LH possesses the largest amount of streamwise vorticity in the environment. The rotation of the mesocyclone is strengthened when the rich streamwise vorticity air is being ingested into the storm. Turning to the maximum vertical vorticity (MVV) near the surface, the results show that the magnitude and the time of the maximum are sensitive to SRH. Specifically, the value and time of appearance of surface MVV in experiments SH, CH, and LH are (0.0674 s^{-1}, 95 min), (0.0728 s^{-1}, 77 min), and (0.0742 s^{-1}, 125 min) respectively.

To explore the reason for the general increase of surface MVV with an increase in SRH (or low-level vertical shear of the environment), we display in Figs. 3.11, 3.12 and 3.13 the evolution of the minimum downdraft below

1 km, the maximum horizontal wind shear at the surface, and the maximum horizontal surface convergence. The extreme values of these variables during the whole integration period are also included in Table 3.1. Inspection of the first panels in these figures and the table entries indicates that the downdraft strength in general increases with SRH, consistent with enhanced mixing when there is larger vertical wind shear of the environment. For example, the maximum downdraft below 1 km is -15 m s^{-1} in LH but is -12 m s^{-1} in SH (Table 3.1).

The strength of the low-level downdraft affects directly the surface horizontal shear and the surface horizontal convergence along the outflow boundaries arising from the RFD. In general, surface horizontal shear is smaller in SH than in LH, and the same applies to the magnitude of the surface horizontal convergence. Specifically, Table 3.1 indicates that the maximum surface horizontal shear and the maximum surface horizontal convergence are respectively (0.0555 s^{-1}, 0.032 s^{-1}) in SH and (0.076 s^{-1}, 0.0545 s^{-1}) in LH.

We summarize the sensitivity experiments in changing the vertical wind shear of the environment below 4 km as follows:

a) Environment with larger vertical wind shear below 4 km produces a stronger mesocyclone due to tilting and stretching, b) Environment with larger vertical wind shear below 4 km causes stronger entrainment to produce a weaker updraft but stronger downdraft, c) The stronger downdraft results in larger horizontal shear and horizontal convergence near the ground to enhance surface vertical vorticity which favors tornadogenesis.

3.4.2 Middle to Upper Tropospheric Dryness and Inclusion of Ice Processes

Fig. 3.9 b shows that before 40 min, the evolution of the maximum updraft for experiments DRY and CH is similar. From 40 min to 75 min, the DRY storm intensifies as a strong updraft pulse develops. This strong updraft pulse may be related to the stronger downdraft in experiment DRY before 55 min (Fig. 3.11 b). However, after this time, the mixing of drier air from the environment with the storm eventually produces a weaker updraft (Fig. 3.9 b), weaker downdraft (Fig. 3.11 b), and smaller surface horizontal shear (Fig. 3.12 b) and surface horizontal convergence (Fig. 3.13 b) along the outflow boundaries. As a result, the MVV near the surface is much weaker in experiment DRY than in CH (Figs. 3.10 a,d and Table 3.1). Thus the middle and upper tropospheric dryness can weaken the low level rotation to disfavor tornadogenesis.

The inclusion of ice/snow and graupel/hail in experiment ICE generates the additional latent heats of sublimation and fusion. As a result, the maximum updraft strength is enhanced (Fig. 3.9 c) and the mesocyclone develops earlier than in CH (Figs. 3.10 a,e). The stronger storm and the presence of graupel/hail with the associated processes like melting and precipitation loading generate stronger downdrafts (Fig. 3.11 c), stronger surface horizontal shear (Fig. 3.12 c) and horizontal convergence (Fig. 3.13 c) to favor low-level rotation (Fig. 3.10 e). As tabulated in Table 3.1, experiment ICE produces the largest surface MVV, the strongest downdraft below 1 km, the strongest surface horizontal convergence and horizontal shear of all experiments. The ice processes in ice/snow and graupel/hail would increase the probability for tornadogenesis.

3.5 Summary and conclusions

Santos et al. (2008a) reported on a qualitative description of a multi-grid simulation of a supercell storm spawning a tornado-like vortex (TLV). In this second paper of the series, we present a quantitative analysis of the vorticity budgets during tornadogenesis, the evolution of the force balance for the mean flow of the TLV, as well as sensitivity experiments on varying the initial conditions and the parameterization of the microphysical processes.

The vorticity budgets cover both the storm scale and the TLV scale. For the storm scale, it was found that at the early stage of storm evolution tilting was the main mechanism for producing midlevel rotation. At 10 min prior to the appearance of the TLV at the surface, stretching is the dominating mechanism for vorticity intensification. This period is marked by a rapid but downward growth of the midlevel mesocyclone which becomes vertically aligned with the maximum vorticity at the surface with peak value of 0.0728 s^{-1}.

For the tornado scale, it was found that during the early part of the intensification stage of the TLV, stretching and advection between 300 m and 500 m are the main mechanisms controlling the time tendency of vertical vorticity. At the final phase of the intensification period, the fastest growth of the TLV occurs in the lowest 200 m, with stretching being the main contributor. During this intensifying stage the force balance of the TLV is subcyclostrophic. However, when the surface horizontal winds of the TLV reach the maximum velocity of 103 m s^{-1}, a state of quasi-cyclostrophic balance in the lowest 200 m appears. This balance is upset during the weakening stage when divergent winds develop near the surface as a result of the development of strong downdrafts throughout the center of the TLV.

The evolution of the azimuthally averaged tangential surface winds and the

radius of maximum wind indicates a process for vortex core contraction every time a steep change in the mean tangential wind happens. Nevertheless the core of the TLV broadens during the late intensifying and weakening stages due to its interaction with a low level jet.

A series of sensitivity experiments were performed to determine the effects of varying the initial conditions and the inclusion of ice phase processes. Significant differences in the evolution of the mesocyclone and the near surface vorticity were observed. In general, a larger environmental SRH produces a stronger mesocyclone and a stronger downdraft. In turn, stronger horizontal convergence and horizontal shear appear near the surface to favor tornadogenesis. A drier environment above the cloud base eventually produced a weaker storm while the inclusion of ice phase processes generates more vigorous updrafts and downdrafts, stronger surface horizontal convergence and horizontal shear to favor tornadogenesis.

Acknowledgements

This research reported here is sponsored by the Canadian Foundation for Climate and Atmospheric Sciences (CFCAS).

Experiment	Max. surface vertical vorticity $\zeta(s^{-1})$	Max. downdraft below 1 km (m s^{-1})	Max. surface horizontal shear (s^{-1})	Min. surface horizontal divergence (s^{-1})
CH	0.0728	-15	0.0793	-0.0484
LH	0.0742	-15	0.0760	-0.0545
SH	0.0674	-12	0.0555	-0.0320
DRY	0.0539	-13	0.0604	-0.0374
ICE	0.0836	-24	0.0936	-0.0591

Table 3.1: Maximum surface vertical vorticity, maximum downdraft in the lowest 1 km, maximum surface horizontal shear and maximum surface horizontal convergence for experiments CH, LH, SH, DRY and ICE.

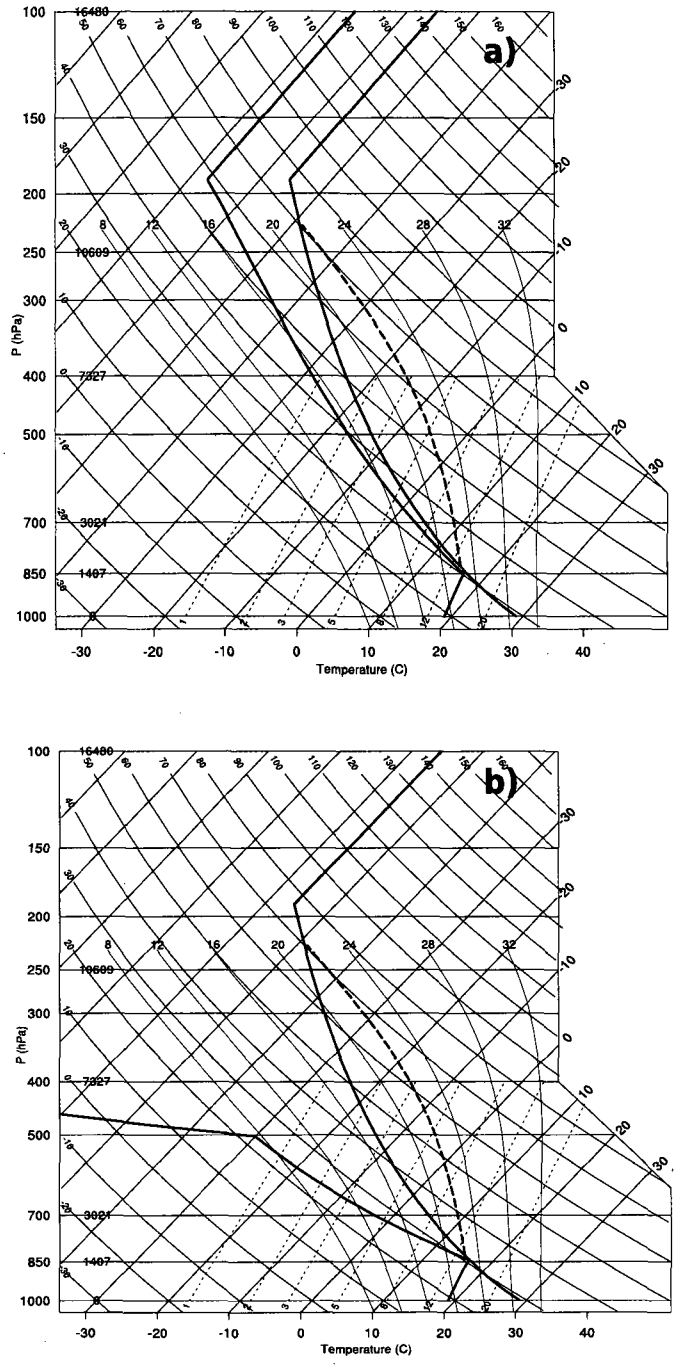

Figure 3.1: Skew-T plot of sounding for a) Control experiment (CH), and b) experiment DRY.

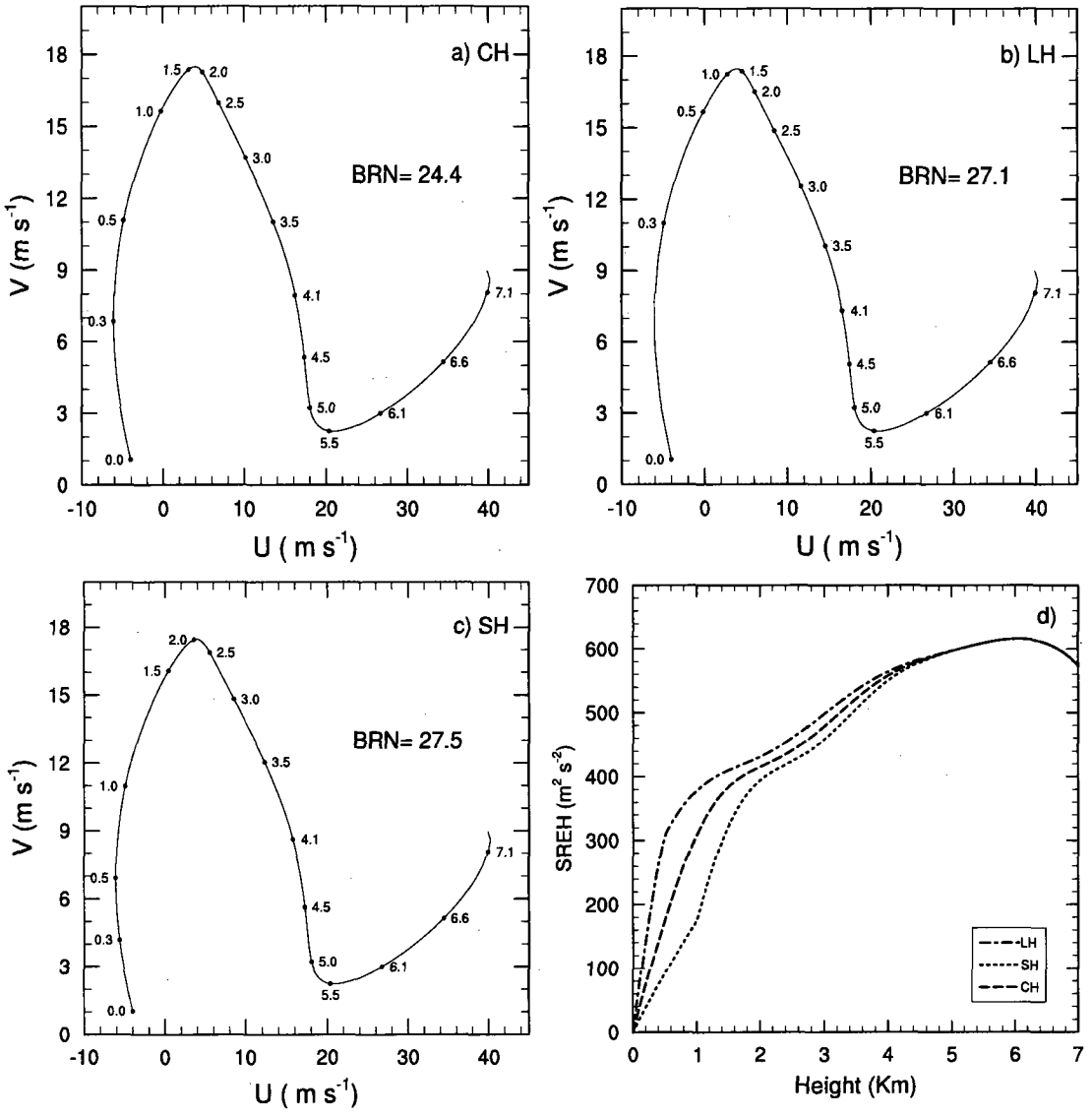

Figure 3.2: Wind hodograph for a) Control experiment (CH), b) experiment LH, and c) experiment SH. The storm relative helicity below 7 km for these experiments are shown in panel d).

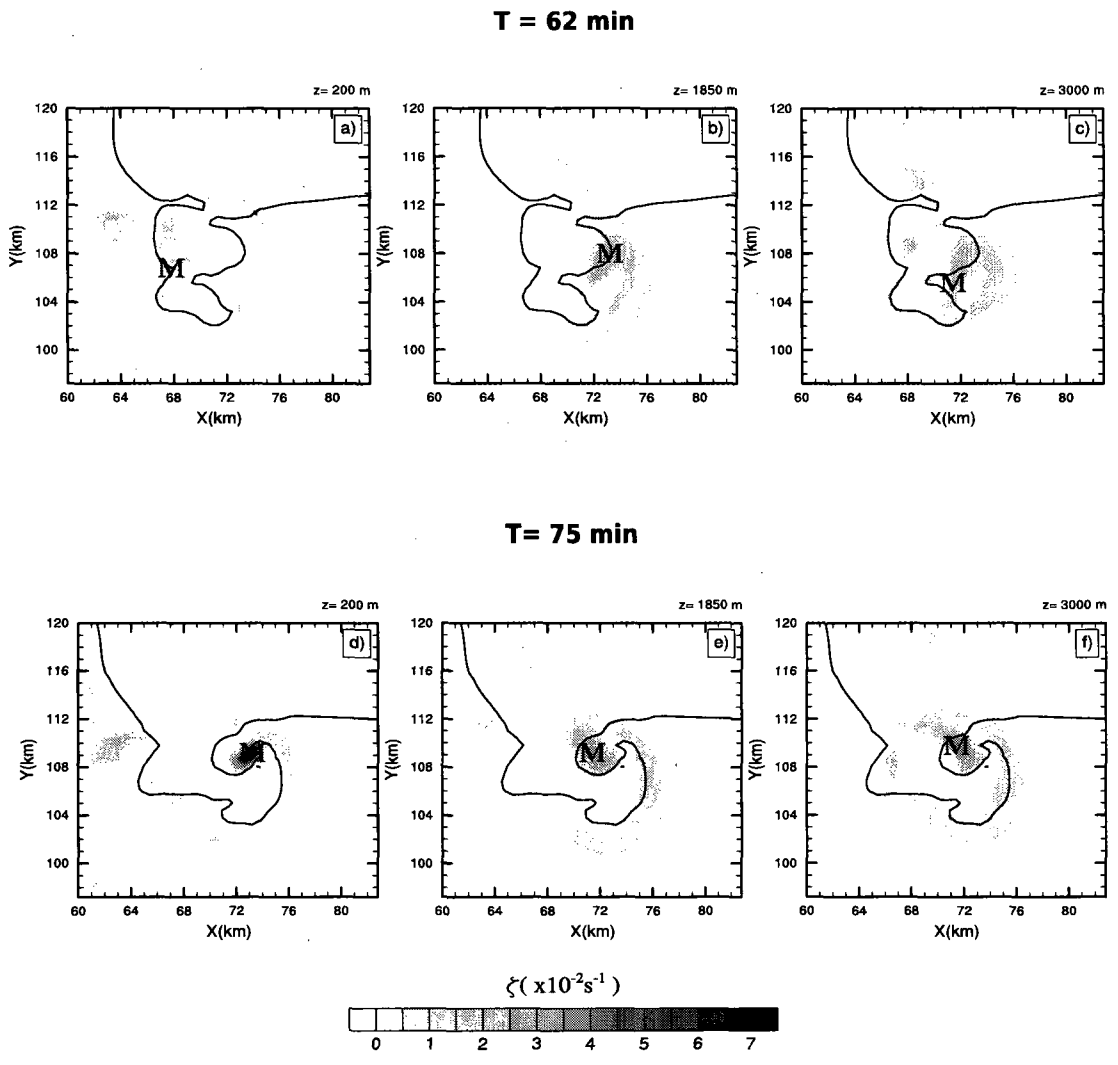

Figure 3.3: Horizontal section of vertical vorticity at 62 min for the level a) 200 m , b) 1850 m and c) 3000 m; and at 75 min for the level d) 200 m, e) 1850 m and f) 3000 m. The solid line denotes the contour for the 1 g kg^{-1} precipitation water content at the surface. The letter M denotes the location of the maximum vorticity center.

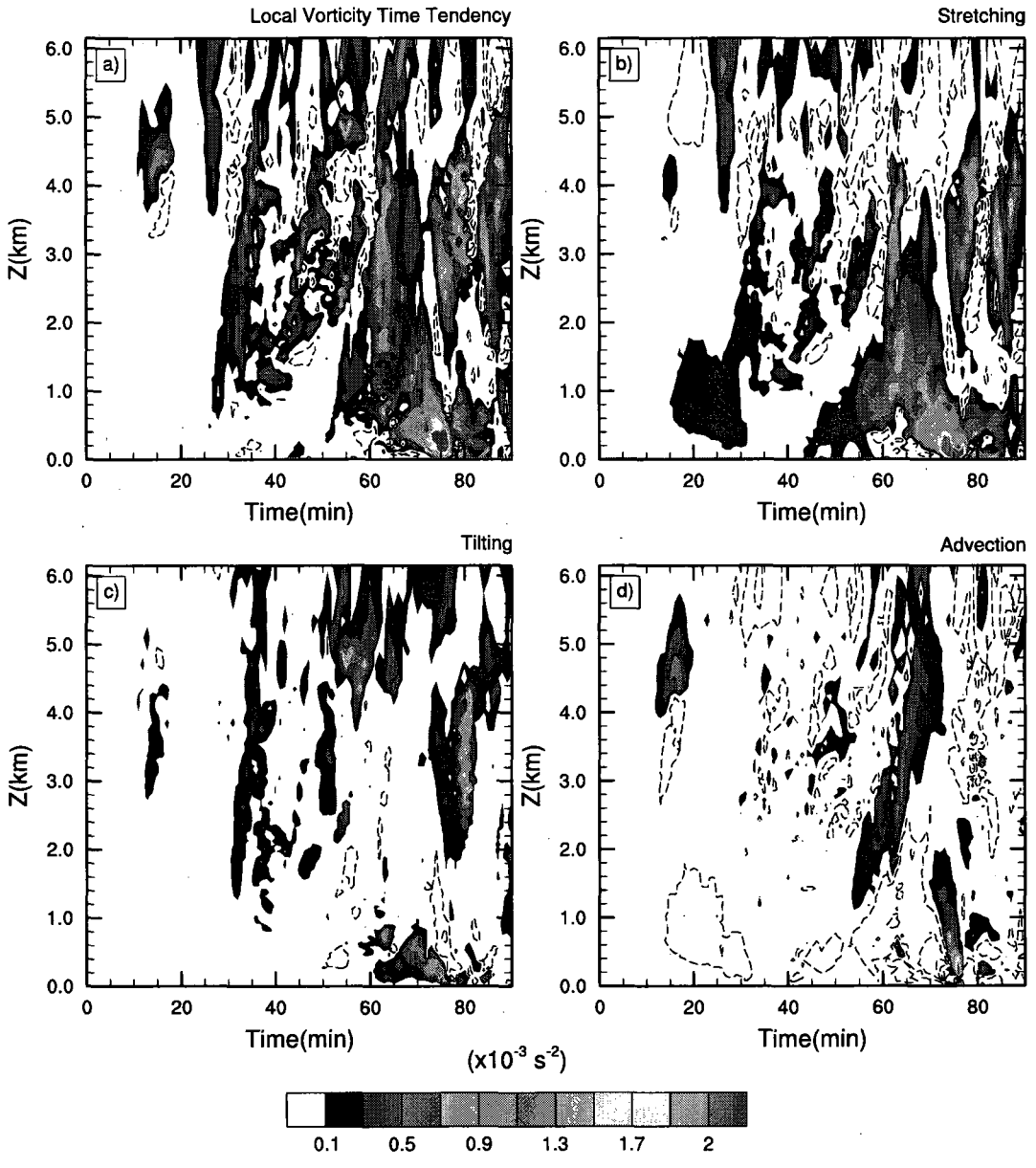

Figure 3.4: Evolution of the maximum in a) local vorticity tendency, b) the stretching term, c) the tilting term, and d) the advection term in the vertical vorticity equation. Positive (negative) values are shaded (dashed). The absolute values of the negative and positive vorticity tendency contours are the same.

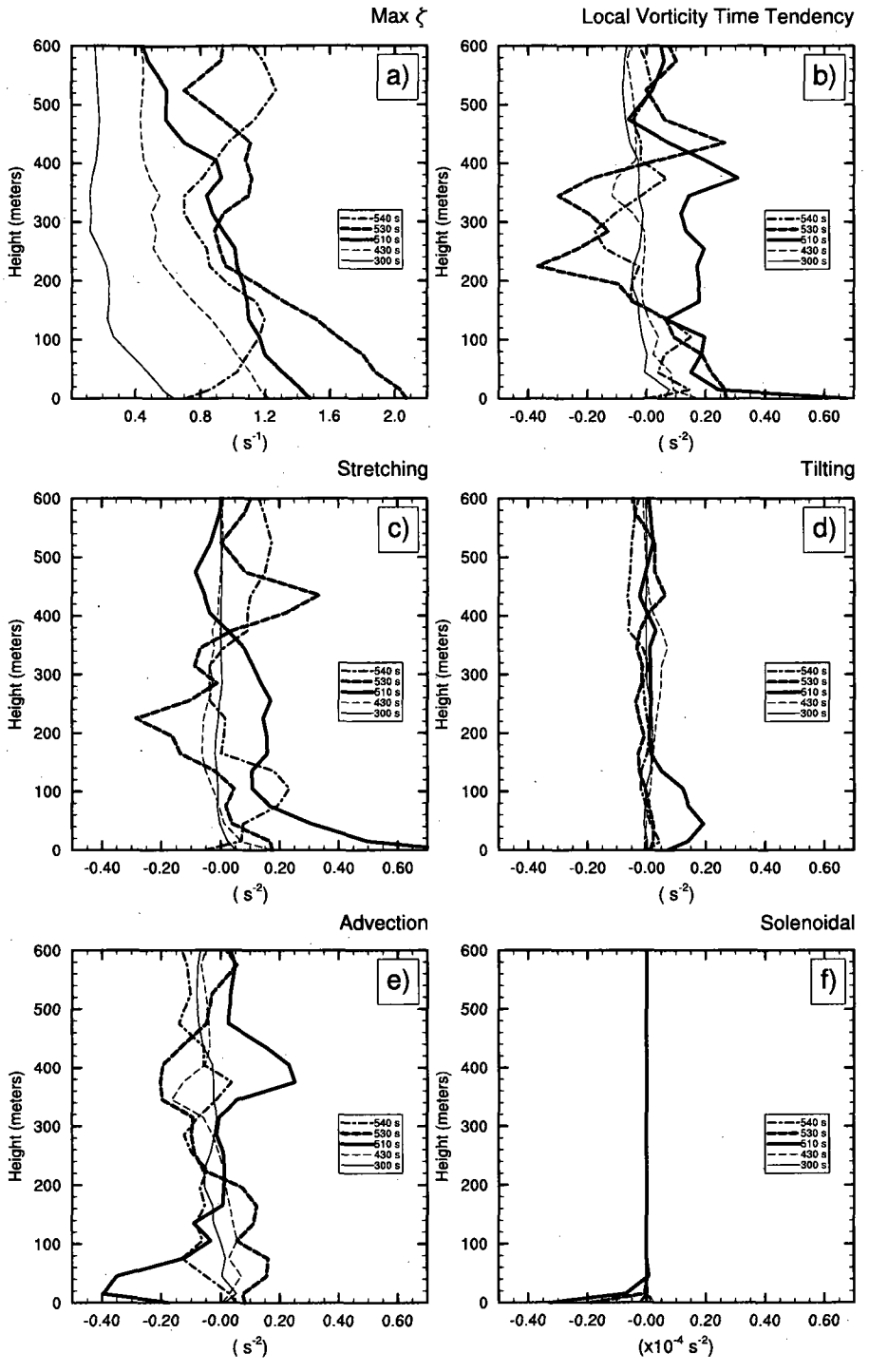

Figure 3.5: Vertical profiles of a) maximum vertical vorticity, b) local vorticity tendency, c) the stretching term, d) the tilting term, e) the advection term, and f) the solenoidal term in the vertical vorticity equation at 300 s, 430 s, 510 s, 530 s and 540 s.

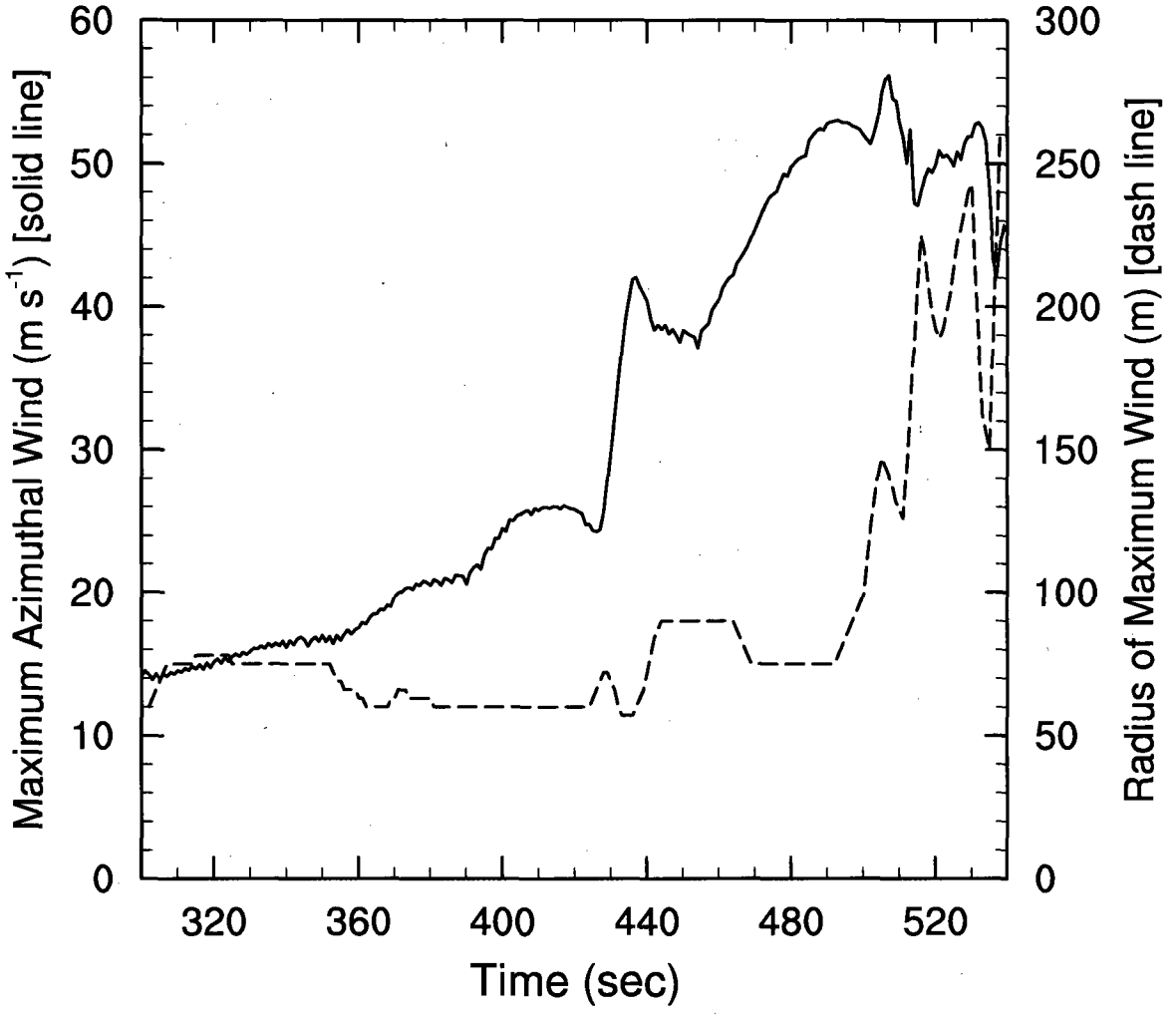

Figure 3.6: Time series of mean tangential wind (solid) and the radius of maximum mean tangential wind (dashed) at the surface.

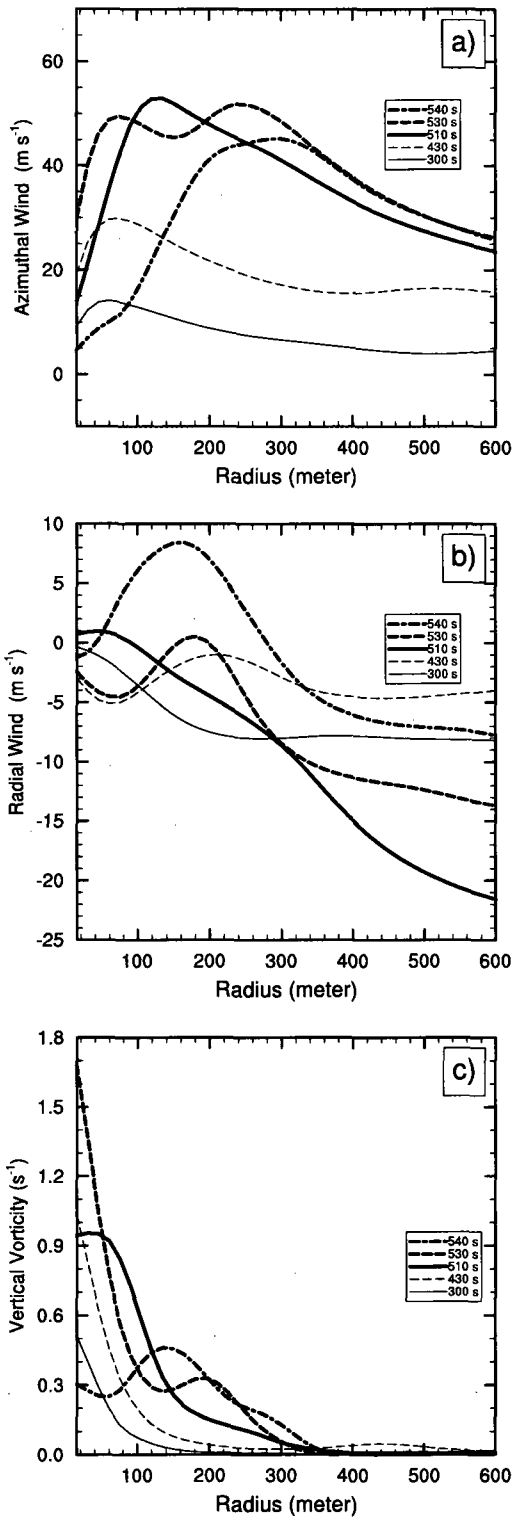

Figure 3.7: Radial distributions of a) mean tangential wind, b) mean radial wind, and c) mean vertical vorticity at 300 s, 430 s, 510 s, 530 s and 540 s.

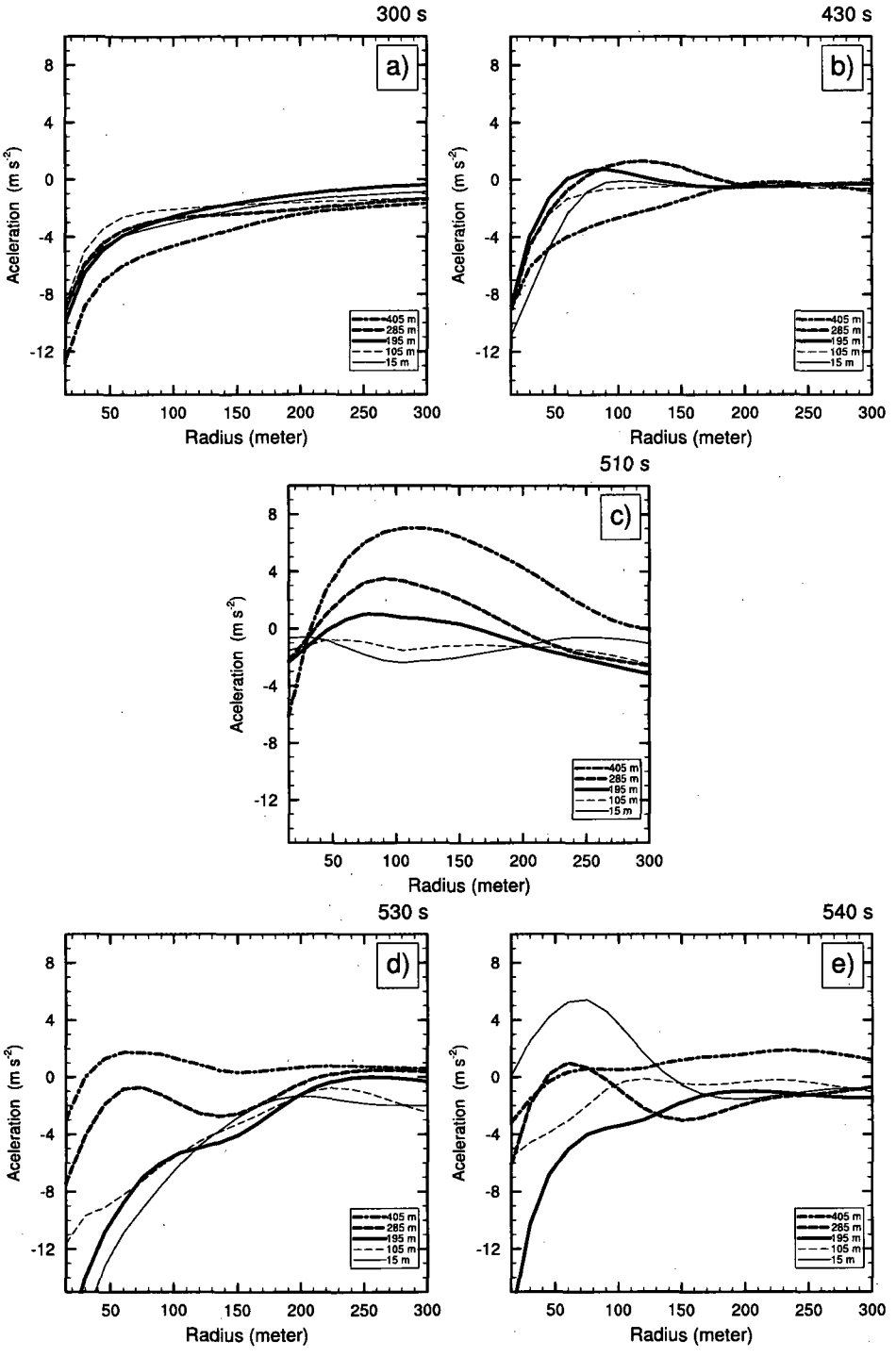

Figure 3.8: Radial distributions of the azimuthally averaged difference between the actual centrifugal forces and the centrifugal force of a cyclostrophic balance at a) 300 s, b) 430 s, c) 510 s, d) 530 s and e) 540 s at 15 m, 105 m, 195 m, 285 m and 405 m AGL.

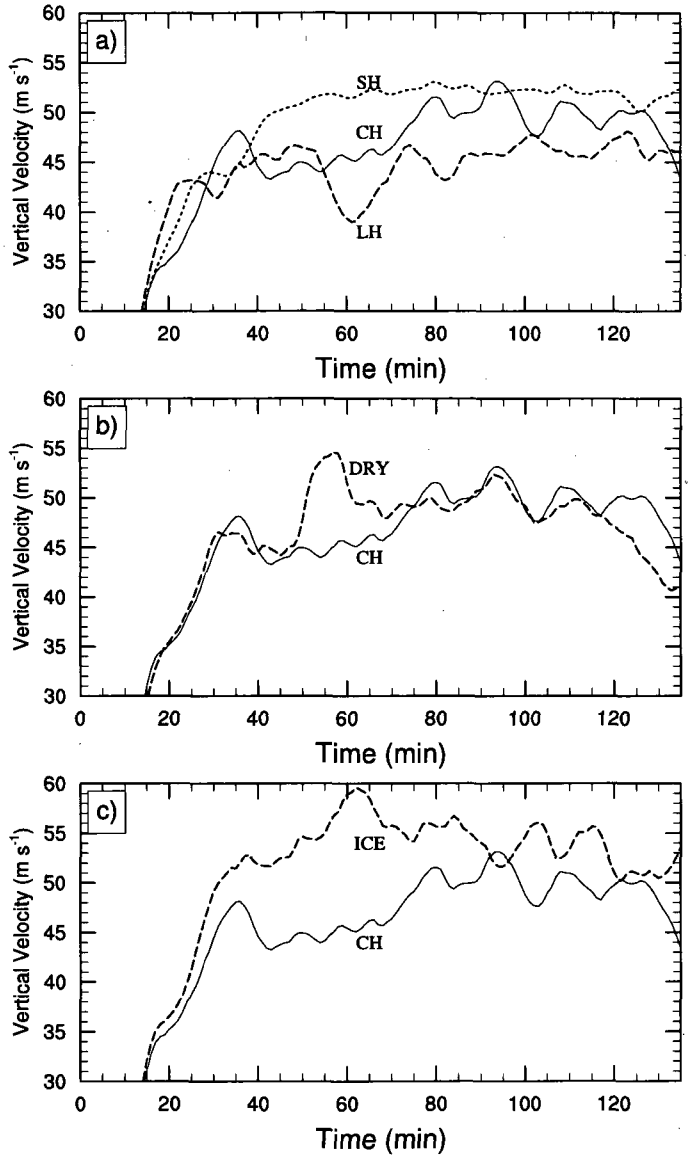

Figure 3.9: Evolution of maximum vertical velocity in the storm for a) experiments SH, CH, and LH, b) experiments DRY and CH and c) experiments ICE and CH.

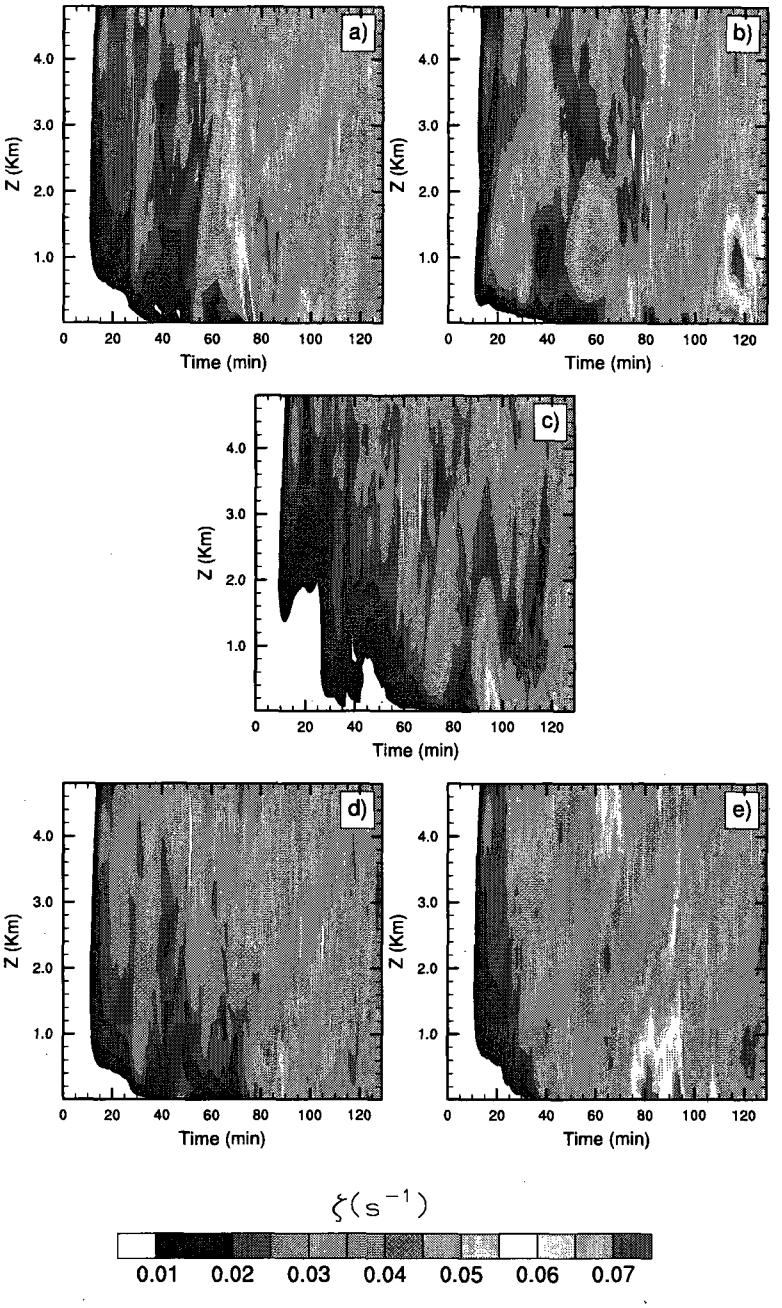

Figure 3.10: Evolution of maximum vertical vorticity in the lowest 5 km for experiments a) CH, b) LH, c) SH, d) DRY and e) ICE.

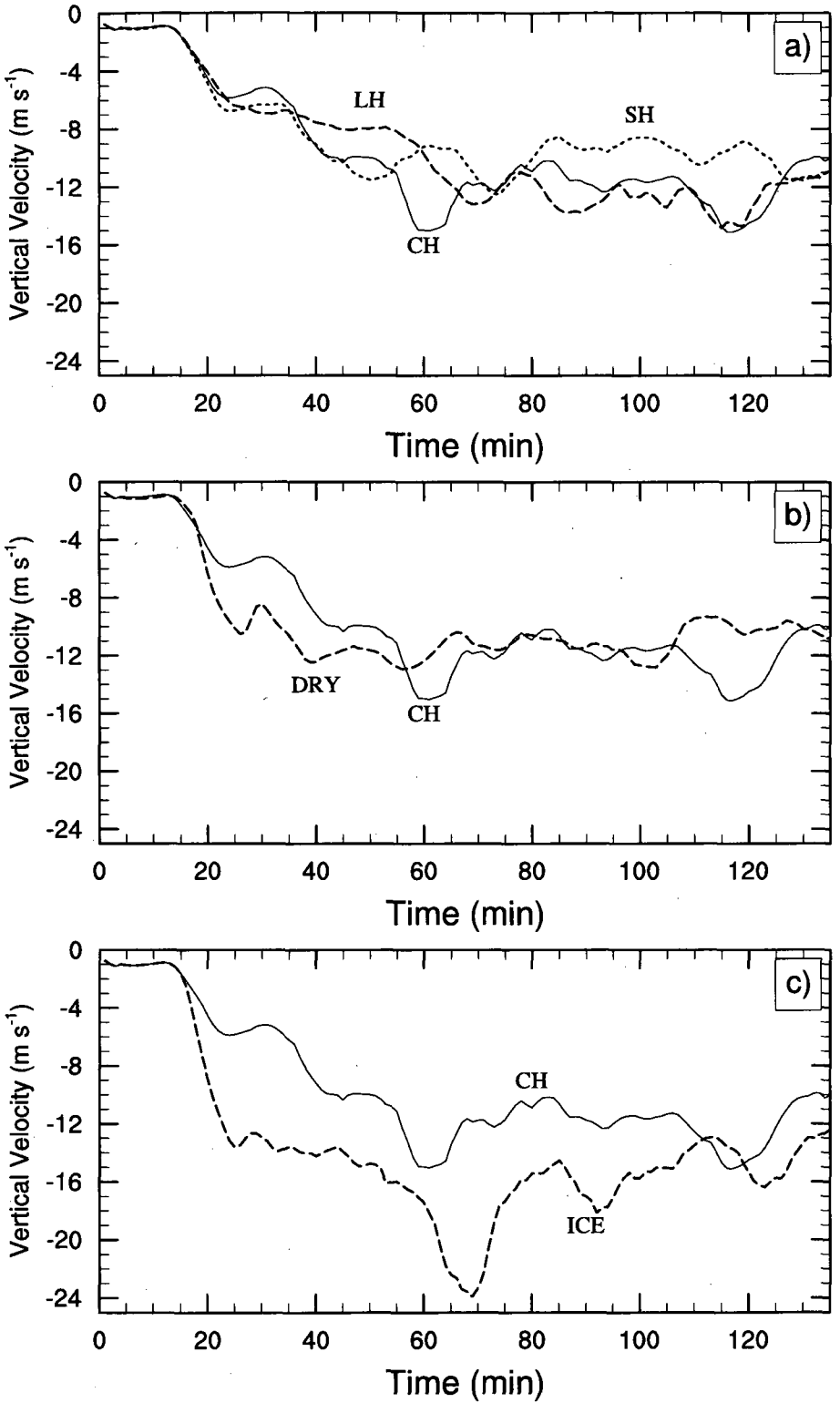

Figure 3.11: Evolution of maximum downdraft in the lowest 1 km for a) experiments SH, CH and LH, b) experiments DRY and CH and c) experiments ICE and CH.

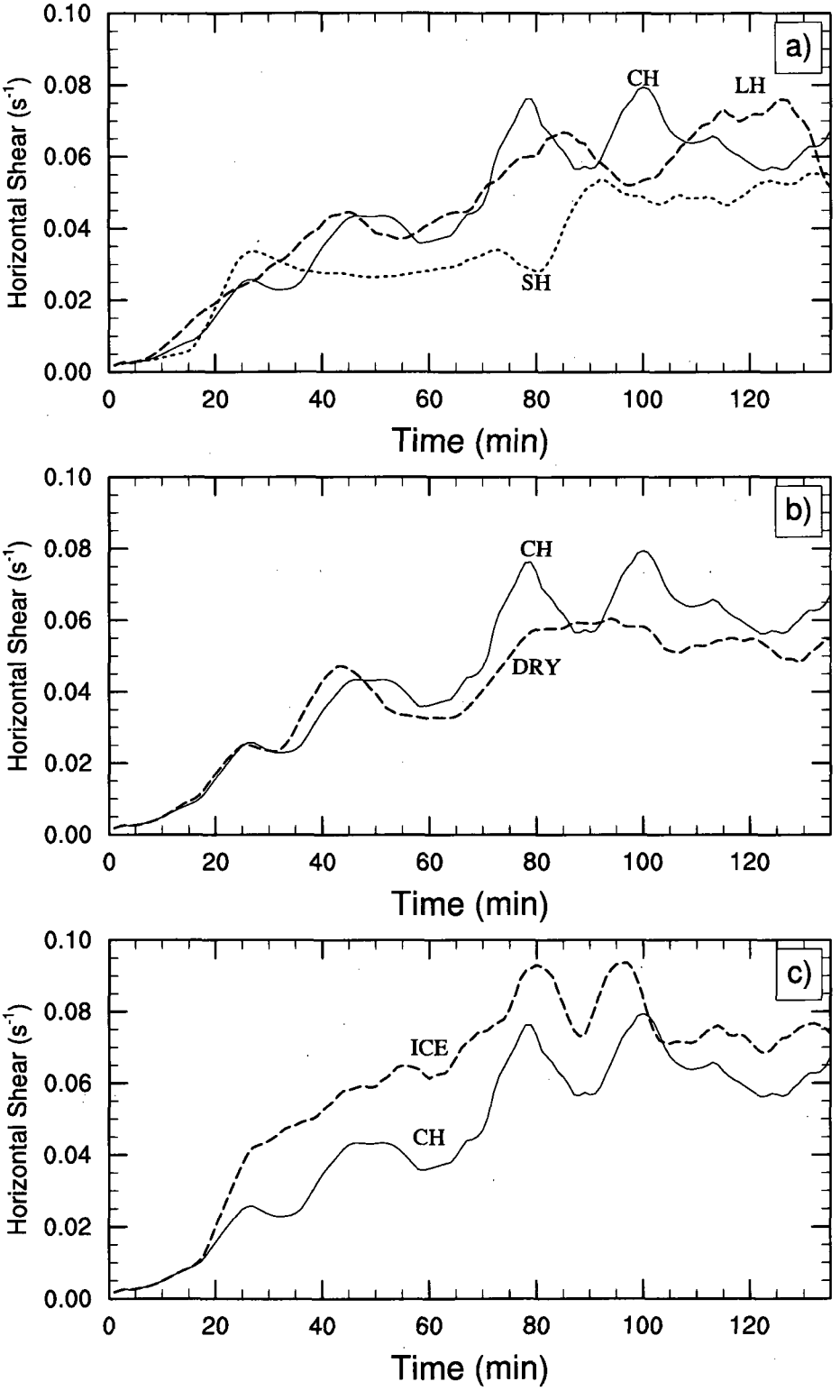

Figure 3.12: Evolution of maximum surface horizontal shear for a) experiments SH, CH and LH, b) experiments DRY and CH and c) experiments ICE and CH.

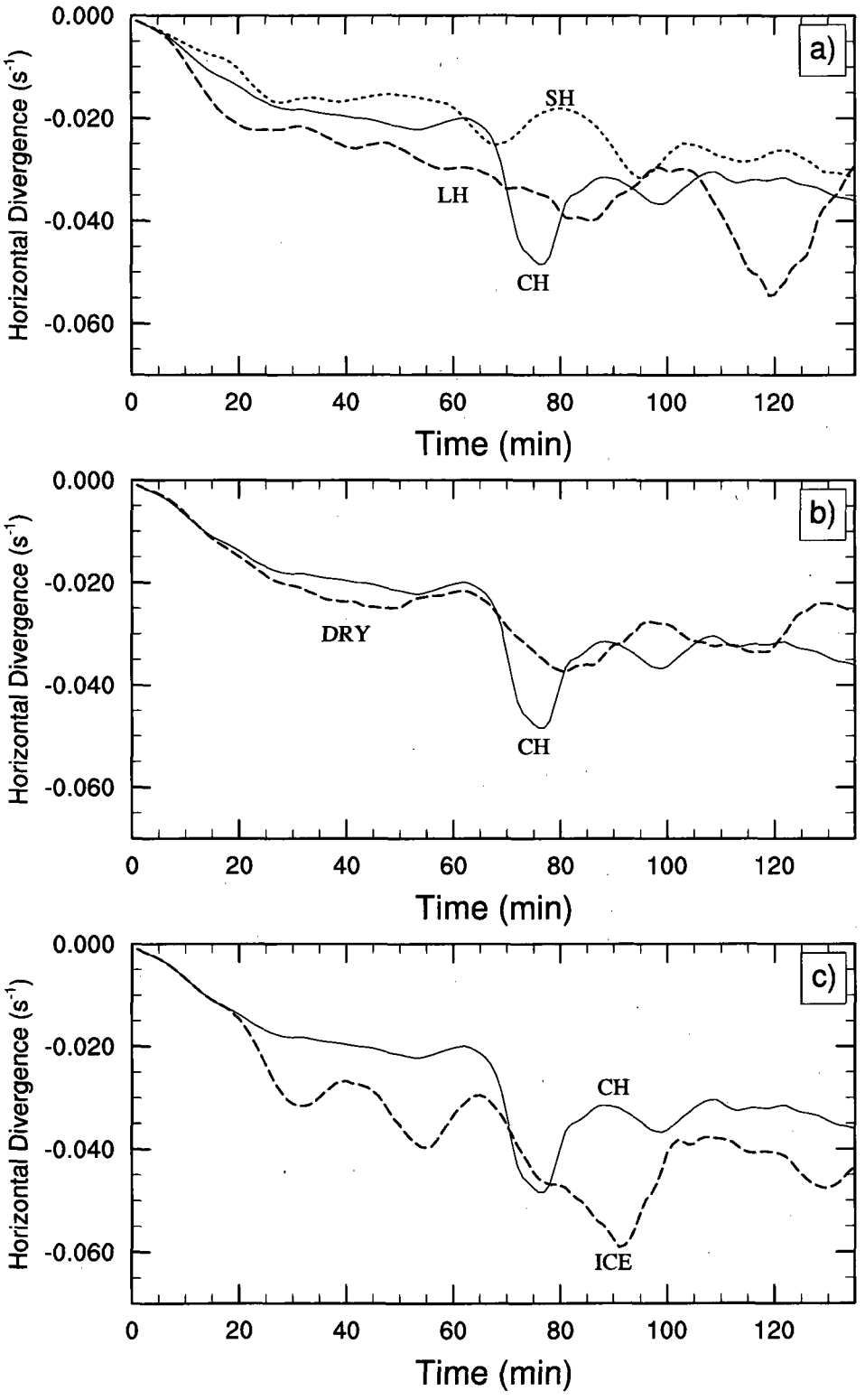

Figure 3.13: Evolution of maximum surface convergence for a) experiments SH, CH and LH, b) experiments DRY and CH and c) experiments ICE and CH.

Chapter 4

Conclusions

Tornadoes are severe weather events that produce severe losses and properties damages all around the world. There are a variety of convective systems spawning this intense vorticies ranging from thunderstorms to hurricanes. This reasearch is particularly dedicated to the study of tornadoes associated with supercell storms. These systems are characterized by a mid-level rotation due to the presence of a mesocyclone, a vortex whose diameter varies between 3 to 10 km. As a consequence of this rotation, the radar reflectivity arising from precipitation near the surface adopts a hook shaped structure and tornadoes are usually form at the tip of this hook. It is worth noting that not all mesoscyclones produce tornadoes. (Burgess et al., 1993) pointed out that tornadogenesis occurs only in between 30-50 % of mesocyclones indicating that sufficient or unique conditions for tornadoes are yet to be found. The problem is a reflection of the fact that the interactions among mesocyclones, tornadoes, and the outflow boundaries associated with the Rear Flank Downdraft (RFD) and the Forward Flank Downdraft (FFD) remain poorly understood.

As a first step toward the understanding of tornadogenesis in supercell storms, an idealized high-resolution simulation of an intense tornado-like vor-

tex in a supercell storm is performed using a three-dimensional nested grid model MC2. The simulated supercell storm spawned one intense tornado-like vortex with maximum surface winds of 103 m s^{-1} and minimum central pressure of 927 hPa. Tornadogenesis was initiated at the surface along an outflow boundary characterized by strong horizontal wind and temperature gradients. Along this boundary, centers of maximum positive vertical vorticity formed from the process of horizontal shear instability. A TLV forms when one of these low-level vortices undergo further interaction with the upper-level mesocyclonic circulation and merges with other surface vortices during its intensification process. Other weaker vortices also developed in the hook region but were less intense because of the absence of the interaction with the mesocyclone and no merging with other surface vortices occurred.

An analysis of the vertical vorticity budget at storm scale reveals that tilting dominates the creation of rotation at the midlevels during the initial stage of storm evolution. Then prior to the tornadic event, vorticity stretching intensifies the storm mesocyclonic circulation which propagates downward. Through the Dynamic Pipe Effect, the low level circulation intensifies and the low level updraft increases at the time when a TLV is produced.

The budget analysis at the scale of the tornado shows that after the seed of vertical vorticity is created, the vertical vorticity intensification is mainly controlled by the intense stretching in the lowest 400 m. Although the radial pressure gradient force dominates over the centrifugal force during the intensification period of the TLV, a cyclostrophic balance near the surface is reached as the TLV reached its maximum strength. The symmetric part of the horizontal winds, given by the maximum azimuthally averaged tangential winds, has a maximum value of 56 m s^{-1}. However, the total wind speed, which includes the asymmetric component, registered a maximum of 103 m s^{-1}. The weakening stage of the TLV is dominated by the presence of diver-

gent surface winds associated with an intense downdraft that developed in the center of the TLV.

To determine the impact of various initial ambient atmospheric conditions conducive to the formation of tornadic supercell storms, a series of sensitivity experiments were performed. It was found that as the environmental wind shear at the lowest 3 km increased, near surface rotation was enhanced and more intense tornado-like vortices were created. It was also found that helicity in these experiments was a good predictor for tornadogenesis as pointed out by Droegemeier et al. (1993) and Dupilka and Reuter (2006b). Another set of experiments indicated that different storm outflow intensities resulted when middle- and upper-level tropospheric moisture was modified and ice phase microphysics parameterization was included. Specifically, it was found that in drier environments aloft, weaker storm outflow boundaries were generated. The weak outflow boundaries produced weaker low level convergence which prevented the intensification of the near surface vortices into a TLV. On the other hand, the inclusion of ice microphysics produced more intense outflow boundaries leading to an increase in the low level convergence that together with the shear-induced vertical vorticity along the leading edge of the gust front enhanced tornadogenesis.

The results from this thesis study are starting to shed some light on the interaction between the tornado and its parent system and the influence of the ambient atmospheric conditions on the vertical vorticity evolution of the storm-tornado system. Nevertheless, to generalize these results further studies are needed. Further research should include not only a proper atmospheric boundary layer parameterization of subscale processes but also a more complete microphysics parameterization. Within the spectra of atmospheric conditions leading to the formation of tornadic supercells, the sensitivity and modulation of tornadogenesis with respect to a larger number of ambient parameters should also be explored.

References

Benoit, R., M. Desgagné, P. Pellerin, S. Pellerin, Y. Chartier, and S. Desjardins, 1997: The Canadian MC2: A semi-implicit semi-Lagrangian wide-band atmospheric model suited for fine-scale process studies and simulation. *Mon. Wea. Rev.*, **125**, 2382–2415.

Blanchard, D. O. and J. M. Straka, 2002: Some possible mechanisms of tornado failure in a supercell.: In *Preprints, 19th Conf. on Severe Local Storms, Mineapolis, MN.* Amer. Meteor. Soc., 116-119.

Bluestein, H. B., S. G. Gaddy, D. C. Dowell, A. L. Pazmany, J. C. Galloway, R. E. McIntoch, and H. Stein, 1997: Doppler radar observations of substorms-scale vortices in a supercell. *Bull. Amer. Meteor. Soc.*, **125**, 1046–1059.

Bluestein, H. B., W. L. Lee, M. Bell, C. C. Weiss, and A. Pazmany, 2003a: Mobile Doppler radar observations of a tornado in a supercell near Basset, Nebraska, on 5 June 1999. Part II: Tornado-vortex structure. *Mon. Wea. Rev.*, **131**, 2968–2984.

Bluestein, H. B. and A. Pazmany, 2000: Observation of tornadoes and other convective phenomena with a mobile 3-mm wavelength Doppler radar: The spring 1999 field experiment. *Bull. Amer. Meteor. Soc.*, **81**, 2939–2951.

Bluestein, H. B. and W. P. Unruh, 1989: Observations of the wind field in tornadoes, funnel clouds and wall clouds with a portable Doppler radar. *Bull. Amer. Meteor. Soc.*, **70**, 1514–1525.

Bluestein, H. B., C. C. Weiss, M. French, E. M. Holthaus, R. Tanamachi, S. Frasier, and A. Pazmany, 2007: The structure of tornadoes near Attica, Kansas, on 12 may 2004: High-resolution, mobile, doppler radar observation. *Mon. Wea. Rev.*, **135**, 475–506.

Bluestein, H. B., C. C. Weiss, and A. Pazmany, 2003b: Mobile Doppler radar observations of a tornado in a supercell near Basset, Nebraska, on 5 June 1999. Part I: Tornadogenesis. *Mon. Wea. Rev.*, **131**, 2954–2967.

Brown, R. A., D. W. Burgess, and K. C. Crawford, 1973: Twin tornado cyclones within a severe thunderstorm. *Weatherwise*, **26**, 63–71.

Browning, K., 1986: *Morphology and classification of middle-latitude thunderstorms.Thunderstorms Morphology and Dynamics.*: E. Kessler, Ed., University of Oklahoma Press, 133-152, 2^{nd} edition.

Burgess, D. W., R. J. D. Jr., and P. R. Desrochers, 1993: The tornado: Its strucutre, dynamics prediction and hazards. *Amer. Geophys. Union*, **79**, 203–221.

Burgess, D. W. and L. R. Lemon, 1990: Severe thunderstorms detection by radar.: Radar in Meteorology. Amer. Meteor. Soc., Eds. D. Atlas, Boston. 619-647.

Davies-Jones, R. P., 1984: Streamwise vorticity: The origin of updraft rotation in supercell storms. *J. Atmos. Sci.*, **41**, 2991–3006.

Davies-Jones, R. P., D. W. Burgess, and M. P. Foster, 1990: Test of helicity as a forecast parameter: In *Preprints,* 16^{th} *Conf. on Severe Local Storms, Kananaskis Park, AB, Canada.* Amer. Meteor. Soc., 588-592.

Davies-Jones, R. P., R. J. Trapp, H. B. Bluestein, and C. A. Doswell III, 2001: Meteorological monograph: Severe convective storms. Tornadoes and tornadic storms. *Amer. Meteor. Soc.*, **50**, Chapter 5.

Droegemeier, K. K., S. M. Lazarus, and R. Davies-Jones, 1993: The influence of helicity on numerically simulated convective storm. *Mon. Wea. Rev.*, **121**, 2005–2029.

Dupilka, M. L. and G. W. Reuter, 2006a: Forecasting tornadic thunderstorm potential in alberta using environmental sounding data. Part I: Wind shear and buoyancy. *Wea. Forecasting*, **21**, 325–335.

Dupilka, M. L. and G. W. Reuter, 2006b: Forecasting tornadic thunderstorm potential in alberta using environmental sounding data. Part II: Helicity, precipitable water, and storm convergence. *Wea. Forecasting*, **21**, 336–346.

Feuerstein, B., N. Dotzek, and J. Grieser, 2005: Assesing a tornado climatology from global tornado intensity distributions. *J. Climate*, **18**, 585–596.

Finley, C. A., W. R. Cotton, and R. A. Pielke, 1998: Numerical simulation of two tornadoes produced by a high-precipitation supercell: In *Preprints, 19^{th} Conf. on Severe Local Storms, Mineapolis, MN.* Amer. Meteor. Soc., 206-209.

Fujita, T., 1981: Tornadoes and downburst in the context of generalized planetary scales. *J. Atmos. Sci.*, **38**, 1511–1534.

Girard, C., R. Benoit, and M. Desgagné, 2005: Finescale topography and the MC2 dynamics kernel. *Mon. Wea. Rev.*, **133**, 1463–1477.

Grasso, L. D. and W. R. Cotton, 1995: Numerical simulation of a tornado vortex. *J. Atmos. Sci.*, **52**, 1192–1203.

Hopfinger, E. J. and G. J. F. van Heijst, 1993: Vortices in rotating fluids. *Ann. Rev. Fluid Mech.*, **25**, 241–289.

Klemp, J. B. and R. Rotunno, 1983: A study of the tornadic region within a supercell storm. *J. Atmos. Sci.*, **40**, 359–377.

Klemp, J. B. and R. Rotunno, 1987: Dynamics of tornadic thunderstorms. *Ann. Rev. Fluid Mech.*, **19**, 369–402.

Klemp, J. and R. Wilhelmson, 1978: Simulations of right- and left-moving storms produced through storm splitting. *J. Atmos. Sci.*, **35**, 1097–1110.

Klemp, J., R. Wilhelmson, and P. Ray, 1981: Observed and numerically simulated structure of a mature supercell thunderstorm. *J. Atmos. Sci.*, **38**, 1558–1580.

Kong, F. Y. and M. K. Yau, 1997: An explicit approach to microphysics in MC2. *Atmosphere-Ocean*, **35**, 257–291.

Lee, B. L. and R. B. Wilhemlson, 1997: The numerical simulation of a non-supercell tornadogenesis. Part I: Initialization and evolution of pretornadic misocyclone circulation along a dry outflow boundary. *J. Atmos. Sci.*, **54**, 32–60.

Lemon, L. and C. A. Doswell, 1979: Severe thunderstorm evolution and mesocyclone structure as related to tornadogenesis. *Mon. Wea. Rev.*, **107**, 1184–1197.

Leslie, L. M. and J. B. Klemp, 1971: The development of concentrated vortices: A numerical study. *J. Fluid Mech.*, **48**, 1–21.

Mailhot, J., S. Belair, R. Benoit, B. Bilodeau, Y. Delage, L. Fillion, L. Garand, C. Girard, and A. Tremblay, 1998: Scientific description of the RPN physics library-Version 3.6, 188 pp., Recherche en Prevision Numerique, Atmospheric Environment Service, Dorval, Quebec.

Markowski, P. M., J. M. Straka, and E. N. Rasmussen, 2002a: Hook echoes and rear flank downdrafts: A review. *Mon. Wea. Rev.*, **130**, 852–876.

Markowski, P. M., J. M. Straka, and E. N. Rasmussen, 2002b: Direct surface thermodynamic observations within the rear-flank downdrafts of tornadic and non-tornadic supercell. *Mon. Wea. Rev.*, **130**, 1692–1721.

Markowski, P. M., J. M. Straka, and E. N. Rasmussen, 2003: Tornadogenesis resulting from the transport of circulation by downdraft: Idealized numerical simulations. *J. Atmos. Sci.*, **60**, 795–823.

Milbrandt, J. A. and M. K. Yau, 2006a: A multimoment bulk microphysics parameterization. Part III: Control simulation of a hailstorm. *J. Atmos. Sci.*, **12**, 3114–3136.

Milbrandt, J. A. and M. K. Yau, 2006b: A multimoment bulk microphysics parameterization. Part IV: Sensitivity experiments. *J. Atmos. Sci.*, **12**, 3137–3159.

Miles, J. W. and L. M. Howard, 1964: Note on the hetereogeneous shear flow. *J. Fluid Mech.*, **20**, 331–336.

Misra, V., M. K. Yau, and B. Nagarajan, 2000: Atmospheric water species budget in mesoscale simulations of lee cyclones over the Mackenzie River Basin. *Tellus*, **52A**, 140–161.

Rasmussen, E. and J. Straka, 1996: Mobile mesonet observations of tornadoes during vortex-95: In *Preprints,*19^{th} *Conf. on Severe Local Storms, San Francisco, CA*. Amer. Meteor. Soc., 1-5.

Rayleigh, L., 1880: On the stability , or instability, of certain fluid motions. *Proc. London Math. Soc.*, **11**, 57–70.

Rotunno, R. and J. B. Klemp, 1982: The influence of the shear-induced pressure gradient on thunderstorm motion. *Mon. Wea. Rev.*, **110**, 136–151.

Rotunno, R. and J. B. Klemp, 1985: On the rotation and propagation of simulated supercell thundestorms. *J. Atmos. Sci.*, **42**, 271–292.

Santos, J. R., M. K. Yau, and B. Nagarajan, 2008a: Simulation of a tornado-like vortex in a supercell storm, Part I: Results on storm scale and tornado scale. Submitted to *J. Atmos. Sci.*

Santos, J. R., M. K. Yau, and B. Nagarajan, 2008b: Simulation of a tornado-like vortex in a supercell storm, Part II: Vorticity budget and sensitivity experiments. Submitted to *J. Atmos. Sci.*

Smith, R. K. and L. M. Leslie, 1979: A numerical study of tornadogenesis in a rotating thunderstorm. *Quart. J. Roy. Meteor. Soc.*, **105**, 107–127.

Trapp, R., 1999: Observations of non-tornadic low-level mesocyclones and attendant tornadogenesis failure during VORTEX. *Mon. Wea. Rev.*, **127**, 1693–1705.

Wakimoto, R. M. and H. Cai, 2000: Analysis of a non-tornadic storm during VORTEX 95. *Mon. Wea. Rev.*, **128**, 565–592.

Wakimoto, R. M. and C. Liu, 1998: The Garden city, Kansas, storm during VORTEX 95. Part II: The wall cloud and tornado. *Mon. Wea. Rev.*, **126**, 393–408.

Weisman, M. L. and J. B. Klemp, 1982: The dependence of numerically simulated convective storms on vertical wind shear and buoyancy. *Mon. Wea. Rev.*, **110**, 504–520.

Weisman, M. L. and J. B. Klemp, 1984: The sructure and classification of numerically sinulated convective storms in directionally varying wind shears. *Mon. Wea. Rev.*, **112**, 2479–2498.

Weisman, M. L. and R. Rotunno, 2000: The use of vertical wind shear versus helicity in interpreting suprecell dynamics. *J. Atmos. Sci.*, **57**, 1452–1472.

Wicker, L. J., D. W. Burgess, and H. Bluestein, 1984: The pre-storm environment of the severe weather outbreak in Western Oklahoma on 22 May

1981: In *Preprints, 13th Conf. on Severe Local Storms, Tulsa, OK.* Amer. Meteor. Soc., 281-282.

Wicker, L. J. and R. B. Wilhelmson, 1995: Simulation and analysis of tornado development and decay within a three-dimensional supercell thunderstorm. *J. Atmos. Sci.*, **52**, 2675–2703.

Wurman, J. and S. Gill, 2000: Fine-scale radar observations of the Dimmit,Texas (2 June 1995), tornado. *Mon. Wea. Rev.*, **128**, 2135–2164.